EFFECTS OF TITANIA PARTICLES ON THE BEHAVIOURS OF POLYLACTIDE BASED COMPOSITES

A THESIS SUBMITTED TO
THE GRADUATE SCHOOL OF NATURAL AND APPLIED SCIENCES
OF
MIDDLE EAST TECHNICAL UNIVERSITY

BY

ULAŞ CAN

IN PARTIAL FULFILLMENT OF THE REQUIREMENTS
FOR
THE DEGREE OF MASTER OF SCIENCE
IN
METALLURGICAL AND MATERIALS ENGINEERING

SEPTEMBER 2018

Approval of the thesis:

EFFECTS OF TITANIA PARTICLES ON THE BEHAVIOURS OF POLYLACTIDE BASED COMPOSITES

submitted by **ULAŞ CAN** in partial fulfillment of the requirements for the degree of **Master of Science in of Metallurgical and Materials Engineering Department, Middle East Technical University** by,

Prof. Dr. Halil Kalıpçılar _____
Dean, Graduate School of **Natural and Applied Sciences**

Prof. Dr. Cemil Hakan Gür _____
Head of Department, **Metallurgical and Materials Eng.**

Prof. Dr. Cevdet Kaynak _____
Supervisor, **Metallurgical and Materials Eng. Dept., METU**

Examining Committee Members:

Prof. Dr. Cemil Hakan Gür _____
Metallurgical and Materials Engineering Dept., METU

Prof. Dr. Cevdet Kaynak _____
Metallurgical and Materials Engineering Dept., METU

Prof. Dr. Hüsnü Emrah Ünalan _____
Metallurgical and Materials Engineering Dept., METU

Assoc. Prof. Dr. Zarife Göknur Büke _____
Materials Science and Nanotechnology Eng. Dept., TOBB ETU

Assist. Prof. Dr. Mert Efe _____
Metallurgical and Materials Engineering Dept., METU

DATE: 04.09.2018

I hereby declare that all information in this document has been obtained and presented in accordance with academic rules and ethical conduct. I also declare that, as required by these rules and conduct, I have fully cited and referenced all material and results that are not original to this work.

Name, Last Name : Ulaş Can
Signature :

ABSTRACT

EFFECTS OF TITANIA PARTICLES ON THE BEHAVIOURS OF POLYLACTIDE BASED COMPOSITES

Can, Ulaş

M. S., Department of Metallurgical and Materials Engineering

Supervisor: Prof. Dr. Cevdet Kaynak

September 2018, 107 pages

In the first part of this thesis, the main aim was to compare influences of various contents of the micron (200 nm) and nano (50 nm) sized titania (TiO_2) particles especially on the mechanical performance of the polylactide (PLA) biopolymer. Micro and nano composites were prepared by twin-screw extruder melt mixing, while the specimens were shaped by compression molding. SEM analyses and mechanical tests revealed that due to the most uniform distribution in the matrix, the best improvements in the strength, elastic modulus and fracture toughness values could be obtained either by 5 wt. % micro-TiO_2 or by only 2 wt. % nano-TiO_2 particles. The secondary aim of this part was to investigate influences of using maleic anhydride (MA) grafted copolymer (PLA-g-MA) compatibilization on the performance of one nanocomposite composition. Due to the improved chemical interfacial adhesion, use of PLA-g-MA compatibilization for the specimen of PLA/2 wt. % n-TiO_2 composition resulted in the highest improvements in the mechanical performance of neat PLA. The improvements were 14% in tensile strength, 20% in flexural modulus and as much as 67% in fracture toughness. Thermal behavior of all specimens were also analysed by DSC and TG analyses.

In the second part of the thesis, the purpose was to investigate mechanical and thermal performance of 2 mm thick PLA specimens against UV irradiation; first when only adding benzotriazole based organic UV absorber (UVA), micron and nano sized TiO_2 particles alone, and then to reveal possible synergism when they are added together. Specimens prepared by the same techniques were exposed to UV irradiation under fluorescent lamps (UVB-313) with 0.50 W/m^2 for the periods of 12 and 24 days. Changes in the performance of UV irradiated specimens were evaluated in terms of % weight loss, changes in color and chemical structure, including the decreases in the mechanical and thermal properties. Various tests and analysis conducted in this part revealed that synergistic benefits of using micro and nano TiO_2 particles together with benzotriazole type UVA were not only due to the effective stiffening, strengthening and toughening actions of titania particles but also due to their very significant "UV screening" actions absorbing the photons of the UV irradiation, thus decreasing the degree of the detrimental photodegradation reactions leading to chain scissions in their PLA matrix.

Keywords: Polylactide; Micro Titania; Nano Titania; Maleic Anhydride; UV irradiation; benzotriazole based organic UV absorber

ÖZ

TİTANYA PARÇACIKLARININ POLİLAKTİT BAZLI KOMPOZİTLERİN DAVRANIŞLARINA ETKİLERİ

Can, Ulaş
Yüksek Lisans, Metalurji ve Malzeme Mühendisliği Bölümü
Tez Yöneticisi: Prof. Dr. Cevdet Kaynak
Eylül 2018, 107 sayfa

Bu tezin birinci bölümündeki ana amaç, çeşitli miktarlardaki mikro (200 nm) ve nano (50 nm) boyutlu titanya (TiO_2) parçacıklarının polilaktit (PLA) biyopolimerinin özellikle mekanik performansı üzerindeki etkilerinin karşılaştırılmasıdır. Mikro ve nanokompozitler çift vidalı ekstrüderde eriyik karıştırma tekniği ile hazırlanırken, numuneler basınçlı kalıplama yöntemi ile şekillendirilmiştir. SEM analizleri ve mekanik testler, matris içinde en etkin homojen dağılımları nedeniyle; mukavemet, elastik modül ve kırılma tokluk değerlerindeki en yüksek gelişmeler ya ağırlıkça % 5 mikro-TiO_2 ya da sadece ağırlıkça % 2 oranında nano-TiO_2 parçacıkları kullanılarak elde edildiğini ortaya çıkarmıştır. Bu bölümdeki ikincil amaç ise, maleik anhidrit (MA) ile graft edilmiş kopolimer (PLA-g-MA) uyumlaştırma tekniğinin seçilen bir nanokompozit bileşiminin performansı üzerindeki etkilerinin araştırılmasıdır. Seçilen PLA/ağ%2 n-TiO_2 numunesi için kullanılan PLA-g-MA uyumlaştırma işlemi, gelişen kimyasal ara yüzey etkileşimi nedeniyle, saf PLA'nın mekanik performansındaki en yüksek gelişmelerin elde edilmesini sağlamıştır. Gelişme oranları çekme mukavemeti değerinde %14, eğme modülü değerinde %20 iken, kırılma tokluğu değerinde %67'ye kadar yükselmiştir. Ayrıca, tüm numune kompozisyonlarının ısıl davranışları DSC ve TG analizleriyle de gözlemlenmiştir.

Bu tezin ikinci bölümündeki amaç, UV ışınımına karşı 2 mm kalınlığındaki PLA numunelerinin mekanik ve termal performanslarının araştırılmasıdır. İlk olarak

benzotriazol tipi organik UV soğurucu (UVA), mikro ve nano boyutlu TiO_2 parçacıkları tek tek, daha sonra ise olası sinerjiyi ortaya çıkarmak için birlikte eklenmişlerdir. Benzer yöntemlerle üretilen numunelere UV ışınımı, 12 ve 24 günlük dönemler boyunca 0.50 W/m^2 şiddetindeki floresan lambalar (UVB-313) kullanılarak uygulanmıştır. UV ışınımına maruz bırakılmış numunelerin performansındaki değişiklikler % ağırlık kaybı, renk ve kimyasal yapıda değişiklikler, mekanik ve termal özelliklerdeki düşüşler ile birlikte değerlendirilmiştir. Yapılan çeşitli testler ve analizler, mikro ve nano TiO_2 parçacıklarının benzotriazol tipi UVA ile birlikte kullanıldığında sinerji oluşturduğunu ortaya çıkarmıştır. Bu sinerji, titanya parçacıklarının yalnızca etkili gerginleştirme, dayanıklaştırma ve toklaştırma mekanizmaları nedeniyle değil, aynı zamanda onların çok önemli "UV perdeleme" etkileri nedeniyledir. Çünkü bu parçacıklar UV ışınımını soğurarak PLA matrisindeki zincir kırılmalarına yol açan zararlı ışıl bozunum reaksiyonlarının derecesini düşürmektedir.

Anahtar Kelimeler: Polilaktit; Mikro Titania; Nano Titania; Maleik Anhidrit; UV ışınımı; benzotriazol tipi organik UV soğurucu

in memory of my dearest auntie Ayla

ACKNOWLEDGEMENTS

First of all I would like to express my thankfulness to my supervisor Prof. Dr. Cevdet Kaynak for not only for his valuable criticism, guidance, insight and efforts at each stage of this thesis; but also his precious support, patience and understanding.

I would like to thank to the members of the examining committee, Prof. Dr. Cemil Hakan Gür, Prof. Dr. Hüsnü Emrah Ünalan, Assoc. Prof Dr. Zarife Göknur Büke and Assist. Prof. Dr. Mert Efe for their valuable discussion and contribution during my thesis defense period.

I would like to gratefully acknowledge Middle East Technical University (METU) Scientific Research Fund – Project Grant No: BAP–03-08-2017-001 and GAP-308-2018-2671. I would like to acknowledge all the technical staff and administrative board of the Metallurgical and Materials Engineering Department for supplying all the research facilities required in this dissertation. I am especially grateful to Serkan Yılmaz, Önder Şahin and Hüseyin Ceylan for their invaluable help. I would also like to express my sincere gratitude to METU Central Laboratory for GPC analyses.

I want to thank my laboratory mates, Yelda Meyva Zeybek, Burcu Sarı, Deniz Varsavaş and Berk Doğu, for their friendship and support. My special thanks go to, Eren Erol, Ezgi Çınar, İpek Bayraktar, Didem Dede, Cansu Demir, Elif Bal, İbrahim İyce, Pınar Tuncer, Tuğçe Altuntop, Miray Mazlumoğlu, Çağatay Taşçı, Ali Karakaya, Baybora Tunahan Matur and Erdi Kandemir for all their support and entertainment.

I would like to express my gratitude to my father Mehmet Murat Can, my mother Serpil Boran Can, my dear brother Boran Zihni Can. They have been a constant love and encouragement in each step of my life from childhood to adulthood. This dissertation would certainly be not possible without their support.

TABLE OF CONTENTS

LIST OF TABLES

LIST OF FIGURES

NOMENCLATURE

σ_{TS}	:	tensile strength
σ_{Flex}	:	flexural strength
ε_f	:	elongation at break, final strain
ΔH_m	:	heat of melting
ΔH_c	:	heat of crystallization
$\Delta H_m°$	:	melting enthalpy of 100% crystalline PLA
E	:	Young's modulus
E_{Flex}	:	flexural modulus
G_{Ic}	:	fracture toughness as critical strain energy release rate
K_{Ic}	:	fracture toughness as critical stress intensity factor
ATR-FTIR	:	attenuated total reflectance Fourier transform infrared spectroscopy
DSC	:	differential scanning calorimetry
PLA	:	poly(lactic acid) or polylactide
PLLA	:	L-enantiomer of polylactide
PDLA	:	D-enantiomer of polylactide
MA	:	maleic anhydrite
SEM	:	scanning electron microscopy
TGA	:	thermogravimetric analysis
$T_{5wt.\ \%}$	:	thermal degradation temperature at 5 wt. % mass loss
$T_{10wt.\ \%}$	:	thermal degradation temperature at 10 wt. % mass loss
$T_{25wt.\ \%}$	:	thermal degradation temperature at 25 wt. % mass loss
T_c	:	cold crystallization temperature
T_g	:	glass transition temperature
T_m	:	melting temperature
T_{max},	:	thermal degradation temperature of maximum mass loss rate
UVA	:	organic UV absorber
X_c	:	degree of crystallinity

CHAPTER 1

INTRODUCTION

1.1 Polylactide

Engineering thermoplastics have been replacing certain conventional metallic and ceramic materials lately due to especially their low density and well established production techniques. Nevertheless, because of the environmental issues associated with engineering polymers derived from petroleum resources, challenges like depletion of available petroleum reserves, sustainability and regulations about the use of petropolymers in some countries like Germany and Japan have arisen [1]. Therefore, the attraction for renewably made polymers, also named as "biopolymers" have grown in the last decade. In this regard, poly(lactic acid), also named as polylactide (PLA), is one of the key substitute biopolymer having aliphatic polyester structure, given in Figure 1.1.

The first attempt to synthesize polylactide was made in 1845 by Peluoze via lactic acid (LA) polycondensation resulted in low-molecular weight PLA. More than a century later, in 1954, DuPont patented high-molecular weight PLA. The commercialization of high-molecular weight PLA production was accomplished by Cargill Inc. following their patent for a continuous manufacture setup for PLA production from corn starch with direct ring-opening polymerization. Thereby, the first industrial PLA production plant was founded in 2002 having an annual capacity of 140 thousand tones [2].

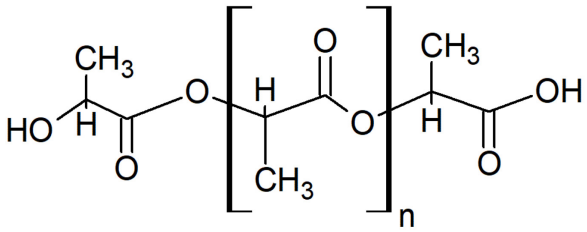

Figure 1.1 Chemical structure of polylactide with end groups

Lactic acid (2-hydroxy propionic acid), the main structural unit of PLA, is generally synthesized via bacterial fermentation of carbohydrates or chemical synthesis. Since lactic acid contains an asymmetric carbon atom, two conformation of PLA can be found; the L and D lactic acid as shown in Figure 1.2. For these two isomers, there are three different possible stereoforms; L,L-lactide, D,D-lactide and D,L-lactide (*meso*-lactide). First two cyclic dimers are optically active but, D,L-lactide form is optically inactive. The mixture of L,L-lactide and D,L-lactide (50/50 ratio) called *racemic*-lactide. Polymerization of these stereoforms are resulted in poly(L-lactic acid) (PLLA), poly(D-lactic acid) (PDLA), and *meso*-PLA, respectively whereas polymerization of racemic-lactide resulted in a polymer blend of PLLA and PDLA also called stereocomplex-type PLA. However, commercial PLA is a copolymer of poly(L-lactide) with small amount of poly(D,L-lactide), since the lactic acid derived from biological sources is composed of mostly L-lactic acid and smaller amount of D-lactic acid [3].

The most common way to synthesize high-molecular weight polylactic acid is through ring-opening polymerization of lactide depicted as first route in Figure 1.3. The lactide, a cyclic lactic acid dimer, is the second intermediate product and formed by depolymerization of low-molecular weight polylactide through back-biting reaction [4]. The first intermediate product is low-molecular weight polylactide oligomer obtained by polycondensation with water removal.

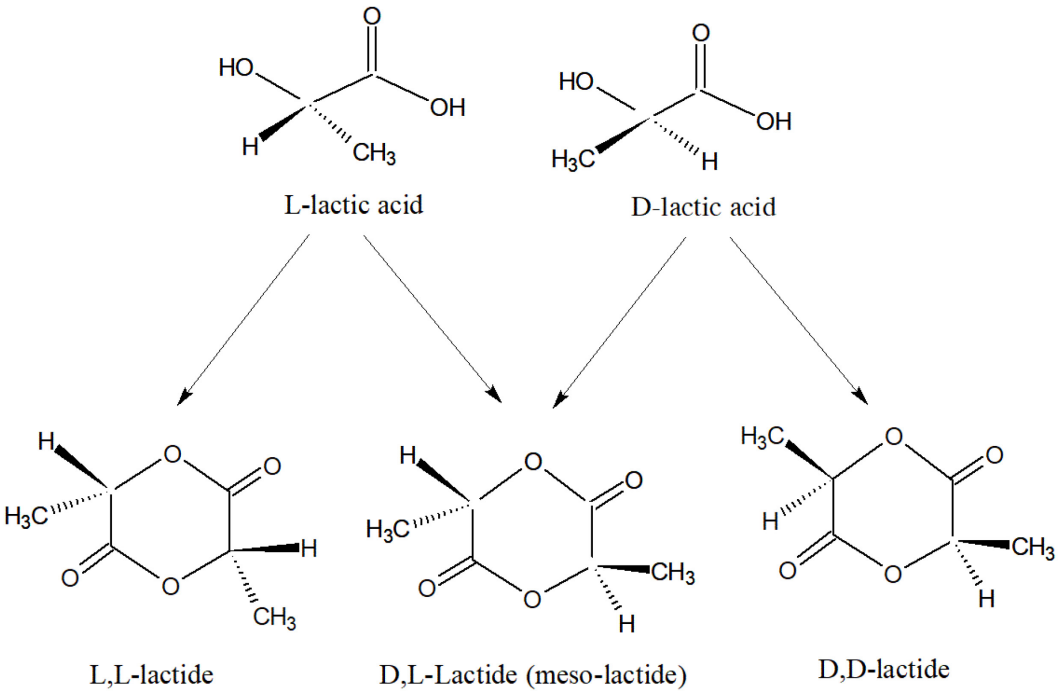

Figure 1.2 Chemical structures of lactic acid isomers and their cyclic dimers

Although, the second route, direct condensation polymerization is the cheapest one to obtain high-molecular weight polylactide because of the difficulty of solvent removal and the need of chain coupling agents and adjuvants, the complexity and cost of the process increase. The main advantage of the third route, azeotropic dehydrative condensation, is the lack of requirement of chain extenders and adjuvants. In this procedure most of condensation water can be removed by means of the distillation at low pressure. The fourth route is rather recently developed one, called solid state polymerization and it needs further improvement because of its long polymerization time in order to reach high-molecular weight [5].

Until last decade, the application of polylactide was limited with biomedical applications like resorbable sutures and degradable implants due to its biodegradability and biocompatibility [6]. With its rather low cost production, PLA had an increasing demand in consumer applications predominantly because of its transparency, processability, renewability and mechanical properties. Polylactide has comparable stiffness and tensile strength to polyethylene terephthalate (PET), but its extensive

implementation in structural applications will be dictated mainly by cost reductions as well as fine control over its mechanical and degradation properties.

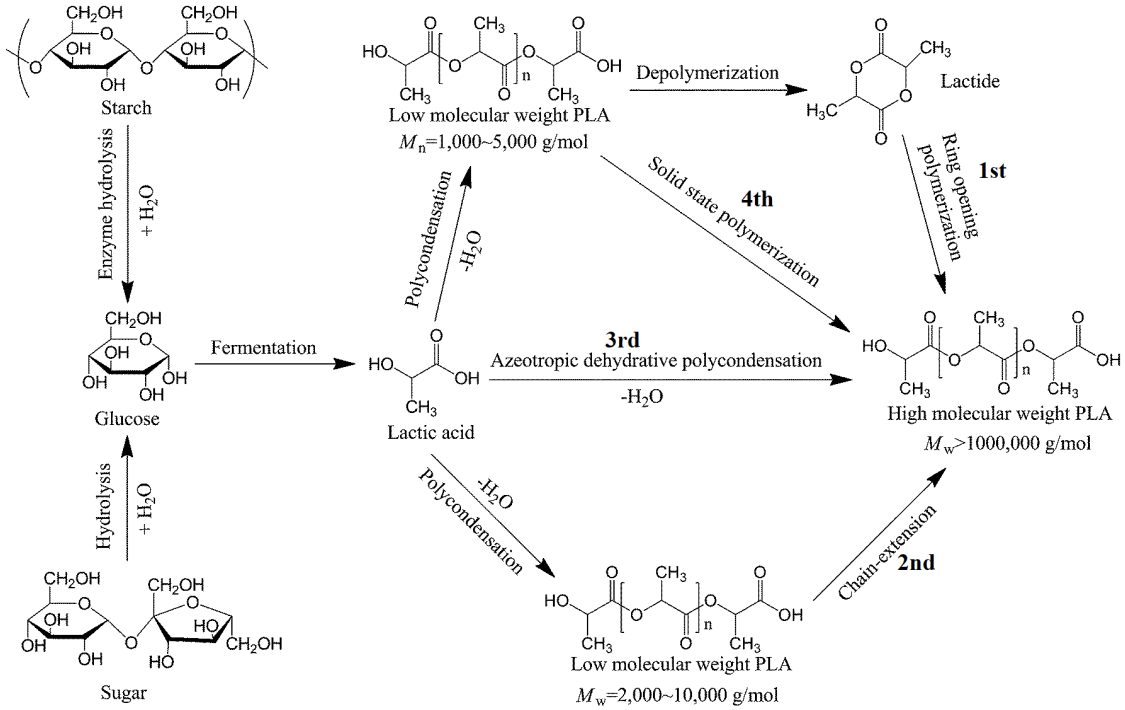

Figure 1.3 Main synthesis routes to high-molecular weight polylactide [3]

1.2 Titania

Titanium dioxide is a metal oxide and as a mineral, it is found most abundantly in the form of ilmenite ($FeTiO_3$) ore in the earth crust and its second largest source is the ore of rutile (TiO_2). The largest rutile and ilmenite reserves in the world are located in China, Australia, India and South Africa. The total world reserve of ilmenite is around 700 million tones whereas rutile reserve is around 50 million tones. The world largest ilmenite and rutile mine are operated in Norway and Sierra Leone, respectively. These ores are converted into pure titanium dioxide with sulphate and chloride processes for ilmenite and rutile ores, respectively.

There are two main approaches for the production of particles: top-down and bottom up approaches. For titania particles, both its industrial production and researches focus

on bottom up synthesis of particles from a precursor such as titanium tetraisopropoxide (TTIP), titanium chloride ($TiCl_4$), titanium hydride (TiH_2) powder and titanium butoxide ($C_{16}H_{36}O_4Ti$), etc. For the industrial production of titania powders utilizing the flame spray pyrolysis method, $TiCl_4$ liquid precursor from chloride process is burned with oxygen flame at high temperatures and titanium oxide obtained [7].

Synthesis of titania particles with controlled sizes and morphology requires fine calibration of the reaction medium. The methods having equal industrial importance other than flame spray reactions are hydrothermal reactions and sol–gel techniques. Titania nanoparticles can be formed in aqueous media, thus allowing for various hydrothermal methods. Hydrothermal synthesis is normally conducted in steel pressure vessels called autoclaves under controlled temperature and/or pressure with the reaction in aqueous solutions. The temperature can be elevated above the boiling point of water, reaching the pressure of vapor saturation. It is a method that is widely used for the production of TiO_2 nanoparticles. In the sol-gel process, a colloidal suspension is formed from the hydrolysis and polymerization reactions of the metal salts or metal alkoxide precursors. Complete polymerization and loss of solvent leads to the formation of the solid gel phase. With this method, ultrafine and uniform ceramic powders are formed by precipitation, spray pyrolysis, or emulsion techniques [7].

There are three commonly known polymorphs of TiO_2 found in nature: rutile (tetragonal), anatase (tetragonal) and brookite (orthorhombic) having different energy band gaps of 3.03, 3.20, and 2.96 eV, respectively [8].

Rutile: This polymorph has a tetragonal structure containing 6 atoms per unit cell. The TiO_6 octahedron is slightly distorted as shown in Figure 1.4. The rutile phase is stable at most temperatures and pressures up to 60 kbar. The stability of the particles also depends on particle size such that the rutile TiO_2 becomes more stable than anatase for particle sizes greater than 14 nm. The activity of the rutile TiO_2 as a photocatalyst is generally very poor compared to anatase TiO_2. The rutile form is widely used as a white pigment and opacifier.

Anatase: This polymorph also has a tetragonal structure but with a slightly larger distortion of the TiO_6 octahedron compared to rutile phase as depicted in Figure 1.4. The anatase structure is preferred over other polymorphs for solar cell applications because of its higher electron mobility and low dielectric constant. The increased photoreactivity is because of the slightly higher Fermi level and higher degree of hydroxylation in the anatase phase.

Brookite: This polymorph belongs to the orthorhombic crystal system. Its unit cell is composed of an octahedra, each has a titanium atom at the center and oxygen atoms at the corners, as shown in Figure 1.4. It is more complicated, has a larger cell volume and is also the least dense of the three forms. It is also the least studied form of TiO_2 due to the difficulty of obtaining it as a pure phase.

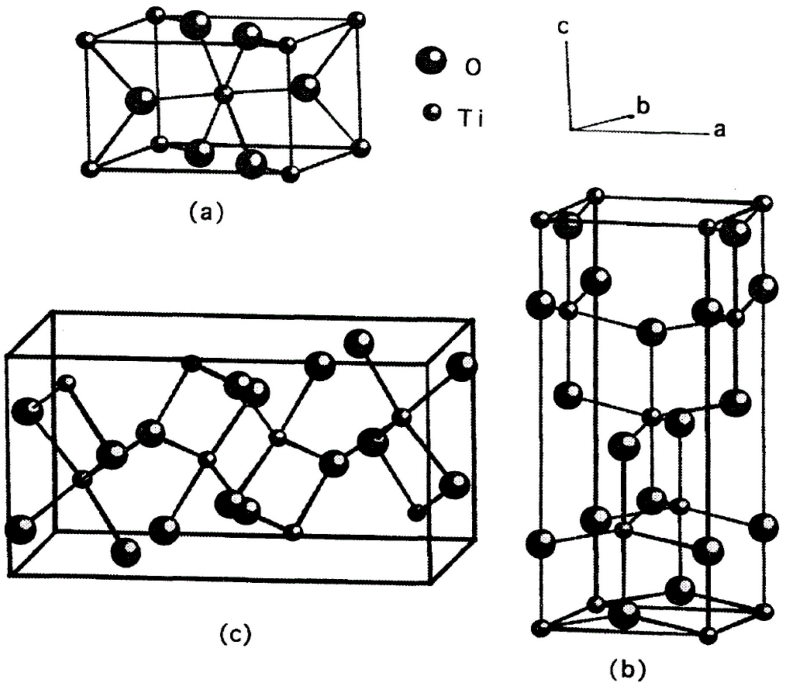

Figure 1.4 Different crystal structures of TiO_2; **(a)** rutile, **(b)** anatase, and **(c)** brookite [9]

Titania nanoparticles have potential to act either as an UV absorber or a photocatalyst. When TiO_2 particles are exposed to UV irradiation, impinging photons with energies equal to or higher than its band gap, electrons are excited from the valence band into

the unoccupied conduction band, leading to the formation of excited electrons (e^-) in the conduction band and positive holes (h^+) in the valence band as shown in Reaction 1 below. These charge carriers can recombine, nonradiatively dissipating the input energy as heat, or get trapped and react with electron donors or acceptors adsorbed on the surface of the TiO_2 particles as illustrated in Figure 1.5. The competition between these processes determines the overall efficiency of TiO_2 particles for various applications. These fundamental processes can be expressed as follows [7]:

$$TiO_2 + h\upsilon \rightarrow e^- + h^+ \quad (1)$$

$$e^- + Ti(IV)O\text{-}H \rightarrow Ti(III)O\text{-}H^-(X) \quad (2)$$

$$h^+ + Ti(IV)O\text{-}H \rightarrow Ti(IV)O^{\bullet}\text{-}H^+(Y) \quad (3)$$

$$h^+ + 1/2\ O^{2-}{}_{lattice} \leftrightarrow 1/4\ O^2(g) + vacancy \quad (4)$$

$$e^-| + O_{2,s} \rightarrow O_{2,s}{}^- \quad (5)$$

$$O_{2,s}\text{-} + H+ \leftrightarrow HO_{2,s} \quad (6)$$

$$h^+ + Ti(III)O\text{-}H^- \rightarrow Ti(IV)O\text{-}H \quad (7)$$

$$e^- + Ti(IV)O^{\bullet}\text{-}H^+ \rightarrow Ti(IV)O\text{-}H \quad (8)$$

$$O_{2,s} + Ti(IV)O^{\bullet}\text{-}H^+ \rightarrow Ti(IV)O\text{-}H + O_{2,s} \quad (9)$$

Reactions 2 – 6 are photocatalytic redox pathways, whereas Reactions 7 – 9 represent the recombination of electron-hole pairs.

These two distinct behavior of titania particles enabled their extensive use for two different purposes. The applications as “UV absorber” includes paints, sunscreens, additives in plastics, pigments and coatings; while they are used in dye-sensitized solar cells, electrode materials in lithium batteries, piezoelectric capacitors, solid oxide fuel cell, gas sensors, polluted water/air treatment and antimicrobial applications as “photocatalyst”.

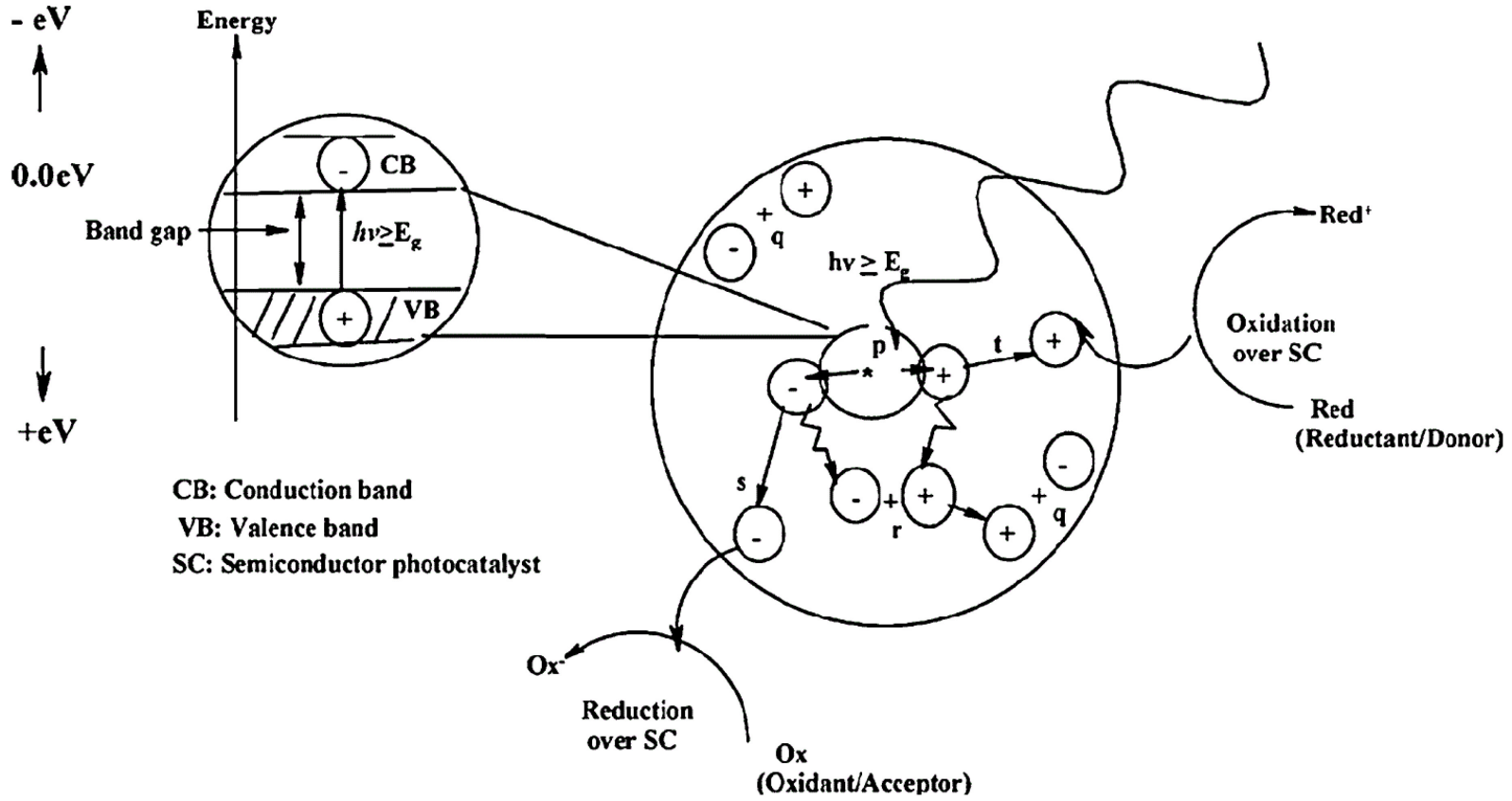

Figure 1.5 Schematic diagram of photocatalytic and UV absorbing process initiated by a photon [10]

They perform these functions depending on their crystal structure and particle size. The anatase structure is preferred over other polymorphs for photocatalyst applications because under UV irradiation, upon photon absorption, electron (e^-) hole (h^+) pairs formed in anatase phase have longer lifetimes before recombination and higher mobility than those they have in rutile. Therefore, e^--h^+ pairs in anatase phase have higher possibility to reduce oxygen and react with OH^-, respectively at particle surface. On the other hand, the activity of the rutile phase as a photocatalyst is generally very poor. Moreover, according to Li *et al*. [11] anatase has an inherent band bending at the surface of the particle that is spontaneously formed in a deeper region with a steeper potential compared to rutile as shown in Figure 1.6. Thus, surface hole trapping dominates recombination in anatase phase because charge separation of e^--h^+ pairs occur via the transfer of holes towards the particle surface along the strong upward band bending. In rutile, however, bulk recombination of electrons and holes prevails such that only the holes very close to surface are trapped and transfer to the surface which makes rutile phase more effective as an UV absorber [12].

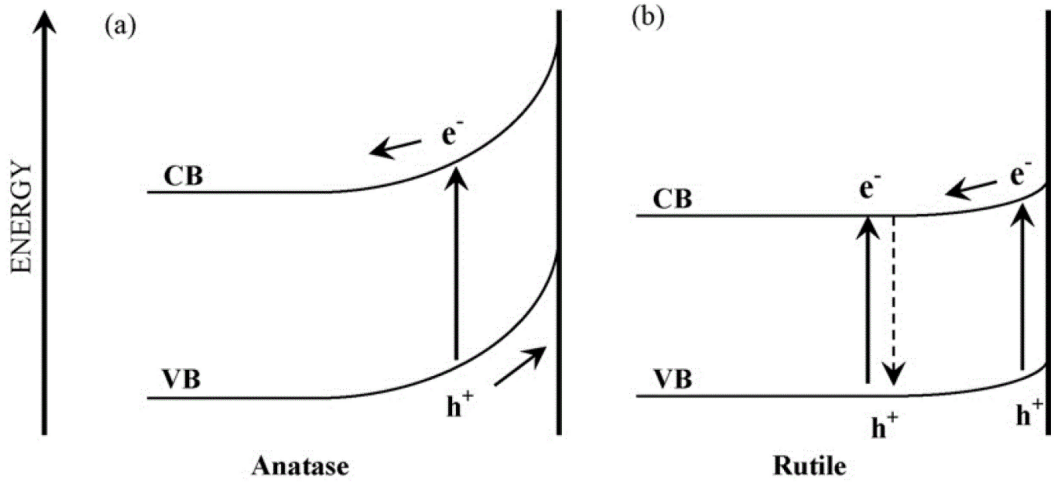

Figure 1.6 Band bending at the surface of **(a)** anatase, **(b)** rutile particles [11]

The photocatalyst function is promoted with smaller particle sizes because as particles become smaller, especially <10 nm, due to the quantum size effect, the possibility of recombination decreases and TiO_2 particles act as photocatalyst. Moreover, it is also known that the previously mentioned band bending will become smaller with the TiO_2

particle size decreasing. On the other hand, the UV absorber behavior becomes dominant over photocatalytic behavior when the size of particles is rather large. The UV light is strongly absorbed by excitation of electrons from the valence band to the conduction band and the recombination of charge carriers followed by the dissipation of the input energy in less harmful way such as heat. TiO_2 has a bandgap energy corresponding to wavelength of 365 nm. Light below these wavelengths has sufficient energy to excite electrons and hence is absorbed by TiO_2 particles. Light having a wavelength longer than the band gap wavelength will not be absorbed.

1.3 Polymer/Titania Composites

Titania particles has already found extensive use in many polymer matrices such as polyvinylchloride, polystyrene, polyamide 6, epoxy, poly(-methyl methacrylate), and polyimide. The introduction of particles cause increase of stiffness, durability, , fire retardation, UV-protection and additional fracture mechanisms like particle pull-out, crack pinning, crack bridging and crack blunting improving the toughness of polymer matrices [13].

Titania particles also receive much attention in food packaging industry to be used in biodegradable polymers like polylactide or polycaprolactone because they are inert, non-toxic, inexpensive, environmentally-friendly and especially have antimicrobial activity against a wide variety of microorganisms [14]. Their most abundant use by mass however is in PVC matrix because of UV absorption and color stabilizing properties of titania and extensive outdoor applications of PVC in construction industry such as doors, window profiles, and fascia boards, etc [15]. Moreover, titania reinforced PMMA thin films is a promising new class of materials for optoelectronic applications. The introduction of titania into a PMMA matrix not only improve thermal

stability of the composites but also their crystallinity, refractive index and more importantly they add non-linear optical behavior [16,17].

In terms of the interactions with UV irradiation, as mentioned in the previous section titania particles may accomplish two different tasks in PLA matrix: (i) shielding UV light and hence decreasing photodegradation rate; (ii) generating radicals at their surface causing chain scission of PLA matrix. Apart from their crystal structure and particle size, according to their surface conditions in the polymer matrix, either one of these effects can be performed by the particles. Under UV irradiation electron hole pairs are formed in particles which may recombine or travel to particle surface forming radicals such as O^{2-}, HOO•, OH• from H_2O and O_2. The encapsulation of the particles in a chemically stable shell prevents direct contact between the particles and molecules that could be converted into a radical. For instance, when the particles are embedded in thick films in which their surface is sealed with the matrix and formation of radicals are inhibited, the possibility of recombination increases and the former effect become dominant [18].

1.4 Photodegradation of PLA

All polymeric materials could be degraded when they are exposed to UV irradiation due to the certain chemical alterations in their structure. The basic degradation mechanisms, namely “main-chain scission”, “cross-linking”, “oxidation”, or “bond cleavage” all lead to discoloration, decreased molecular weight, lower mechanical properties and brittle fracture behavior. The photodegradation of polymers is accelerated especially when they are used in outdoor applications because of the high energy UV irradiations of the sunlight further divided into UVA, UVB, and UVC regions as 380-315, 315-280, 280-200 nm, respectively [19].

As PLA has gained much attention as a non-petroleum biobased polymer in recent years, it is important to focus on the degree of photodegradation of PLA for its durable outdoor applications. It is known that PLA is also becoming one of the most preferable

material in the biomedical sector due to its mechanical properties and biodegradability/biocompatibility. Today, most of these biomedical parts are sterilized under UV irradiation. Therefore, to study level of photodegradation of PLA in this field is also critical.

According to Grotthuss – Draper law only the photons absorbed by the molecule can initiate photochemical reactions. When a photon is absorbed, the molecule in the ground state is electronically excited into a higher energy state. Generally, the photon is absorbed by a particular group in the molecule which is C=O bond in PLA known to have n-π* excitation at 280 nm. The other single bonds like C-C, C-H, and C-O have excitations at wavelengths shorter than 180 nm. Since PLA is rarely exposed to these high energy photons, C=O carbonyl group is the main subject of the photodegradation of PLA. The excitation of carbonyl group having antibonding and bi radical properties (Figure 1.7 (a)) tends to cause α and β cleavage (Figure 1.7 (b)), atom abstraction (Figure 1.7 (c)), radical addition, and electron abstraction or electron transfer [19].

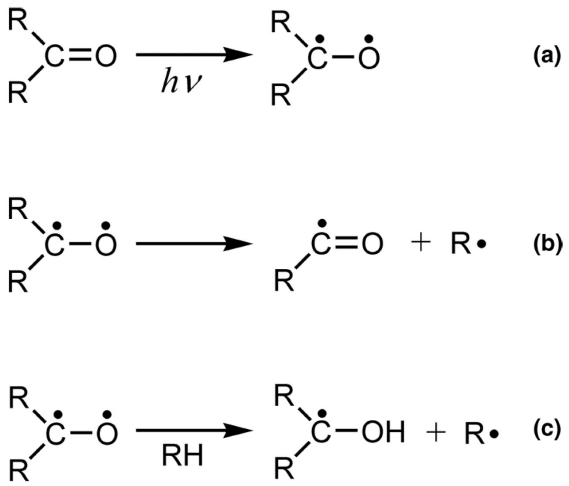

Figure 1.7 Excited states of C=O bond in carbonyl group [19]

The first study in 1985 proposing the photodegradation mechanism of PLA was reported by McNeill *et al.* [20] suggesting that PLA decomposition under UV radiation occurred by photolysis of the C-O bond in the ester linkage, at the position (b) as depicted in Figure 1.8.

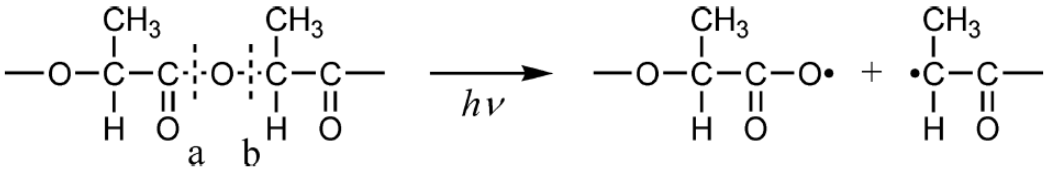

Figure 1.8 PLA photodegradation by Norrish I reaction according to McNeill *et al.* [20]

The second study about polylactide photodegradation was published in 1997 by Ikada [21] and later accepted by many scientist like Tsuji *et al.* [22]. Based on the increased C=C double bonds and OH groups in their IR spectra, Ikada claimed that chain scission in the backbone of polylactide occurred via Norrish type II mechanism, shown in Figure 1.9 at the ester group and the subsequent two methylene groups adjacent to the ester oxygen.

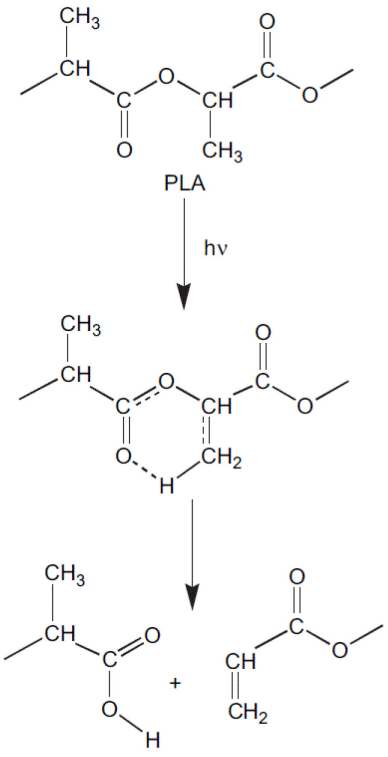

Figure 1.9 PLA photodegradation by Norrish II reaction according to Ikada [21]

Janorkar *et al.* [23] applied low energy UV irradiation having wavelength range of 300–500 nm in order to minimize photodegradation of polylactide. Two alternative mechanisms were proposed: (i) photolysis of C=O followed by dehydrogenation indicated as Mechanism A and (ii) photooxidation forming hydroperoxide derivatives dissociated into carboxylic acid and unstable diketones compounds as shown in Mechanism B of Figure 1.10. However, it should be noted that these reactions cannot explain the increase of C=C bonds reported by Ikada [21].

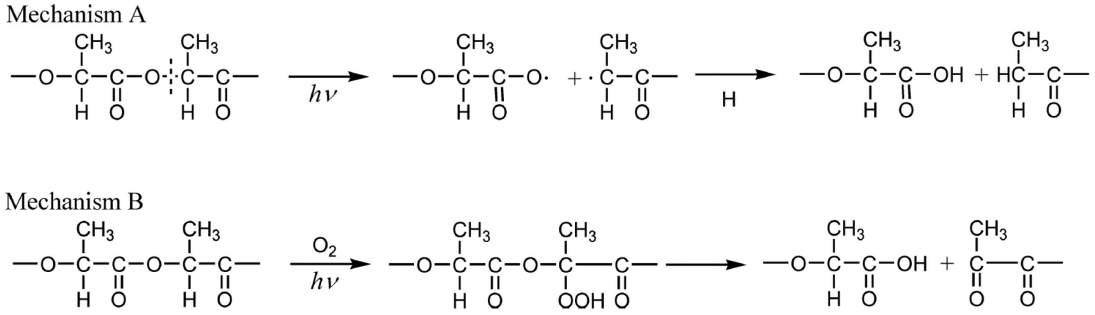

Figure 1.10 Photodegradation mechanisms via photolysis (Mechanism A), and photooxidation (Mechanism B) proposed by Janokar *et al.*[23]

Bocchini *et al.* [24] proposed two different photodegradation mechanisms which are Norrish II mechanism and photooxidation radical mechanism. Among these two mechanisms, which one is predominant largely depend on the wavelength of the photon. If the wavelengths of the photon is below 300 nm, it can be directly absorbed by PLA molecule and photodegradation occurs via well-known Norrish II type chain cleavage. However, if the wavelength of the photon is above 300 nm, it cannot be directly absorbed. In this case, the photooxidation radical mechanism takes place as shown in Figure 1.11. This mechanism usually begins with radical formation from impurities by UV-irradiation or thermal decomposition. First, a tertiary hydrogen is abstracted from PLA chain and a tertiary radical P• is formed as shown in Reaction (1) of Figure 1.11. This radical can react with oxygen to form a peroxide radical (2), which may easily abstract another hydrogen from a tertiary carbon with the formation of an hydroperoxide and the initial radical P• (3). Then, the hydroperoxide undergoes photolysis (4) with the formation of the HO• and a PO• radical that can further evolve by β-scission (5). Taking into account the stability of the different fragments the most

probable β-scission appears to be the (5b) reaction, leading to the formation of anhydride groups. In this study, presence of anhydride groups were observed with new peak formation at 1845 cm^{-1} in FTIR spectra of PLA specimen.

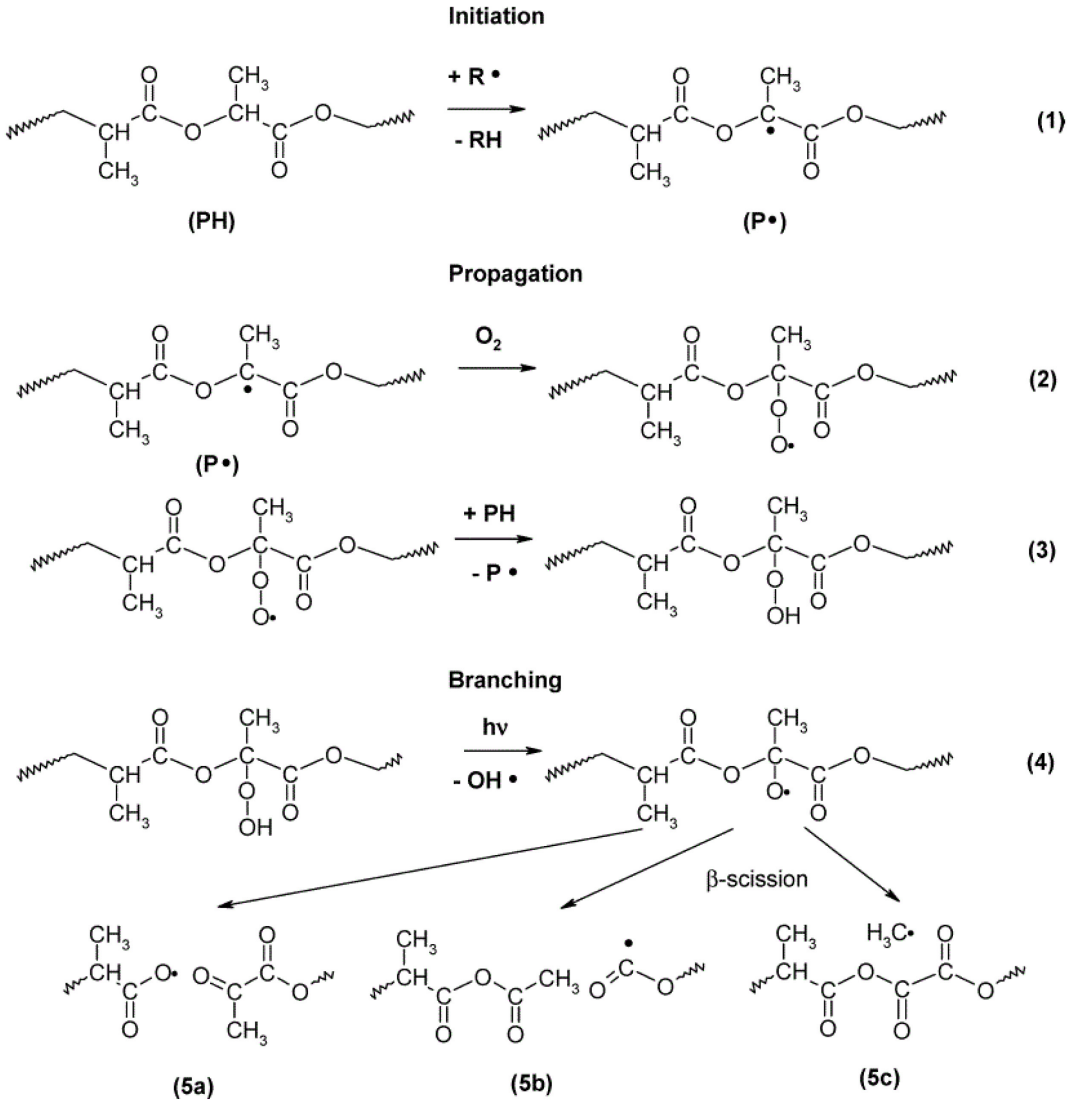

Figure 1.11 Radical oxidation process of irradiated PLA samples: Hydroperoxide chain propagation and formation of anhydrides by photolysis of hydroperoxide [24]

It should be also pointed out that, the decreased molecular weight by chain scissions result in the increased mobility of polylactide chains and ultimately ease the crystallinity as reported by Tsuji et al. [22]. In their study, they compared the photodegradation of crystalline and amorphous PLA. It was found that degradation occurred both in amorphous and crystalline regions of PLA but photodegradability of crystalline regions was rather low. The decrease in the cold crystallization temperature

(T_{cc}) was explained by the crystallization amount, promoted via decreased molecular weight, caused by annealing in a 65 ºC UV irradiation chamber. Because as the degradation proceeds, the chains become short enough to rearrange spatially of the amorphous parts in crystalline regions. Polarized optical microscopy (POM) studies of amorphous PLA also revealed the newly formed spherulites while no significant change were observed at size and amount of spherulites in crystalline PLA.

In their FTIR analysis, Copinet *et al*. [25] observed decreasing intensities and shifting peak positions to lower wavelengths of the –C–O– and –C=O stretching bands with UV irradiation because of the hydrolysis of ester linkages while decreased intensity of –C–C– stretching was ascribed to modification of the degree of crystallinity.

Santonja-Blasco *et al.* [26] observed that –C=O stretching band broadened and shifted to lower frequencies due to increased concentrations of acid end groups. It is stated that photodegradation occurs via Norrish II type chain cleavage and photolysis leading to formation of anhydride groups by β-scission. The spectra belonging to longer degradation times displayed anhydride carbonyl adsorption at 1845 cm^{-1}.

1.5 Literature Survey

1.5.1 Previous Studies on the Effects of Micron and Nano Sized Titania on the Behavior of Polylactide

It is very well known that due to the depletion of petroleum resources, there is a growing interest in the use of biosourced polymers classified as “biopolymers”. For instance, polylactide (PLA) being a renewable thermoplastic that can be produced from annually renewable resources (such as corn starch or sugar cane) is recently becoming a significant candidate for short-time uses, e.g. in food packaging and medical device market [27], especially due to its rather high-strength, high-modulus, biodegradable/biocompatible aliphatic polyester structure. Hereafter, PLA has started to gain more and more importance as a promising alternative candidate material to

replace conventional petrochemical-based polymers for also long-term industrial applications, such as automotive industry. However, for such rather structural applications, PLA suffers from some shortcomings such as lower values of toughness, thermal resistance and rate of crystallization. Although PLA has the highest mechanical properties among other biopolymers, it still needs reinforcements in order to fulfill structural integrity requirements in many engineering applications. Therefore, there is a demanding interest in the number of the researches investigating the effectiveness of the "composite approach" for PLA matrix.

In this respect, effects of various types of fillers have been studied as the composite approach to PLA matrix, such as: (i) natural fibers; kenaf, hemp, flax, jute, ramie and sisal [28–33], (ii) engineering fibers; carbon and glass short fibers [34–37], (iii) micro-fillers; talc, hydroxyapatite, calcium carbonate, calcium sulfate, mica, and microcrystalline cellulose [38–43], and (iv) nano-fillers; carbon black, carbon nanotube, graphene, silicate, nanoclays, POSS, halloysite nanotube, cellulose nanofibers and silica nanoparticles [44–54]. Moreover, micron and nano-sized titanium dioxide (TiO_2) particles, also named as "titania", have been used as the reinforcing material.

Titania particles are widely used commodity powders (annual production of > 4 million tons), especially in micron size as an inorganic pigment in paints, plastics, paper, leather, textiles, foods and personal care products. On the other hand, recent studies showed that TiO_2 nanoparticles have potential to be used in areas of chromatographic separation, lithium-ion batteries, dye-sensitized solar cells, photo catalytic redox reactions and water splitting, gas sensors and drug delivery vehicles [55].

As a composite reinforcement, TiO_2 particles have been investigated for many thermoplastic matrices such as PVC, PP, PS, PE, etc. due to their high photostability and biocompatibility. In the literature, titania particles were generally investigated in two groups of size-ranges; micro and nano. If the particle size range was between 200-1000 nm, then they are named as either "sub-micron" or simply just "micro"; whereas

they are named as “nano” when their size range is less than 100 nm. In the literature, for the PLA matrix, majority of the studies investigate effects of TiO_2 nanoparticles with less than 100 nm range. Some of these studies can be summarized as follows:

Dural-Erem *et al.* [56] produced PLA nanocomposite films containing 0, 1 and 5 wt. % TiO_2 nanoparticles (< 25 nm) for medical applications by melt intercalation method via twin screw extrusion through a film die. Thermal analysis showed that transition temperatures T_g, T_c, T_m and crystallinity amount did not significantly change whereas thermal degradation temperatures $T_{d\,0.5}$ and $T_{d\,0.05}$ increased with the filler content. This means that the addition of TiO_2 nanoparticles increased thermal stability of the PLA films by decreasing the heat transfer rate. According to the tensile tests results strength and modulus values were reduced possibly due to the distribution problems of the nanoparticles. On the other hand, the water absorption properties of the nanocomposite films increased exhibiting bacteriostatic and limited bactericidal efficacy.

Farhoodi *et al.* [57] used anatase TiO_2 nanoparticles (20 nm) for the production of PLA/TiO_2 (1, 3, 5 wt. %) composite films with solution casting. DSC analyses showed that crystallinity amount increased slightly at 1 wt. % due to nucleation agent effect; but at higher loadings opposite effect was observed, this time due to the restriction in the spherulite growth. On the other hand, T_g was affected adversely because nanoparticles disturb the packing and regularity of polymer chains and cause free volume increment in the system. Results of the tensile test showed that strain at break increased 57% at 3 wt. % content, but tensile strength decreased and no significant change observed in elastic modulus. This toughening effect could be the consequence of the breaking up of agglomerates, void nucleation, crack deflection, nanofiller debonding or pull out, matrix deformation and bridging mechanisms. SEM micrographs revealed uniform distribution of TiO_2 nanoparticles at 1 and 3 wt. % loading levels. UV-visible spectra showed that TiO_2 nanocomposite films had high ultraviolet shielding compared to neat polymer, but there was significant reduction in transparency.

Fonseca *et al*. [58] produced PLA/TiO_2 (anatase, 10 nm) composites with 1, 3, 5 and 8 wt. % compositions by melt-mixing method. DSC results showed that T_g and T_m were not affected from nanoparticle incorporation while T_c increased from 106ºC to 120ºC showing that it promotes crystallinity due to the nucleation agent effect of the particles. However, percent crystallinity did not show a significant change. Polarized optical microscope (POM) images showed that the number of spherulites increased, i.e. higher nucleation density with finer spherulite size compared to neat PLA. A significant change was not present in the degradation temperatures according to TGA results. The increase in the Young's modulus of PLA/TiO_2 nanocomposites were as much as 55% with 5 wt. % TiO_2. On the other hand, elongation at break values decreased with nanoparticle incorporations.

In the study of Zhang *et al.* [59], PLA/TiO_2 (20 nm, anatase) nanocomposites were prepared by vane extruder with 0, 0.5, 1, 2, 5, 10 and 15 wt. % TiO_2 while specimens were fabricated by injection molding. According to SEM images homogeneous distribution was obtained when particle content was not more than 5 wt. %. DSC results suggested that TiO_2 nanoparticles do not play an active role in heterogeneous nucleation. According to TGA, thermal stability of the PLA/TiO_2 nanocomposites were improved as compared with that of pure PLA resin. This is possible because TiO_2 particles could act as heat barrier in the early stages of thermal decomposition. According to the results of tensile tests, properties increased up to only 2 wt. % TiO_2. For this nanocomposite, the increase in tensile strength and elongation at break values were 1.5% and 107%, respectively.

One of the biggest problem in the polymer nanocomposite investigations is the extreme difficulty to obtain random and uniform distribution of the nanoparticles in polymer matrices. In the literature, there exist substantial amount of effort in order to improve dispersibility of titania in PLA matrix because of the bad influences of aggregated TiO_2 nanoparticles especially in terms of reduced mechanical properties which would prevent use of PLA/TiO_2 nanocomposites in structural applications. Literature survey indicated that, these studies especially focused on the use of different TiO_2 surface modification techniques as some of them summarized below:

Lu *et al.* [60] modified surfaces of TiO_2 (20 nm) nanoparticles by surface-grafting with L-lactic acid oligomer and produced PLA/TiO_2 nanocomposite specimens by solvent casting method at 5, 10, 15, 20 wt. % compositions. It was observed that grafted particles (g-TiO_2) had approximately uniform distribution, while unmodified TiO_2 nanoparticles tended to aggregate. Crystallinity of the PLA matrix decreased with increasing the amount of g-TiO_2 particles which might be due to the interfacial chemical bond between g-TiO_2 and PLA, decreasing the PLA chain mobility required for crystallization. Tensile tests showed that compared to neat PLA, 5 wt. % g-TiO_2 increased tensile strength as 23%, while this increase was 11% with unmodified TiO_2. This behavior can be attributed to better interaction and adhesion between g-TiO_2 particles and PLA matrix.

Similarly, in order to eliminate their agglomeration in PLA matrix, Luo et al. [61] functionalized TiO_2 (20 nm, anatase) surfaces by lactic acid grafting. PLA/TiO_2 nanocomposites with 0.2, 0.5, 1, 2, 5 and 8 wt. % grafted and bare TiO_2 compositions were produced by co-rotating twin-screw extruder while test specimens were shaped by injection molding. TEM studies showed that bare TiO_2 particles formed agglomerates even at 0.5 wt. %, but grafting prevented their agglomeration effectively up to 2 wt. %. The strain at break and tensile strength values of the composites with 1 and 2 wt. % grafted TiO_2 nanoparticles increased certain amount compared to neat PLA. Because, PLA chains having compatibility with grafted TiO_2 establish rather strong interaction leading to increased stress transfer from the matrix to the particles. However, for composites reinforced with non-grafted TiO_2 particles, both tensile strength and strain at break values decreased for all filler contents. SEM images also showed that composites reinforced with bare TiO_2 nanoparticles had very smooth fracture surfaces indicating the semi-brittle fracture behavior whereas specimens reinforced with grafted TiO_2 nanoparticles had very rough fracture surfaces with extensive ligament stretching.

In the study of Meng *et al.* [62] titania (400 nm, anatase) sub-micron particles were surface treated by coating with this time poly(ε-caprolactone) (PCL). Then,

microcomposites were fabricated by melt-blending and compression molding at compositions of 2, 5, 10, 30 and 40 wt. % bare and coated TiO_2 particles. Agglomerations were observed at and above 5 wt. % bare TiO_2 loadings whereas coated TiO_2 particles resulted in no agglomeration even at 20 wt. % loading. For composites reinforced with coated TiO_2, strain at break increased with increasing TiO_2 loading and reached a maximum value of 64.7% at 30 wt. %. A stress whitening phenomenon induced by large amount of crazes and necking was observed easily during the tensile test of samples filled with coated TiO_2 indicating ductile fracture. On the other hand, for composites reinforced with bare TiO_2 particles strain at break values were lower than neat PLA. However, for all cases, tensile strength of composites were lower than the PLA matrix.

Zhuang *et al.* [63] fabricated PLA/TiO_2 (20 nm, anatase) nanocomposites with 1, 3, 5 and 10 wt. % loadings via in-situ polymerization and shaped them with solution casting method. Particles used in their study were organically surface modified with a silane (γ-methacryloxypropyltrimethox-ysilane). They proved by SEM studies that, silanized TiO_2 particles at 1 and 3 wt. % were well dispersed in PLA matrix. Thermal stability of the polymer was enhanced because the presence of nano-TiO_2 particles constraining the mobility of PLA molecular chains and simultaneously acting as thermal insulators during the thermal transport. Change in the glass transition temperature was proportional to particle dispersion level in the matrix, because chain mobility of the matrix decreased by the hydrogen bonds formed between carbonyl groups on the PLA chains and the hydroxyl groups on the surfaces of silanized TiO_2. Increasing the homogeneity of the dispersion increased the chain mobility restriction and consequently T_g. Tensile strength, modulus and elongation at break improved to a certain degree as 17 MPa, 287 MPa and 262%, respectively, for the 3 wt. % TiO_2 reinforced composite. When a load is imposed on the PLA, it will be transmitted to the TiO_2 particles nearby, and then to the matrix around the particles; even the rupture of some of the chains would not endanger the whole system. In this way, the load can be dissipated quickly and effectively with both the strength and toughness enhanced.

In the study of Marra *et al.* [64], PLA/TiO_2 (25 nm) (80% anatase and 20% rutile) nanocomposite films were prepared by twin screw mixer and compression molding. Compatibility between polymer matrix and nanoparticles were improved by functionalizing TiO_2 surfaces with fluorocarbons plasma treatment. They used 2 and 5 wt. % untreated and functionalized TiO_2 nanoparticles. Thermal degradation temperatures shifted to higher temperatures but the improvement was more significant for functionalized nanocomposites. For example, at 5 wt. % particle loading, the improvement in T_{max} was 27 ºC whereas it was only 14 ºC for composites reinforced with untreated TiO_2 particles. Similarly, for 5 wt. % loading, yield strength and tensile strain at break values have been improved by 18.6% and 22.8%, respectively with functionalized TiO_2 particles; whereas these properties were deteriorated as much as 12.0% and 14.5% with untreated TiO_2 particles. The morphological analysis has evidenced that all these improvements were basically due to the rather homogeneous distribution of the functionalized TiO_2 nanoparticles in the PLA matrix.

1.5.2 Previous Studies on the UV Irradiation of PLA and PLA/TiO_2 Composites

Polymers derived from the renewable agricultural resources, called as “biopolymers” are recently being considered as a probable way out from the today’s petroleum based traditional polymeric materials, because of the significant environmental concerns and the depletion of fossil resources. In this regard, poly(L-lactic acid), i.e. polylactide (PLA), among other available biopolymers, is becoming one of the most promising candidate replacement material due to its attractive mechanical properties and biodegradability/biocompatibility.

Nowadays, apart from its widespread applications in food packaging industry, use of PLA is becoming common in the fields of “agricultural mulch” films, “biomedical devices” such as sutures, stents, drug carrier, orthopedic devices, scaffolds and “automotive parts” such as pillar cover, door trim and front panel. In all these applications, investigation of the performance of PLA against UV irradiation become

crucial. Because, agricultural mulch films and outer automotive components are exposed to UV irradiation of sunlight; while UV irradiation itself is used extensively for the periodic sterilization of many medical devices because of its simplicity, effectiveness and low cost of operation [22,23,65,66].

The energy of UV light between 200 nm (598 kJ/mole) and 400 nm (299 kJ/mole) are higher than the bond energies of C-O (358 kJ/mole), C-C (347 kJ/mole) and C-H (414 kJ/mole) in the molecular chain structure of PLA. It is known that, UV absorption taking place especially by the low energy C-O bond in the ester linkage of the PLA structure leads to bond breakage, i.e. "chain scission", via Norrish I type photodegradation reaction [20,21,23]. It is also known that photons could be absorbed by the C=O (745 kJ/mole) bond in the carbonyl group of the PLA ester backbone leads to excitations resulting in Norrish II type photodegradation reactions again causes significant chain scission [21–23,25,26]. Many researches [21,22,25,26,38,67–70] revealed that this type of chain cleavage of course results in significant decreases in the molecular weight of the PLA, consequently deteriorated mechanical properties.

In the polymer industry, in order to decrease deteriorative influences of UV irradiation, there are many commercial organic UV absorbers containing certain absorption bands in different wavelength regions below 400 nm. Examples of the commercially available organic UV absorbers are; benzotriazole, benzimidazole, benzophenone, triazine, oxanilide, salicylate and cinnamate types [71,72]. In this group, "benzotriazole-type" organic UV absorbers are known as one of the most effective one. In the literature, although there are certain number of studies revealing the effectiveness of this type of UV absorber for many polymeric materials including aromatic and aliphatic polyesters [73–75], no work has been reported for the neat PLA structure. Therefore, one of the purpose of the second part of this thesis will be to indicate influence of benzotriazole based organic UV absorber on the performance of PLA.

In terms of organic UV absorbers, n-type semiconductors are consideration, especially rutile phase titania (TiO_2) particles due to its nontoxicity and chemical stability under

UV irradiation [76]. Rutile TiO_2 having energy band gap of 3.0 eV is capable of absorbing UV light at wavelengths less than 410 nm. Li *et al.* [77], Man *et al.* [78], and Xiu *et al.* [79] indicated that use of both micron sized (~200 nm) and nano sized (<100 nm) titania, if uniformly distributed, increase the resistance of the PLA structure against UV irradiation with very high rate of electron-hole recombination mechanism. These improvements were obtained for both sheet specimens and thick specimens.

Anatase crystal structure of TiO_2 having an energy band gap of 3.2 eV is also capable of absorbing UV light wavelength less than 384 nm. However, for this TiO_2 there is another possibility, i.e. having "photocatalytic" effect. Because, in the anatase structure under UV irradiation, electron hole pairs not only recombine but they may also travel to the particle surface forming certain radicals such as O^{2-}, HOO•, OH• with H_2O and O_2 present in the environment. As particles become smaller especially <10 nm due to the quantum size effect, the possibility of recombination decreases and TiO_2 particles act as effective photocatalyst. Although photocatalytic effects have certain usefulness in other sectors, it would accelerate the photodegradation reactions in the polymer structures. Li *et al.* [77], Buzarovska *et al*. [80], Nakayama *et al.* [81], Zhuang *et al.* [63] revealed that use of ≤21 nm sized anatase TiO_2 particles resulted in significant reductions in the molecular weight of the PLA with lowered mechanical properties. This detrimental photocatalytic effect was especially important in the film specimens [63,80,81], but in thick specimens [78,79]., since surfaces of the particles were covered with the matrix material, the possibility of the contact of the anatase particles with oxygen or water prevented, leading to no photocatalytic action.

It is known that use of only one type of UV absorber could not prevent the photodegradation reactions taking place in the polymer structures fully. One way to improve resistance against photodegradation is use of mixtures of different UV absorbers. In the literature there are studies investigating the influences of using mixtures of two or more different organic UV absorbers/stabilizers [71,73,82–85], or using mixtures of organic and inorganic UV absorbers [86–92]. In this respect, there are limited number of studies using TiO_2 particles together with an organic UV absorber especially for polymeric coatings [89–92].

1.6 Aim of the Thesis

Literature survey for the PLA matrix, some of them summarized in Section 3.5.1, revealed that there is no published study on the effects of both micron and nano sized titania particles. Therefore, the main aim of the first part of this thesis was to compare influences of various contents of the micro (200 nm) and nano (50 nm) titania particles on especially the mechanical and thermal properties of PLA. To the best of our knowledge, all the published work on the interfacial improvement between the PLA matrix and TiO_2 particles were related to using different "surface modification" techniques of TiO_2 particles, but use of "copolymer compatibilization" approach was not reported. Therefore, the secondary purpose of the first part of this thesis, as the first time, was to investigate influences of using "maleic anhydride" copolymer compatibilization on the performance of one of the nanocomposite composition.

Literature survey in Section 3.5.2 indicated that, to the best of our knowledge, no investigation was reported using benzotriazole type organic UV absorber together with TiO_2 particles for the PLA matrix. Therefore, the purpose of the second part of this thesis was, as the first time, to investigate performance of 2 mm thick PLA specimens against UV irradiation, first when only using benzotriazole based UV absorber, micro and nano titania particles used alone, and then to reveal possible synergism when they are used together.

CHAPTER 2

EXPERIMENTAL WORK

2.1 Materials Used

Polylactide (PLA) matrix material used in this thesis, was commercial L-lactic acid type polylactide with an extrusion grade (NaturePlast, PLE 001). According to technical data sheet of this PLA, it melts between 145-155°C and degrades in the range of 240°-250°C; its melt flow index range is 2-8 g/10 min at 190°C under 2.16 kg, as well as a density of 1.25 g/cm^3. Moreover, weight average molecular weight of this PLA was determined using Gel Permeation Chromatography as 105 800 g/mol.

In this thesis, as the reinforcement material, effects of two different size ranges of titania were compared. The first one, named as “micro-titania” was a commercial one (Sachtleben R 210, Germany) used in polymer masterbatch industry with 94% purity. Average particle size, d (50), of these TiO_2 particles determined by the particle size analyzer (Malvern Mastersizer 2000) was 200 nm, as shown in Figure 2.1. The second one, named as “nano-titania” was laboratory grade nanopowders supplied from US Research Nanomaterials (USA) having a purity of 99.9%. SEM analysis (FEI Nova Nano 430) revealed that the average size range of these nanoparticles were around 50 nm, which can be observed in Figure 2.2. It was also determined by XRD diffractograms (Bruker D8 Advance A25) that both micron and nano sized TiO_2 particles were composed of 100% rutile phase. Because, as given in Figure 2.3, all those well-known diffraction angles of the rutile phase were matched with the labelled peak positions.

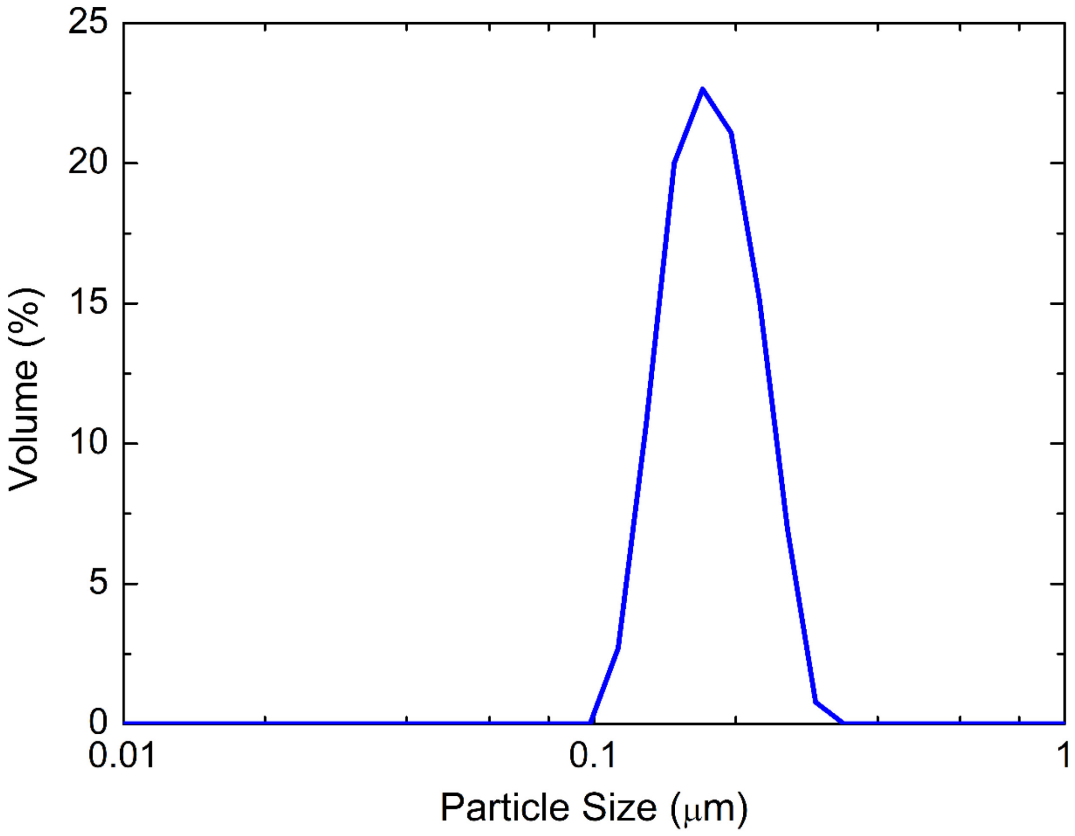

Figure 2.1 Particle size distribution of micron sized titania (m-TiO_2) particles

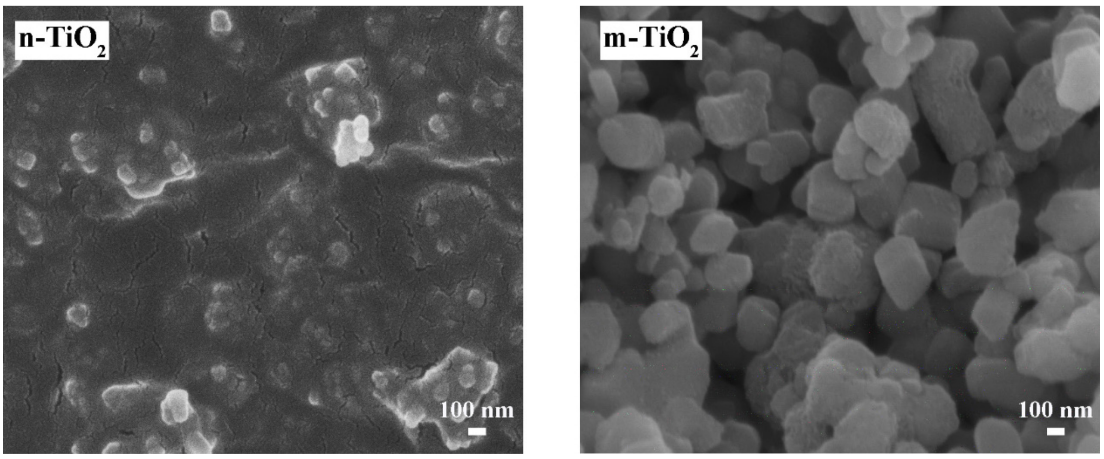

Figure 2.2 SEM images of nano (n-TiO_2) and micron (m-TiO_2) sized titania particles

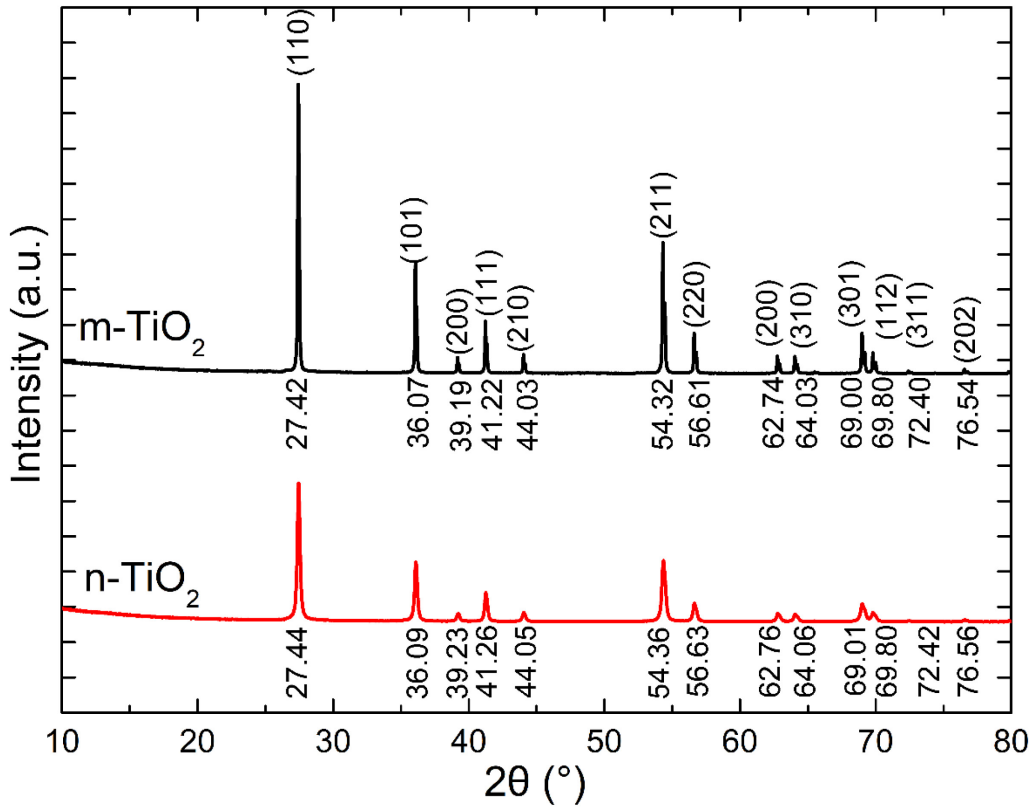

Figure 2.3 X-ray diffractograms of micron (m-TiO_2) and nano (n-TiO_2) sized titania particles indicating the well-known diffraction angles of the rutile phase (JCPDS card number 01-072-1148)

Maleic anhydride (MA) whose chemical structure is shown in Figure 2.4 was used during copolymer compatibilization studies in the first part of this thesis. It was purchased from Sigma-Aldrich with 99% purity and 98 g/mol molecular weight. Its melting temperature was in the range of 51-56ºC with boiling temperature of 200ºC. Dicumyl peroxide (DCP) used as the initiator for the reaction of MA grafting was also supplied from Sigma-Aldrich with a purity of 99% and a melting temperature of 39ºC.

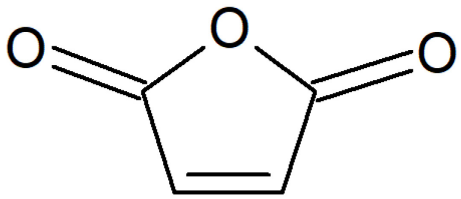

Figure 2.4 Chemical structure of maleic anhydride

The commercial organic UV absorber (SONGSORB® 2340, Songwon Ind. Co. Ltd., South Korea) used in the second part of the thesis has the chemical formula of 2-[2-Hydroxy-3,5-di(1,1-dimethylbenzyl) phenyl]-2H-benzotriazole, as schematically shown in Figure 2.5. It was supplied in powder form with a minimum purity of 99% and a molecular weight of 448 g/mol. Its melting temperature is in the range of 137-141 ºC with strong UV irradiation absorbing capability in the 300-400 nm region.

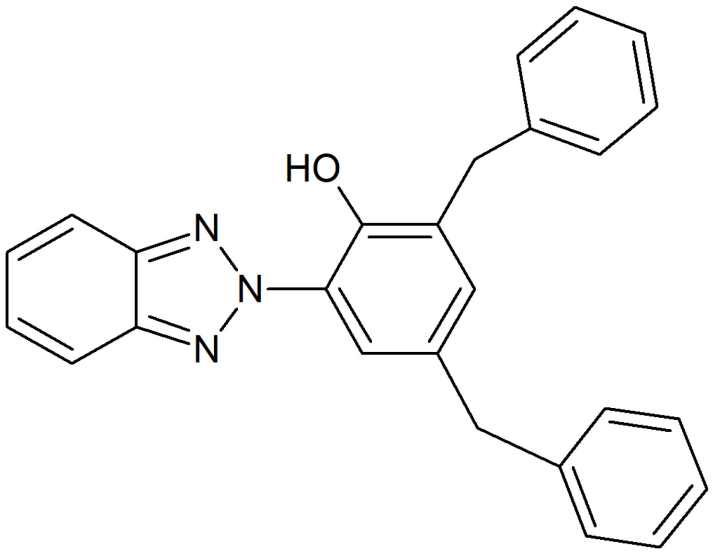

Figure 2.5 Chemical structure of the benzotriazole type organic UV absorber

2.2 Production of the PLA/Titania Micro and Nanocomposites

In the first part of this thesis, composite specimens of PLA reinforced with micron and nano sized TiO_2 were all compounded via melt mixing and compression molding techniques using laboratory size equipment. Before melt mixing, PLA powders and TiO_2 particles were dried in a vacuum oven at 60°C for 15 hours. Then, according to the composition, PLA and TiO_2 powders were pre-mixed manually just before feeding into side feeder of the extruder. These mixtures were then melt compounded via laboratory size twin-screw extruder (Rondol Microlab 300, D=10 and L/D=20). The temperature profile used for this production from feeder to die were 115°-170°-180°-175°-145°C, and the screw speed used was 75 rpm all through the compounding stage;

followed by air cooling and pelletizing of the continuous strands into 2-3 mm pellets using a four blade cutter.

Before specimen shaping, pellets were allowed to re-dry for another 15 hours at 60°C in a vacuum oven. Specimens required for testing and analyses were melt-shaped via laboratory scale compression molder (MSE Press Series, LP_M2SH05, Turkey) in accordance to the related standards. Maximum loading capacity and heating plate size of the compression molder were 50 kN and 20x20 cm, respectively. Temperature of the steel molds and the applied compressive load were kept at 160°C and 25 kN throughout the shaping processes, respectively. In order to prevent mold sticking, inner surfaces of the molds were first sprayed with a commercial mold release agent. Then, thin sheets of PTFE were also inserted in between the upper and lower surfaces of the molds and heating plates. During compression molding, before application of full pressure for 5 minutes, a period of 6 minutes without pressure was applied in order to homogeneously melt pellets of the compounds (placed in the molds). Finally, shaped specimens were carefully unmolded after sufficient time of cooling down to room temperature.

PLA/titania microcomposites were produced with loadings of 1, 2, 5, 10 and 15 wt. %; while the nanocomposites with 0.5, 1, 2 and 3 wt. % loadings. Micron and nano sized titania particles were designated as m-TiO_2 and n-TiO_2, respectively; therefore, the produced composites were designated using the format of "PLA/m-TiO_2 *x*%" or "PLA/n-TiO_2 *x*%", where *x* denotes wt. % of the particles used.

In order to investigate the effects of maleic anhydride copolymer compatibilization, PLA was grafted with MA and a copolymer, namely PLA-g-MA was formed using the reactive extrusion technique by twin-screw melt mixing of PLA together with 2 wt. % MA and 0.5 wt. % dicumyl peroxide (DCP) as a free radical initiator. Afterwards, the amount of grafted MA to PLA was found by titration method as 2.67 %. Details of these procedures are explained in our former study [93]. As it will be discussed in the following results and discussion section, since use of 2 wt. % n-TiO_2 revealed the optimum mechanical properties; PLA-g-MA approach was used only for this

nanocomposite. Hence, this nanocomposite specimen is designated as PLA/g-MA/n-TiO_2 2%. In this composition, the amount of PLA-g-MA copolymer used was also 2 wt. %.

In the second part of this thesis, during compounding and shaping of the specimens the same process parameters mentioned above were used. The only difference was the addition of the organic UV absorber in certain composition. In this part, in order to reveal the proposed synergism of the organic UV absorber (designated as UVA) with micron and nano sized titania, totally six different compositions were produced. Designations of these compositions were as follows: PLA, PLA/UVA, PLA/m-TiO_2, PLA/n-TiO_2, PLA/UVA/m-TiO_2 and PLA/UVA/n-TiO_2. In these compositions, the amount of each filler added were all 2 wt. %. Because, in the first part of the thesis, investigating the effects of the micron and nano sized titania contents on the mechanical performance of PLA, the optimum and common amount determined for each particle was 2 wt. %. For comparative purposes, the amount of the added UVA was also 2 wt. %. Therefore, since the added amounts were all the same, 2 wt. % contents were not indicated in the designations of the specimens

All the specimen compositions used in the first and second part of the thesis were tabulated in Table 2.1.

2.3 Structural and Morphological Characterization

In the first part of the thesis, Fourier transform-infrared (FTIR) spectroscopy was conducted to PLA, PLA/n-TiO_2 and PLA/g-MA/n-TiO_2 2% composites via Bruker ALPHA IR spectrometer in order to reveal certain interactions between PLA, MA and n-TiO_2. Signals of at least 32 scans were averaged by attenuated total reflectance (ATR) unit with 4 cm^{-1} resolution in the wavenumber range of 400 to 4000 cm^{-1}.

Table 2.1 Compositions (wt. %) of the specimen produced in the first and second part of the thesis

	Specimens	PLA	m-TiO_2	n-TiO_2	g-MA	UVA
First Part of the Thesis	**PLA**	100	-	-	-	-
	PLA/m-TiO_2 1%	99	1	-	-	-
	PLA/m-TiO_2 2%	98	2	-	-	-
	PLA/m-TiO_2 5%	95	5	-	-	-
	PLA/m-TiO_2 10%	90	10	-	-	-
	PLA/m-TiO_2 15%	85	15	-	-	-
	PLA/n-TiO_2 0.5%	99.5	-	0.5	-	-
	PLA/n-TiO_2 1%	99	-	1	-	-
	PLA/n-TiO_2 2%	98	-	2	-	-
	PLA/n-TiO_2 3%	97	-	3	-	-
	PLA/g-MA/n-TiO_2 %2	96	-	2	2	-
Second Part of the Thesis	**PLA**	100	-	-	-	-
	PLA/UVA	98	-	-	-	2
	PLA/m-TiO_2	98	2	-	-	-
	PLA/n-TiO_2	98	-	2	-	-
	PLA/UVA/m-TiO_2	96	2	-	-	2
	PLA/UVA/n-TiO_2	96	-	2	-	2

In the first part of the thesis, morphological analysis was carried out using scanning electron microscope (SEM) (FEI Nova Nano 430) for the fracture toughness specimens whose fracture surfaces were sputtered with gold right after drawing a conductive path from silver paste. Secondary electron detector was used together with 5 kV accelerated voltage and 2 mm spot size in order to prevent the specimen surface damage. Distribution of m-TiO_2 and n-TiO_2 particles in PLA matrix and the interface between them were analyzed.

2.4 Mechanical Tests and Thermal Analyses

In the first part of the thesis, in terms of mechanical testing, both three point bending flexural tests and tensile tests were applied to the specimens to measure their strength and modulus values under two different loading types. These tests were carried out via 5 kN Instron 5565A universal testing system according to ISO 178 and ISO 527-2 standards, respectively. Besides tension and flexural tests; fracture toughness tests were also carried out to determine K_{IC} and G_{IC} values of the specimens. Single-edge-notched-bending specimens were notched and pre-cracked with Ceast Notchvis system as defined in the standard ISO 13586, again using the Instron 5565A system. All mechanical tests were conducted for 5 specimens of each micron and nanocomposite combinations and the properties were determined as the average values including their standard deviations.

In order to determine the transition temperatures, the enthalpies and thermal degradation temperatures of each specimen composition, differential scanning calorimetry (DSC) (SII X-DSC 700 Exstar) and thermogravimetric analyses (TGA) (SII TG/DTA 7300 Exstar) were conducted. The heating profile used for DSC was -80 to 220°C, whereas for TGA it was 30 to 550°C. For both analyses, the heating rate and the purging gas were 10°C/min and nitrogen gas flow, respectively.

2.5 UV Irradiation of the Specimens

In the second part of the thesis, degree of the photodegradation in each six specimen compositions under UV irradiation were measured using Q-LAB QUV/se model accelerated weathering test system without any moisture cycle. The specimens were exposed to UV light with fluorescent lamps (UVB-313, Q-Lab Corp., Cleveland, USA) providing irradiance in the range of 280-400 nm and having their peak emission at 310 nm. The light intensity was 0.50 W/m^2 (at 310 nm) and the distance between the UV lamps and the samples was 5 cm. During UV irradiation of the 2 mm thick flexural and fracture toughness test specimens mounted onto the plates of the testing

unit, the temperature was set to 50ºC. Effects of UV irradiation were investigated for the periods of 12 and 24 days. Therefore, specimen designations (PLA, PLA/UVA, PLA/m-TiO_2, PLA/n-TiO_2, PLA/UVA/m-TiO_2, PLA/UVA/n-TiO_2) were suffixed with 0d, 12d and 24d where 0d is used for the non-irradiated specimens.

2.6 Analyses for the Changes after UV Irradiation of Specimens

Degree of the photodegradation in each specimen compositions after UV irradiation period was evaluated by comparing results of the following tests and analyses performed.

2.6.1 Measurement of Weight Losses

In order to reveal the possible mass losses, weight of each specimen compositions were measured with a precision balance (Denver Instruments, SI-234) before (0d) and after (24d) UV irradiation. The % weight losses were calculated using the following simple relation:

$$\% W_{Loss} = \frac{W_{0d} - W_{24d}}{W_{0d}} \times 100$$

, where W_{0d} is the initial weight while W_{24d} is the weight of the specimen after UV irradiation. For each specimen composition, five weight measurements were made.

2.6.2 Analyses for Color Changes

For the possible color changes under UV irradiation, each specimen compositions were inspected both visually and quantitatively. Visual inspection was made by comparing the digital photographs of the exposed (24d) and non-exposed (0d) specimen surfaces.

The quantitative analyses for the color changes were conducted using the Diffused Reflectance Analysis (DRA) which determines the CIELAB color space parameters (L*, a*, b*) with the DRA unit of Agilent Cary 60 UV-Vis spectrophotometer. The measurements were performed in accordance with the CIE 1976 standards from the surfaces of five specimens for each composition, before (0d) and after (24d) UV irradiation.

2.6.3 Analysis for Molecular Weight Changes

To be able to evaluate possible changes in the molecular weight of the PLA matrix, gel permeation chromatography (GPC) analysis was conducted. The decrease in the weight average molecular weight (M_w) of the neat PLA specimens were measured in tetrahydrofuran at 35 ºC using a Malvern OMNISEC GPC system. The analysis was conducted with triple detection method by use of refractive index, viscometer and light scattering detectors together with two columns (T6000M). The solutions were prepared through 40 hours of magnetic stirring at concentrations above 2 mg/ml and filtered using a 0.2 μm pore-sized membrane.

2.6.4 Analyses for the Changes in the Chemical Structure, Fracture Surface Morphology, Mechanical and Thermal Properties

The changes in the chemical structure, fracture surface morphology, flexural strength and modulus, K_{IC} and G_{IC} fracture toughness, transition temperatures along with the thermal degradation temperatures of all specimen compositions before and after UV irradiation periods were evaluated by FTIR, SEM, mechanical tests and thermal analyses as explained in detail above in the Sections 2.3 and 2.4.

CHAPTER 3

RESULTS AND DISCUSSION

As stated before, since this dissertation has two different parts, their results are presented and discussed successively in the following two subsections.

3.1 Effects of Micro-Nano Titania Contents and Maleic Anhydride Compatibilization on the Mechanical Performance of PLA

3.1.1 Effects of Micron and Nano Sized TiO_2 Contents on their Distribution in PLA Matrix

SEM has been proven to be a powerful tool not only for studying the dispersion of micro and nanofillers embedded within a polymer matrix, but also for exploring fracture surface morphology of the specimens revealing certain information on their fracture behavior. Hence, fracture surfaces taken from the fracture toughness test specimens of each composition were investigated under SEM in order to observe effects of micro and nano filler content on their distribution and morphology in the PLA matrix. The fractographs of neat PLA and its micro and nanocomposites were given in two different magnification levels, i.e. (a) low [10000X] and (b) high [40000X], in Figures 3.1 and 3.2, respectively.

First of all, these figures indicate that fracture surfaces of the neat PLA at all magnifications were rather flat and smooth revealing its inherent high level of brittleness. When micro or nanoparticles were incorporated, both Figures 3.1 and 3.2

show that fracture surface morphology become very rough due to the certain level of shear banding and plastic deformation around the ligaments of particles in the matrix. Thus, as will be seen in the next section, fracture toughness of the all micro and nanocomposites were higher than that of the neat PLA.

It can be observed from the low magnification fractographs given in Figure 3.1 (a) that all loadings of the micron sized titania particles were distributed rather homogeneously in the PLA matrix. However, the higher magnification fractographs given in Figure 3.1 (b) revealed that there are slight differences especially in terms of particle agglomeration. For instance, at low micro filler contents (i.e. 1, 2, 5 wt. % m-TiO_2) almost no agglomeration was observed, while at higher micro filler contents (i.e. 10 and 15 wt. % m-TiO_2) there were certain level of particle coalescence leading to formation of micron sized agglomerates. Therefore, as will be discussed in the next section, there was a gradual increase in strength and toughness of the microcomposites when filler contents were 1, 2, 5 wt. % m-TiO_2, contrarily these properties started to decline with 10 and 15 wt. % m-TiO_2.

In the case of nanoparticles, Figure 3.2 shows that there was a similar situation. That is, under low magnification (Figure 3.2 (a)) almost all nanoparticle loadings seemed to be homogeneously distributed. However, under high magnification, Figure 3.2 (b) indicated that incorporation of 3 wt. % n-TiO_2 resulted in certain level of particle agglomeration. Hence, the highest mechanical properties in this group were obtained with the loading of 2 wt. % n-TiO_2.

It should be noted that micron size TiO_2 particles were started to form agglomerates beyond 5 wt. % loading, whereas for the TiO_2 nanoparticles this threshold content was beyond 2 wt. % loading. Agglomeration tendency of the nanoparticles at much lower loading amount should be due to their larger specific surface area and higher surface tension between the n-TiO_2 particles.

Apart from morphology and distribution of particles, another significant aspect influencing all mechanical properties of the composites is the interfacial adhesion

between the polymer matrix and particle surfaces. It is known that depending on the production and storage conditions, there might be certain number of hydroxyl groups on the surfaces of TiO_2 particles. Therefore, in addition to the certain polar attractions between the matrix and the particles, formation of certain level of hydrogen bonding between the hydroxyl groups present at the PLA chain ends and the hydroxyl groups on the surfaces of the TiO_2 particles can be also expected.

On the other hand, SEM fractographs taken especially at high magnifications given in Figures 3.1(b) and 3.2 (b) revealed that, there were certain level of debonding between the PLA matrix and titania particles, including certain number of particle pull-out holes left in the PLA matrix. Therefore, it can be said that the interfacial adhesion between the PLA matrix and TiO_2 particles used was not so strong. However, even these slightly bonded particles resulted in improvements in the mechanical properties of PLA.

In the first part of the thesis, in order to improve interfacial interaction between the PLA matrix and TiO_2 particles, maleic anhydride (MA) copolymer compatibilization was applied for the PLA/n-TiO_2 %2 composite specimen. Figure 3.2 showed that when only 2 wt. % PLA-g-MA copolymer was present, there were better distribution with lower level of particle agglomeration, all leading to further improvements in the mechanical properties, as will be discussed later in detail.

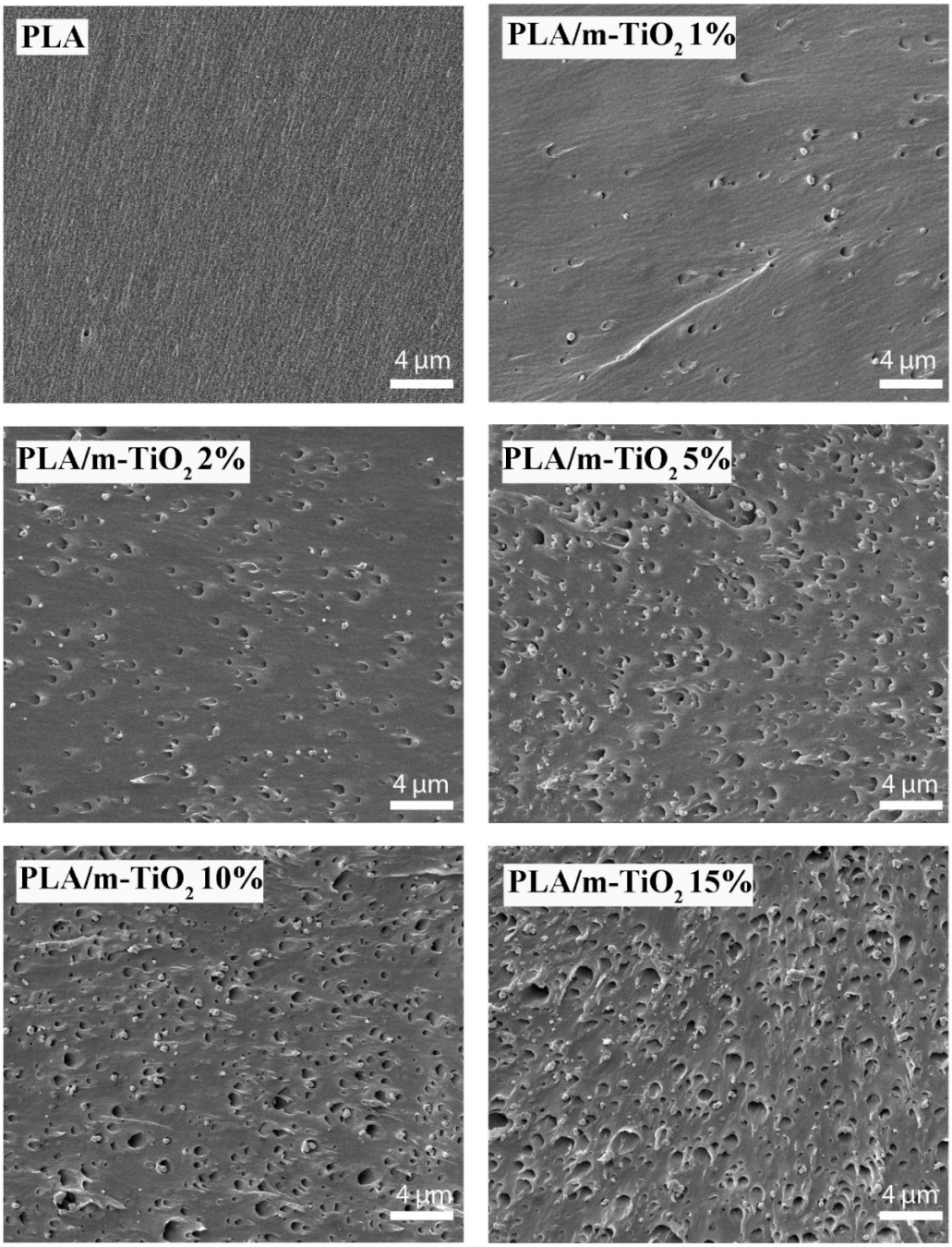

(a)

Figure 3.1 (a) Low and (**b)** high magnification SEM fractographs of neat PLA and PLA/m-TiO_2 microcomposites

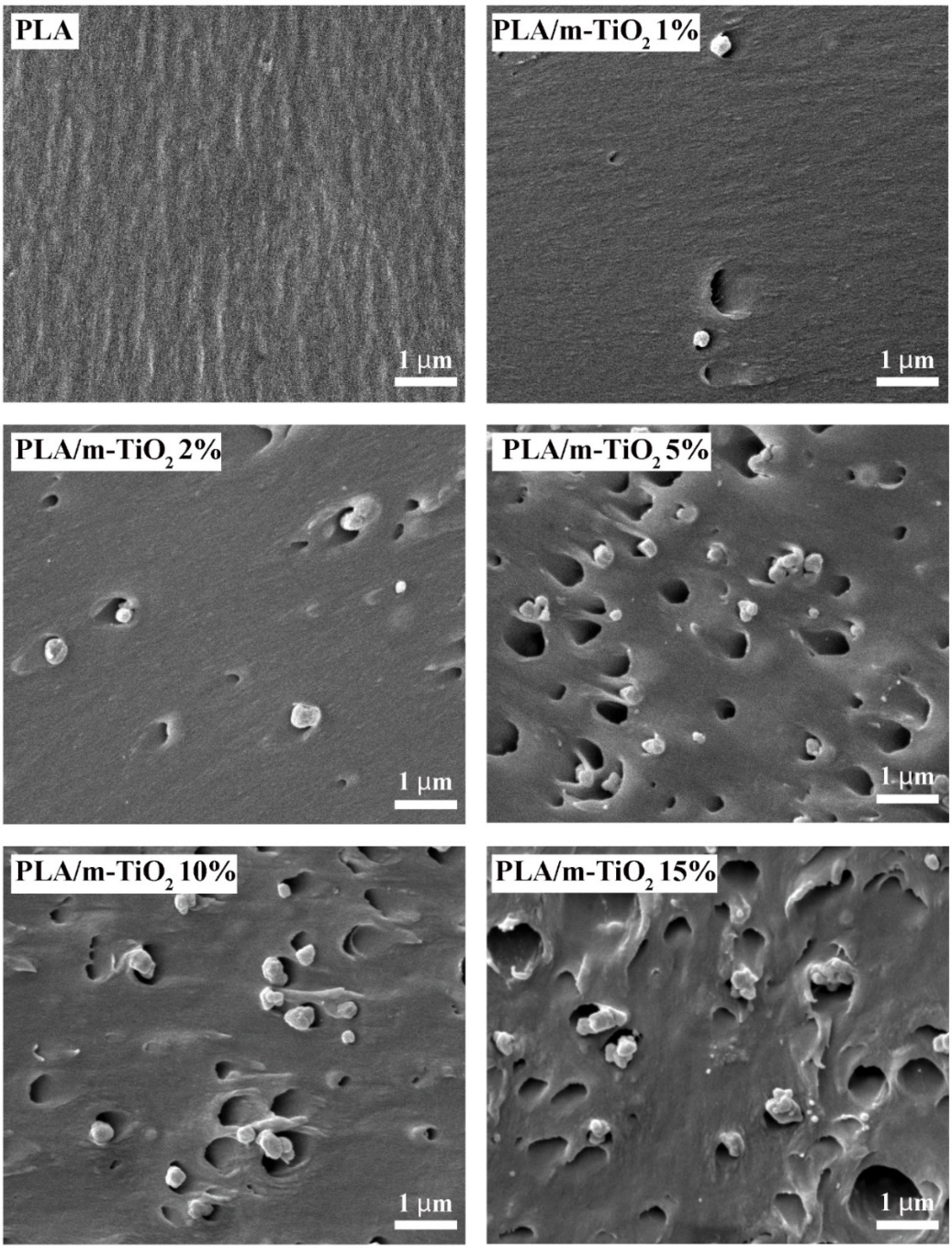

(b)

Figure 3.1 (continued)

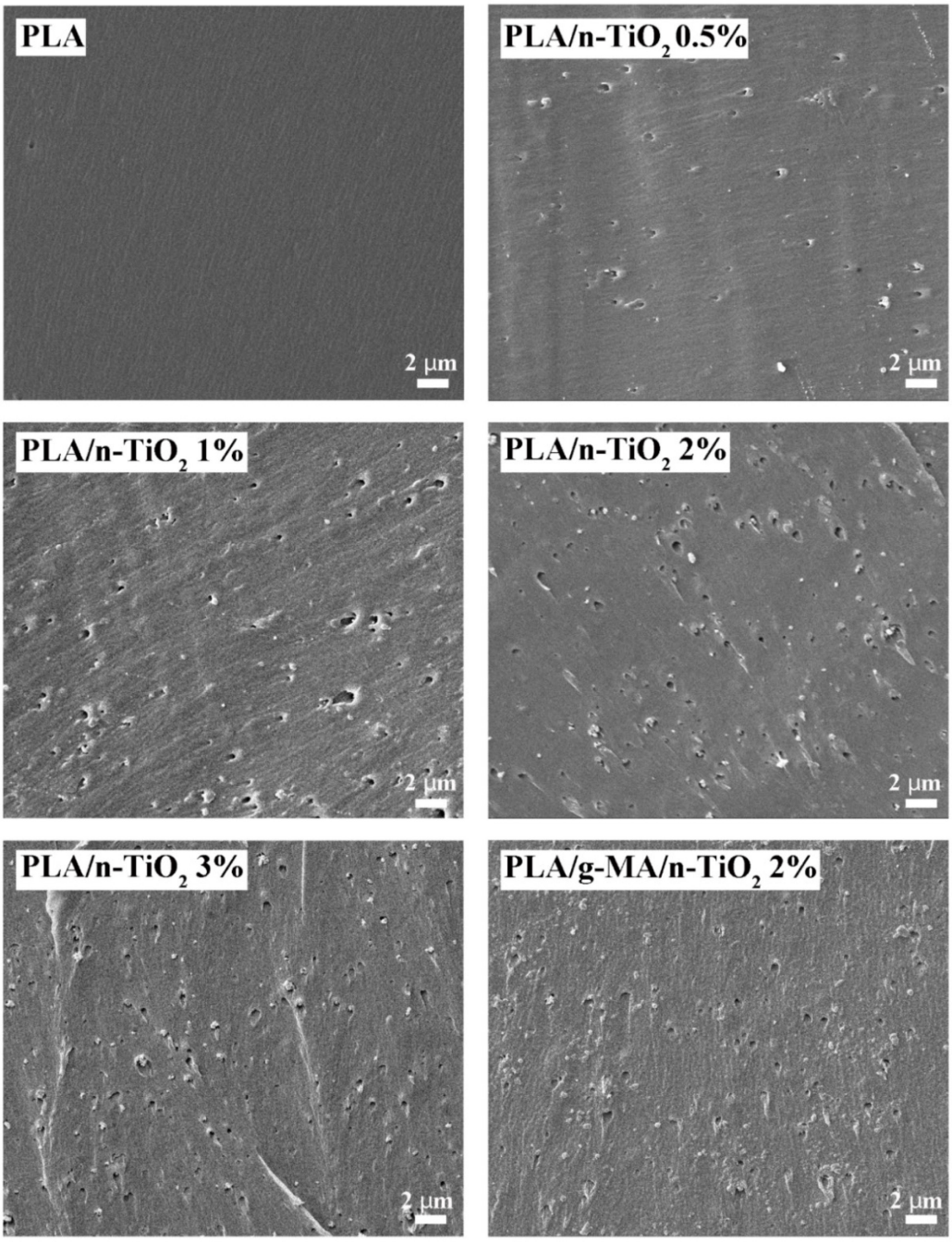

(a)

Figure 3.2 (a) Low and (**b)** high magnification SEM fractographs of neat PLA and PLA/n-TiO_2 nanocomposites

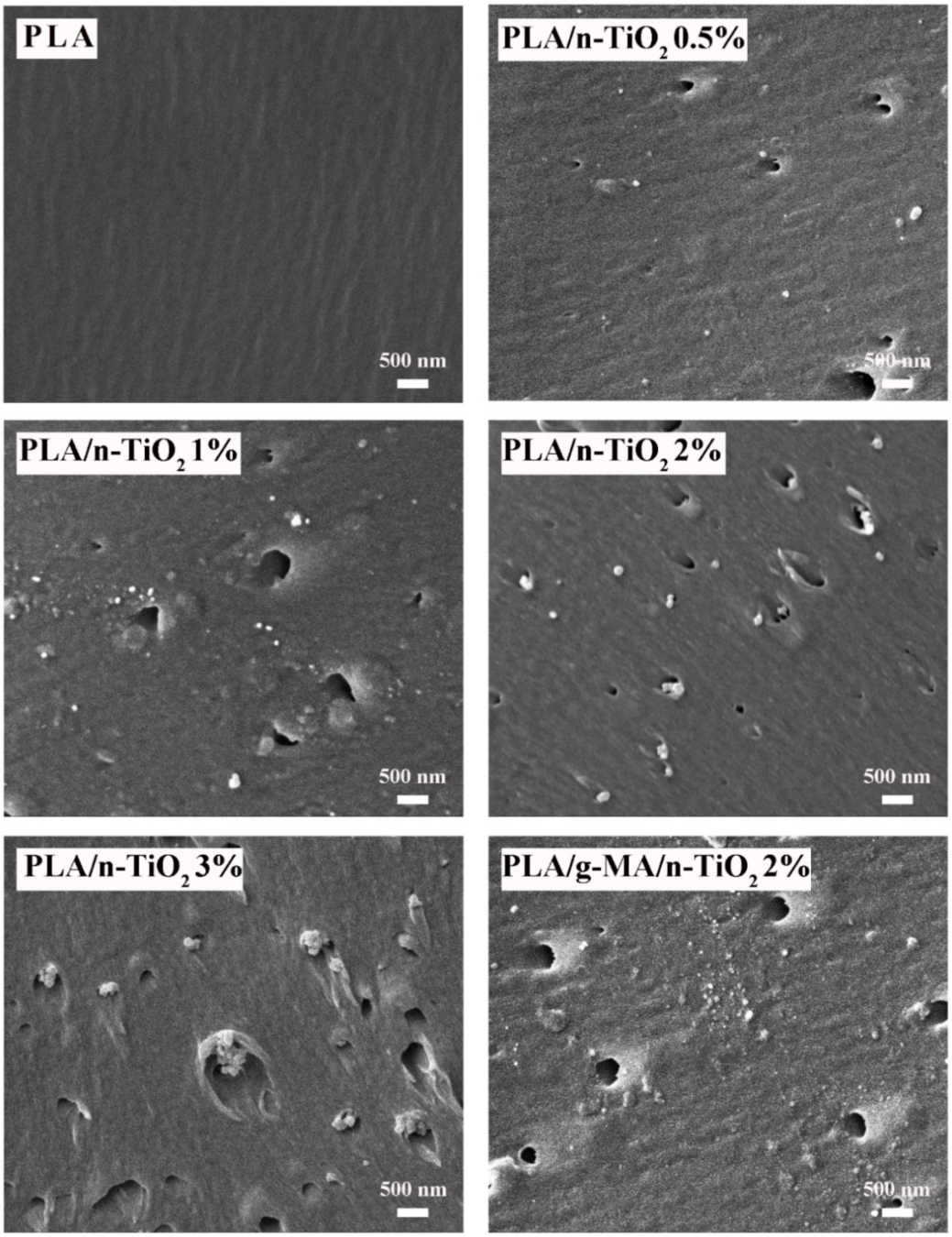

(b)

Figure 3.2 (continued)

3.1.2 Effects of Micron and Nano Sized TiO_2 Contents on the Mechanical Properties of PLA

Tension tests, three-point bending tests and fracture toughness tests were carried out to determine the mechanical properties of PLA, PLA/m-TiO_2 and PLA/n-TiO_2 composites. The values of "Tensile Strength (σ_{TS})", "Young's Modulus (E)" and "% strain at break" determined by tension tests; "Flexural Strength (σ_{Flex})" and "Flexural Modulus (E_{Flex})" values obtained from bending tests; and "Critical Stress Intensity Factor (K_{IC})" and "Critical Strain Energy Release Rate (G_{IC})" values calculated from the results of fracture toughness tests are all tabulated in Table 3.1. "Tensile stress-strain" curves and "flexural stress-strain" curves of specimens are given separately in Figures 3.3 and 3.4, respectively. Moreover, influences of increasing TiO_2 contents on the strength, elastic modulus and fracture toughness values of PLA/m-TiO_2 and PLA/n-TiO_2 composites were compared in Figures 3.5, 3.6 and 3.7, respectively.

Figures 3.5, 3.6 and Table 3.1 simply show that use of micron and nano sized TiO_2 particles at all contents improved strength and modulus values of the PLA matrix to a certain extent. It is known that the basic strengthening mechanisms of polymer matrix composites are the decreased mobility of the macromolecular chains of polymer matrix, and the applied load transfer from the polymer matrix to the reinforcement particle. The level of the effectiveness of these strengthening mechanisms especially depends on the degree of interfacial adhesion between the matrix and reinforcement surfaces. In this thesis, apart from the polar interactions, there is a certain tendency of the formation of hydrogen bonding due to the interactions between the hydroxyl groups present on the TiO_2 surfaces and the carboxyl and hydroxyl groups present at the chain ends of the PLA macro molecules.

Another important parameter on the level of composite strengthening mechanisms is the amount of the fillers incorporated into the matrix. Strength of the matrix polymer increases with increasing the filler content, of course only up to certain content, beyond which due to the agglomeration and consequent distribution problems, strength values start to decrease gradually. Therefore, it is seen in Figure 3.6 that, tensile and flexural

strength of the microcomposites increase up to 5 wt. % m-TiO_2; while for the nanocomposites, it was up to 2 wt. % n-TiO_2. At these optimum TiO_2 contents, the improvement in tensile and flexural strength in the microcomposite were 15% and 8%, respectively; whereas for the nanocomposite they were both 9%. Beyond these optimum contents, tensile and flexural strengths of the micro and nanocomposites started to decline, but still remained above the strength values of neat PLA matrix.

Improvement in the elastic modulus of the polymer matrices depends particularly on the stiffness and content of the reinforcing filler. Since TiO_2 particles are rather stiff inorganic materials, Figure 3.6 shows that increasing the content of the m-TiO_2 particles increases the Young's and flexural modulus of the PLA matrix. For instance, when 5 wt. % m-TiO_2 was used, the increases in E and E_{Flex} were 11% and 10%, respectively. Increasing the m-TiO_2 content to 15 wt. % resulted in further improvement as 15% in E and 19% in E_{Flex}. For the nanocomposite, improvements were up to a n-TiO_2 content of 2 wt. %. For this composition, E and E_{Flex} of the PLA matrix increased by 5% and 9%, respectively. In the nanocomposite with a n-TiO_2 content of 3 wt. %, due to the distribution problems, no improvement was observed.

It is known that the values of the "% tensile strain at break" can be interpreted as "ductility" of materials. Tensile stress-strain curves of all compositions, shown in Figure 3.3 exhibited yielding with short quasi-constant stress region followed by fracture without necking. Percent Tensile Strain at Break (%ε_f) values tabulated in Table 3.1 indicated that ductility of the PLA matrix decreased gradually with the increasing micron and nano sized titania particle contents. Similar results were also reported in the literature [60,64] after the addition of TiO_2 nanoparticles. It has been discussed that the ductility decrease in the nanocomposites were due to the increased number of the "pinning point" action of the nano fillers preventing the sliding of the PLA chains required for plastic deformation.

One of the most critical shortcoming of PLA is its inherent brittleness; therefore, its improvement is essential for most of the engineering applications. Consequently, in this thesis, fracture toughness tests (one of the most important parameter required for

structural designs) were conducted to investigate influences of micro and nano TiO_2 particle contents on the fracture toughness of PLA. Results of this test, measuring the ability of the materials to withstand crack initiation and propagation, were evaluated in terms of both "Critical Stress Intensity Factor (K_{IC})" and "Critical Strain Energy Release Rate (G_{IC})" values as tabulated in Table 3.1. Effects of micron and nano sized TiO_2 contents on the K_{IC} and G_{IC} values were evaluated in Figure 3.7.

It is known that fracture toughness of the brittle matrices can be improved by both delaying the crack initiation and decreasing the crack propagation rate. In the micro and nanocomposites, delay in the crack initiation mainly depends on the interfacial adhesion between the matrix and the fillers. In this thesis, it is believed that the level of the polar attractions and the hydrogen bonding mentioned before would not be sufficient to prevent crack initiation. On the other hand, some of the toughening mechanisms to decrease crack propagation rate known as "crack deflection", "crack bowing", "debonding", and "pull-out" would be operative in this thesis. For the mechanism of crack deflection and bowing, a certain level of interfacial adhesion formed by the polar attractions and the proposed hydrogen bonding would be sufficient. Oppositely, for the debonding and pull-out mechanisms to be effective, rather a weaker interfacial adhesion would be effective, which was evidenced from the SEM fractographs given in Figures 3.1 and 3.2.

Therefore, Table 3.1 and Figure 3.7 indicate that fracture toughness of the brittle PLA matrix was improved with the incorporation of m-TiO_2 particles up to 10 wt. %. For instance, for the 5 wt. % m-TiO_2 content, the improvement in K_{IC} and G_{IC} values were 12% and 38%, respectively. However, due to the highest level of uniform distribution, use of only 1 wt. % m-TiO_2 resulted in the highest improvement in this group, being 15% in K_{IC} and 42% in G_{IC}. In the nanocomposite group, use of all contents of n-TiO_2 resulted in improved fracture toughness values. In this group, due to the better distribution level and much higher surface area/volume ratio of the nanoparticles, use of 2 wt. % n-TiO_2 resulted in highest improvement, being as much as 18% in K_{IC} and 49% in G_{IC}.

Table 3.1 Tensile Strength (σ_{TS}), Flexural Strength (σ_{Flex}), Young's Modulus (E), Flexural Modulus (E_{Flex}), Tensile Strain at Break (ε_f), and Fracture Toughness (K_{IC} and G_{IC}) values of neat PLA, PLA/m-TiO_2 and PLA/n- TiO_2 composites

Specimens	σ_{TS}**(MPa)**	σ_{Flex}**(MPa)**	E**(GPa)**	E_{Flex} **GPa)**	ε_f**(%)**	K_{IC}**(MPa√m)**	G_{IC}**(kJ/m^2)**
PLA	56.0±0.6	94.8±0.5	2.71±0.02	3.16±0.04	5.11±0.06	3.75±0.04	6.28±0.07
PLA/m-TiO_2 1%	60.5±0.8	97.2±0.9	2.84±0.07	3.20±0.03	4.21±0.20	4.30±0.07	8.93±0.28
PLA/m-TiO_2 2%	61.7±0.8	99.7±0.3	2.89±0.04	3.38±0.07	4.19±0.14	4.23±0.08	8.72±0.19
PLA/m-TiO_2 5%	64.4±0.3	102.7±1.5	3.02±0.04	3.47±0.07	4.15±0.19	4.19±0.11	8.64±0.02
PLA/m-TiO_2 10%	62.9±1.1	100.7±1.4	3.08±0.01	3.66±0.07	4.15±0.25	3.97±0.02	6.47±0.17
PLA/m-TiO_2 15%	60.2±0.7	99.5±0.83	3.12±0.02	3.75±0.10	3.91±0.34	3.73±0.07	5.60±0.21
PLA/n-TiO_2 0.5%	56.3±0.7	97.0±0.7	2.75±0.03	3.17±0.07	4.53±0.13	3.90±0.15	7.35±0.21
PLA/n-TiO_2 1%	57.6±0.3	100.5±0.4	2.76±0.03	3.31±0.02	4.35±0.54	4.02±0.03	7.76±0.20
PLA/n-TiO_2 2%	61.1±0.4	103.5±1.0	2.85±0.03	3.44±0.04	3.98±0.30	4.43±0.06	9.35±0.27
PLA/n-TiO_2 3%	56.5±0.7	98.8±1.5	2.71±0.02	3.30±0.05	3.81±0.25	4.05±0.05	8.13±0.29
PLA/g-MA/n-TiO_2 2%	63.8±0.4	104.1±0.9	3.15±0.03	3.78±0.04	5.35±0.26	5.05±0.03	10.50±0.18

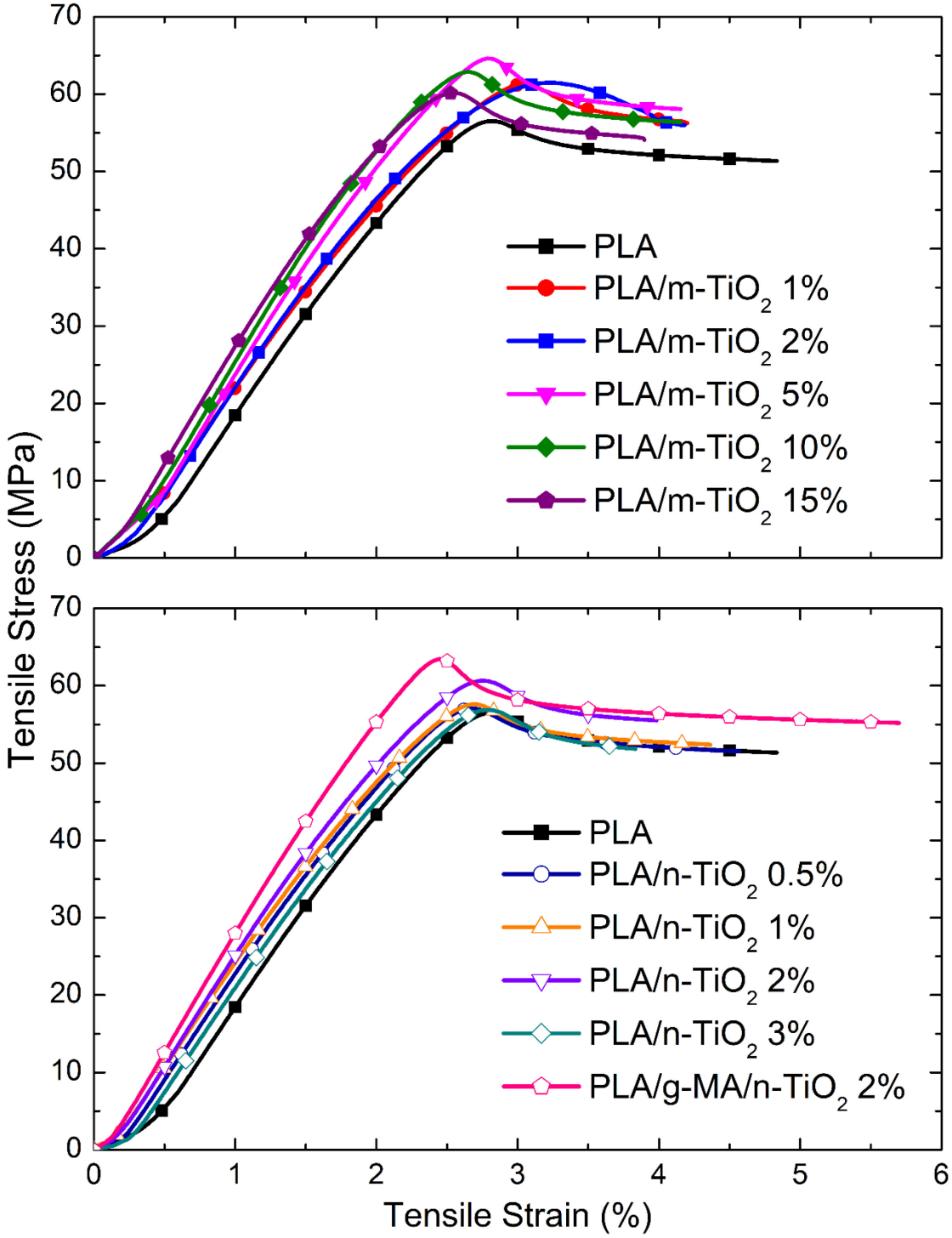

Figure 3.3 Stress-strain curves of the specimens obtained from tensile tests

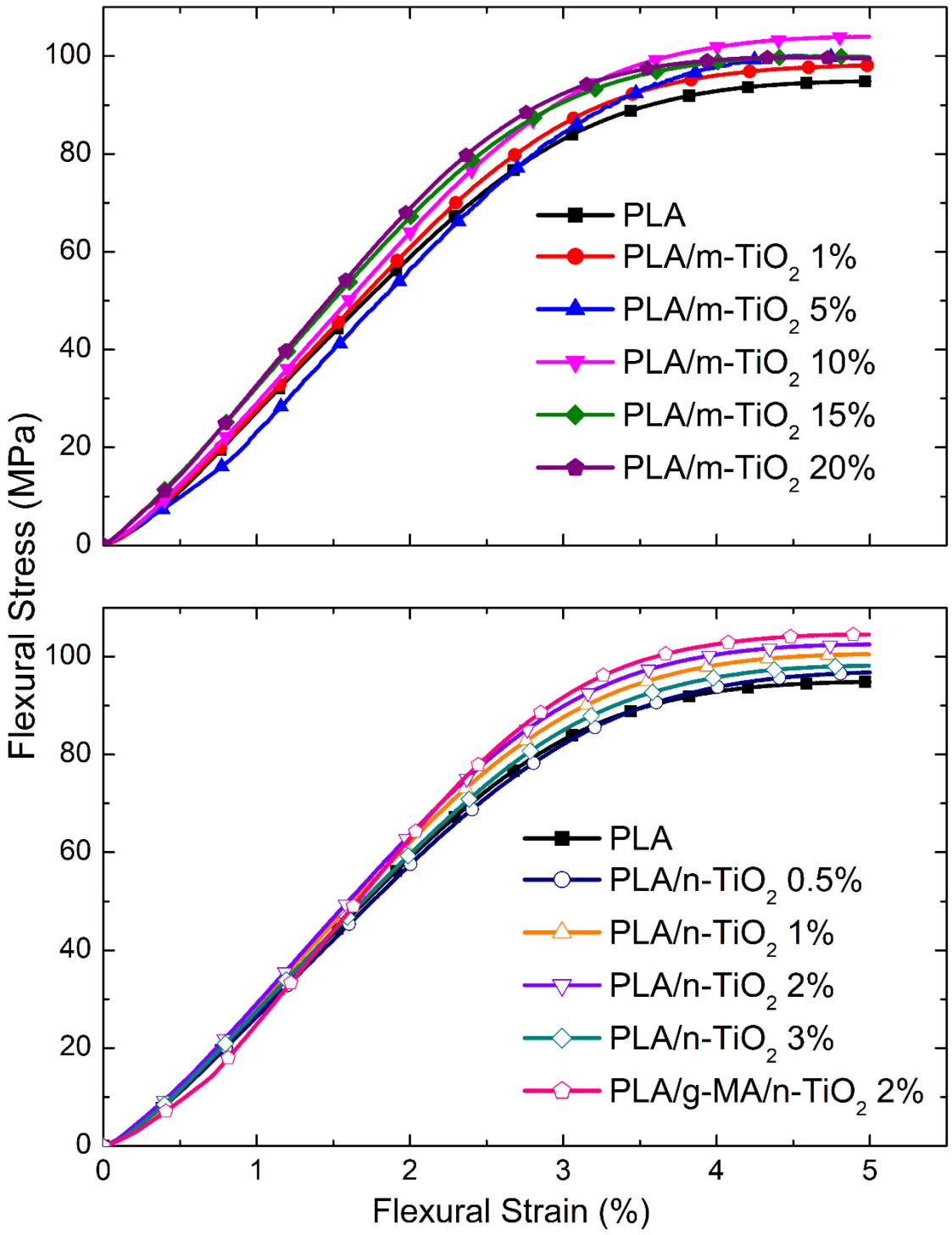

Figure 3.4 Stress-strain curves of the specimens obtained from 3-point bending flexural tests

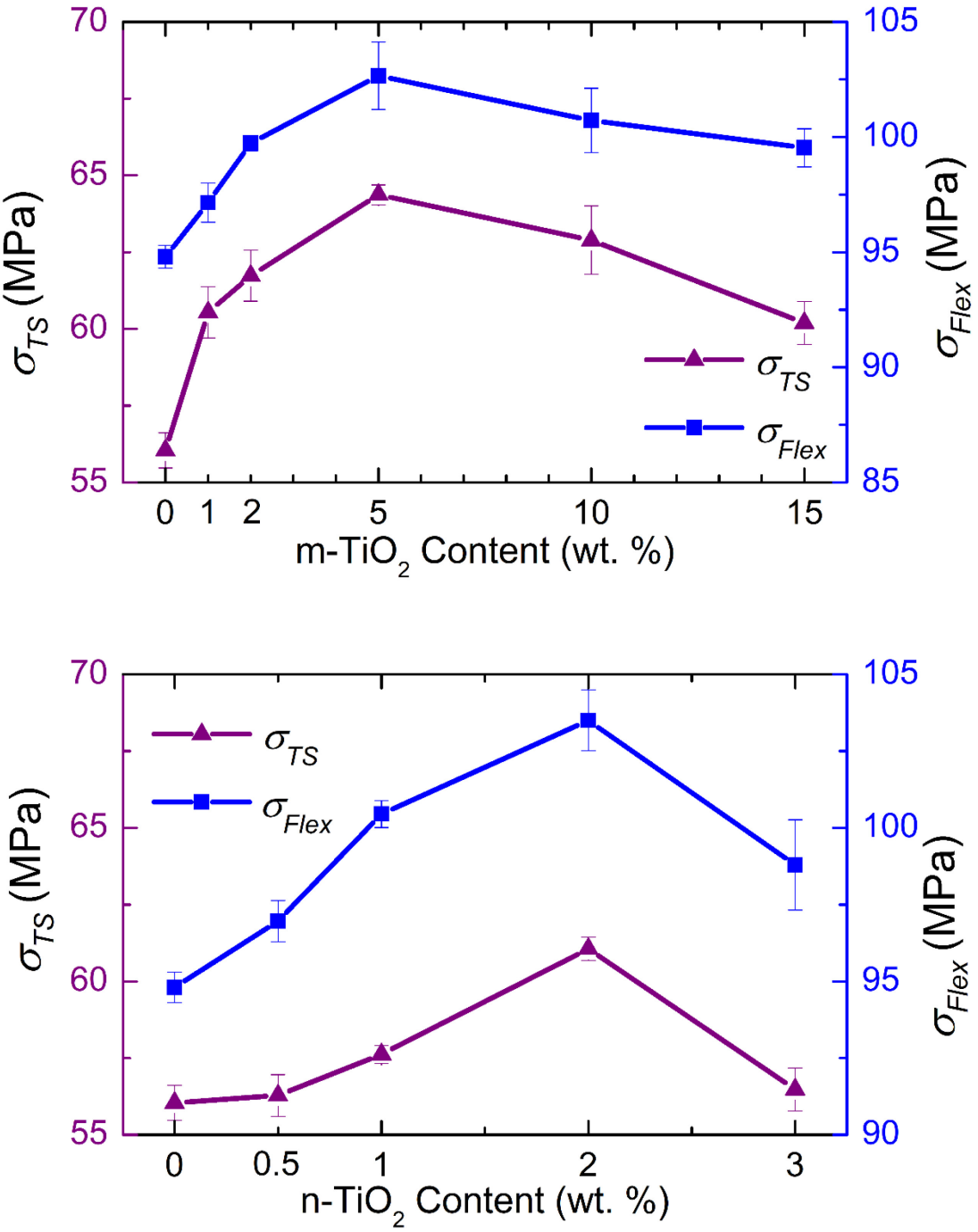

Figure 3.5 Effects of micron and nano sized TiO_2 contents on the tensile (σ_{TS}) and flexural (σ_{Flex}) strength of the composites (The lines are for visual aid only)

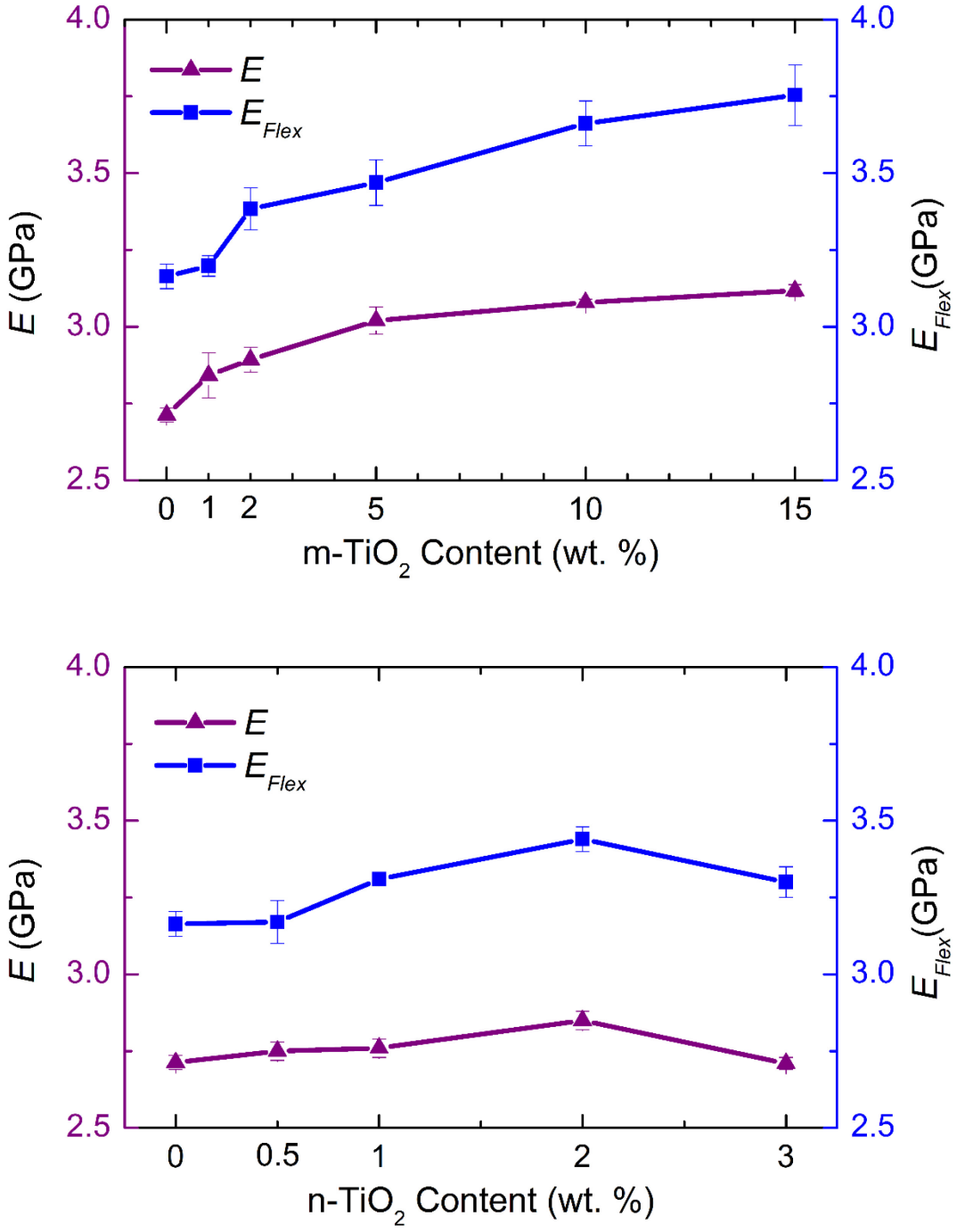

Figure 3.6 Effects of micron and nano sized TiO_2 contents on the Young's (E) and flexural (E_{Flex}) modulus of the composites (The lines are for visual aid only)

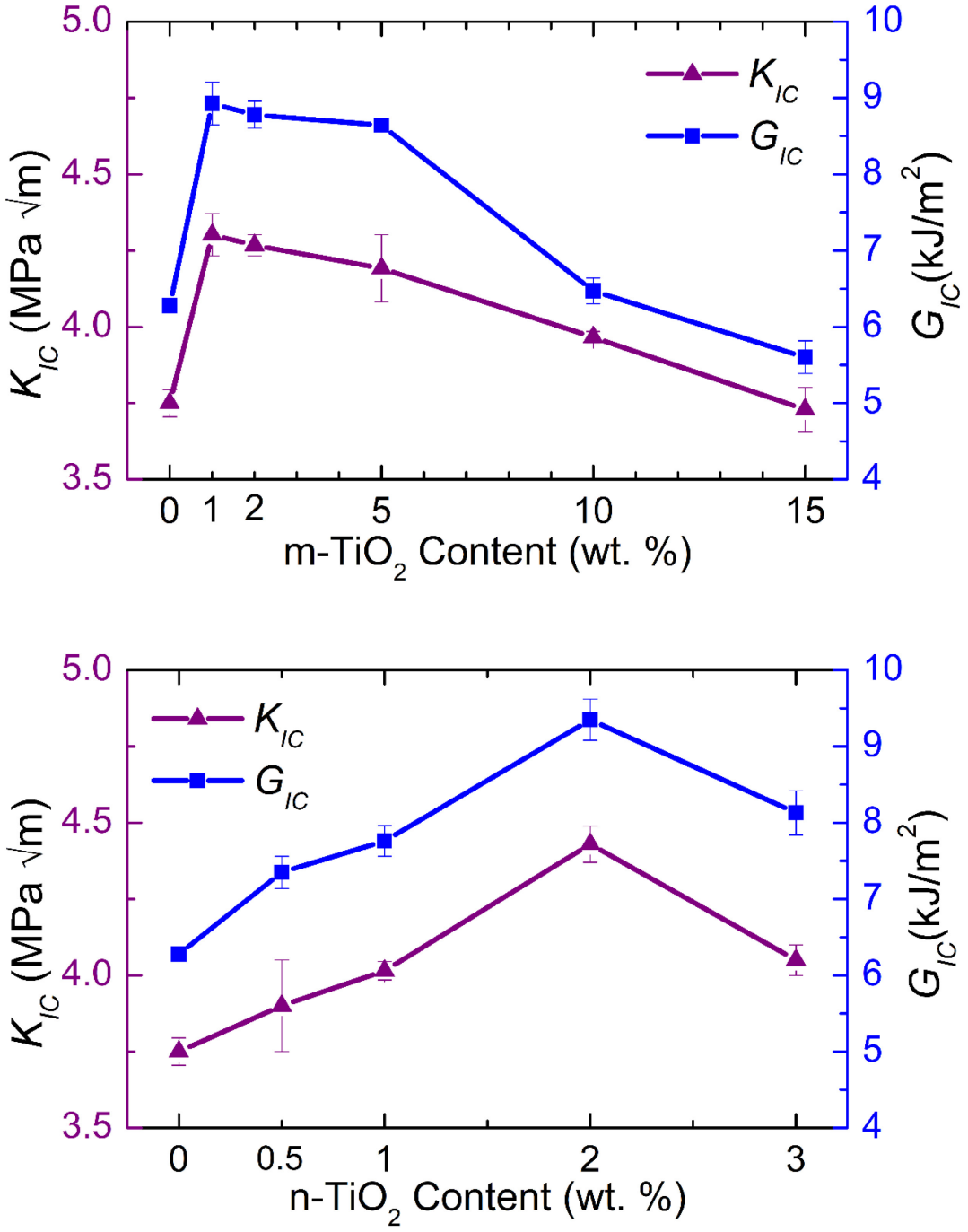

Figure 3.7 Effects of micron and nano sized TiO_2 contents on fracture toughness (K_{IC} and G_{IC}) of the composites (The lines are for visual aid only)

It can be summed up that apart from ductility; strength, elastic modulus and fracture toughness of the PLA can be improved by a certain extent either by using micron sized (200 nm) or nanosized (50 nm) TiO_2 particles. The main difference observed between them was the amount of the particles necessary for the highest improvement. That is, use of only 2 wt. % n-TiO_2 resulted in either similar or higher improvements compared to the use of 5wt. % m-TiO_2.

3.1.3 Effects of MA Copolymer Compatibilization on the Mechanical Performance of a PLA/TiO_2 Nanocomposite

In this part, in order to further investigate the effects of the improving interfacial interactions further between the PLA matrix and TiO_2 particles, maleic anhydride (MA) grafted PLA copolymer (PLA-g-MA) compatibilization was used only for one of the nanocomposite compositions having the highest mechanical performance, i.e. for PLA/n-TiO_2 2% specimen. Before comparing the mechanical properties of the neat PLA, PLA/n-TiO_2 2% and PLA/g-MA/TiO_2 2% specimens, ATR-FTIR analyses were conducted for these three compositions (as given in Figure 3.8) to reveal the possible interactions.

The first IR spectrum in Figure 3.8 belongs to neat PLA indicating the five main absorption bands of the PLA structure starting from low energy bands as: (i) C-H stretching vibrations of $R_3C–H$ stretching at 2995, 2944, 2925 and 2853 cm^{-1}; (ii) C=O stretching mode vibrations of the carbonyl group at 1746 cm^{-1}; (iii) CH_3 vibrations in two different modes as the antisymmetric CH_3 bending mode at 1452 cm^{-1} and $C–CH_3$ deformation mode at 1382 and 1360 cm^{-1}; (iv) C–O stretching vibrations in between 1300 – 1000 cm^{-1} in three different modes as (O=)C–O stretching of ester group at 1180 cm^{-1} and 1264 cm^{-1}, antisymmetric C–O–C stretching mode at 1079 cm^{-1} and 1127 cm^{-1}, and C–C–O stretching mode at 1041 cm^{-1}; and (v) C–C stretching mode at 955 and 867 cm^{-1}. All these characteristic IR bands observed in this thesis were very well matching with the ones reported in the literature [94].

The second IR spectrum in Figure 3.8 is for the PLA nanocomposite specimen with 2 wt. % n-TiO_2 particles. In this spectrum, only those bands different than the characteristic PLA bands were labelled. It was seen that the characteristic IR bands of the titania structure as established in the literature [34, 41], Ti–O and Ti–O–Ti stretching modes were observed in between 800–400 cm^{-1} as broad peaks with rather low intensity; due to both very low amount (2 wt. %) of titania present and also due to detection difficulty because of the overlapping skeletal vibrations of the C-C bands of PLA structure, which was also discussed elsewhere [96]. In this spectra, apart from Ti–O and Ti–O–Ti stretching vibrations, two tiny low intensity Ti-OH assignments were observed. The first one was in between 3800-3600 cm^{-1} indicating the characteristic tetrahedral and octahedral coordinated vacancies; designated as $_4Ti^{4+}$-OH and $_6Ti^{3+}$-OH. In the literature [96], these bands are discussed as non-hydrogen bonded hydroxyl groups left on the surface of TiO_2 particles after their production. The second tiny broad Ti-OH absorption band observed at around 1620 cm^{-1} was generally attributed to the absorbed water on the surface of TiO_2 nanoparticles in the form of hydroxyl groups [95].

In this study, as mentioned before, formation of certain level of hydrogen bonding was proposed between the hydroxyl groups on the TiO_2 surfaces and the carboxyl and hydroxyl groups at PLA chain ends. Therefore, one of the reason of the very low intensity of these Ti-OH bands seen in the spectrum can be due to the formation of mentioned hydrogen bonding. It is also known that after this type of interaction between the PLA matrices and inorganic particle surfaces, there might be certain shifts or decrease in the intensity of the characteristic IR bands of the PLA structure including its end groups. In this respect, in this study, there was a very slight shift at C=O stretching adsorption band from 1746 cm^{-1} to 1747 cm^{-1}. Moreover, intensities of all of the C-H stretching, C-CH_3 deformation and antisymmetric CH_3 bending vibrations of the PLA structure decreased with nanoparticle loading, together with a slight shift in two of the four peaks of C-H stretching vibrations from 2853 cm^{-1} and 2925 cm^{-1} to 2850 cm^{-1} and 2917 cm^{-1}, respectively.

The third spectrum given in Figure 3.8 was for the 2 wt. % n-TiO_2 nanocomposite specimen after the use of PLA-g-MA copolymer compatibilization. In the literature, typical IR assignments observed for MA structure are cyclic C=C stretching band at 1590 cm^{-1}, asymmetric and symmetric carbonyl C=O stretching at 1774 cm^{-1} and 1850 cm^{-1}, respectively. Of course, after the formation of PLA-g-MA copolymer structure, the C=C stretching band disappears. In the literature [97], it is discussed that the expected interaction between MA and TiO_2 is the adsorption of MA onto the TiO_2 surface by electronic donation, which occurs from one surface oxygen to one of the two C=O carbonyls of MA, followed by electronic donation from the s-bonded oxygen of MA to Ti^{4+}. Normally, this type of chemical interaction between the MA and TiO_2 surfaces can be revealed by the formation of Ti-O-C bands corresponding to 1160 cm^{-1} and 1096 cm^{-1}. It is also known that after that type of interaction, shifting and/or decrease in the intensity of the MA carbonyl C=O stretching vibrations (at 1774 cm^{-1} and 1850 cm^{-1}) could be observed. However, due to the overlapping of the broad and intense C–O stretching vibrations (around 1100-1200 cm^{-1}) and the antisymmetric C=O stretching (at 1746 cm^{-1}) of PLA matrix, it was not possible to distinguish them in Figure 3.8.

In order to observe the effects of the PLA-g-MA copolymer compatibilization on the mechanical performance of the PLA/n-TiO_2 2% nanocomposite specimen, all mechanical properties before and after compatibilization were compared with that of the neat PLA in Figure 3.9, which was constructed using the data tabulated in Table 3.1. Figure 3.9 shows that MA compatibilization resulted in further improvements in all mechanical properties of the PLA/n-TiO_2 2% composite specimen. For instance, compared to neat PLA, the improvement in the tensile strength (σ_{TS}) of the nanocomposite was 9%, but after MA compatibilization this improvement increased to 14%. For the flexural modulus (E_{Flex}), the improvement before and after compatibilization were 9% and 20%, respectively. Similarly, in terms of G_{IC} fracture toughness, the improvements before compatibilization was 49%, after MA compatibilization it was as much as 67%.

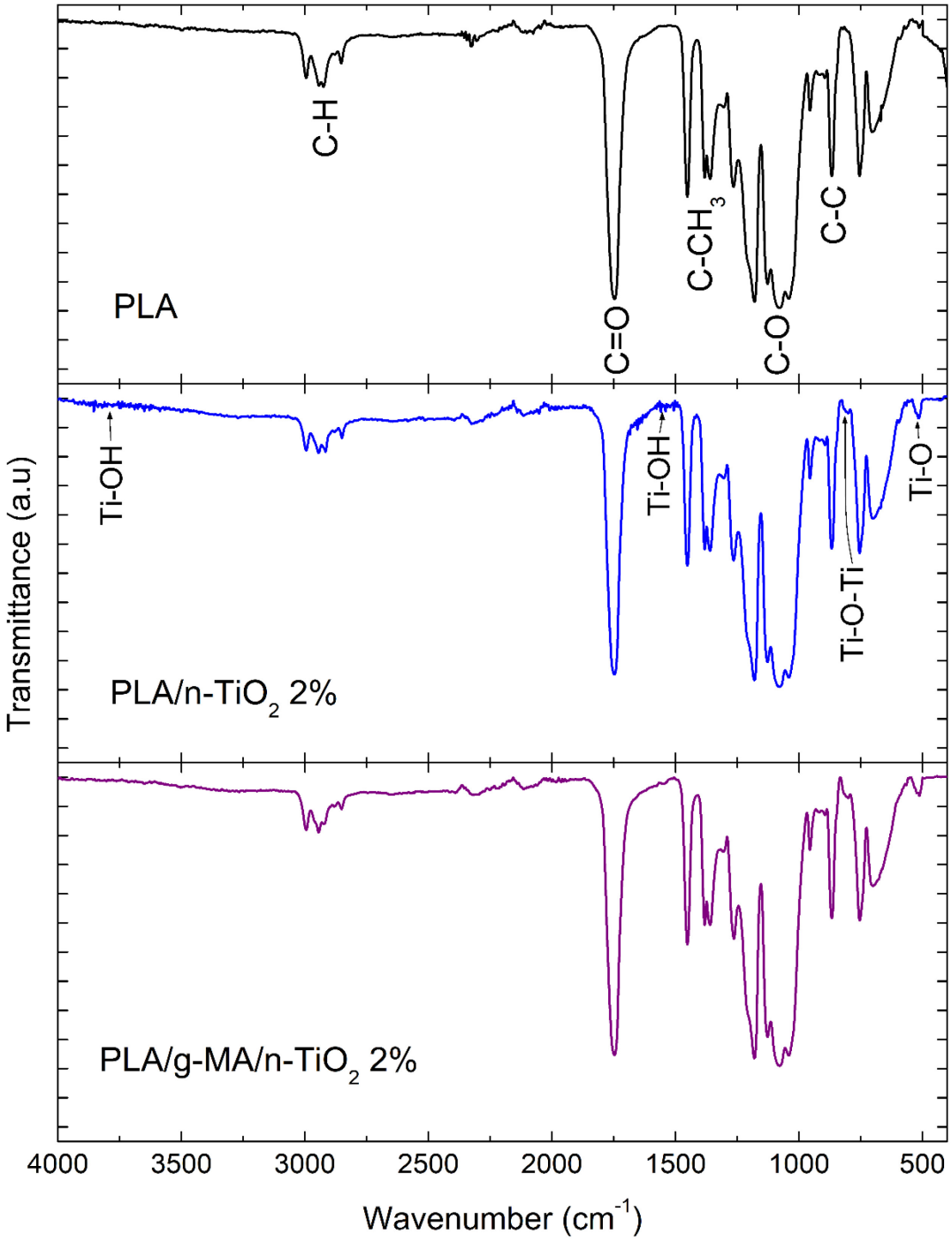

Figure 3.8 ATR-FTIR spectra of the neat PLA, PLA/n-TiO_2 2% nanocomposite specimen, before and after its PLA-g-MA copolymer compatibilization

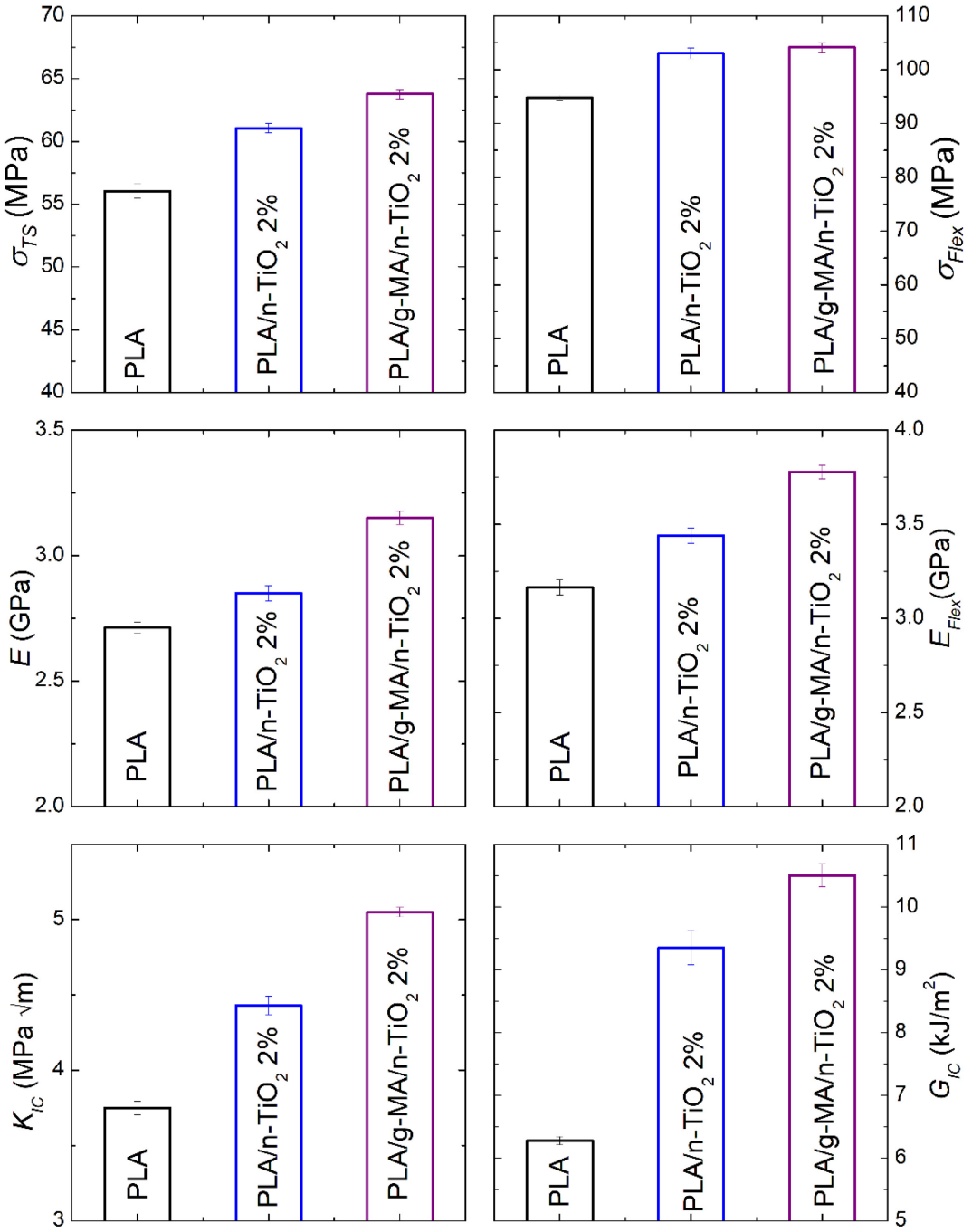

Figure 3.9 Mechanical performance comparison of the neat PLA with PLA/n-TiO_2 2 % nanocomposite specimen, before and after its PLA-g-MA copolymer compatibilization

The main reason of these further improvements was the further improvements achieved in the interfacial adhesion. As discussed in the FTIR analysis section above, the expected interaction between the PLA matrix and TiO_2 particles was only polar attractions and formation of the certain level of hydrogen bonding; while after MA compatibilization, certain level of covalent chemical bonding was also expected. Therefore, improvement in the interfacial adhesion increased effectiveness of the not only strengthening mechanisms (i.e. load transfer and chain mobility decrease) but also effectiveness of the certain toughening mechanisms (such as crack deflection and bowing).

3.1.4 Effects of Micron and Nano Sized TiO_2 Contents on the Thermal Behavior of PLA

Two different analysis were conducted to investigate the thermal behavior of all specimen groups. As the first one, differential scanning calorimetry (DSC) analysis was conducted in order to determine the important transition temperatures; i.e. glass transition (T_g), cold crystallization (T_c) and melting (T_m) temperatures, together with the enthalpy of melting (ΔH_m) and enthalpy of crystallization (ΔH_c) including percent crystallinity (X_c). The relation used in the calculation of percent crystallinity is given below;

$$X_c = \frac{\Delta H_m - \Delta H_c}{w_{PLA} \cdot \Delta H_m} \cdot 100$$

, where w_{PLA} is the weight fraction of the PLA matrix and ΔH_m^o is the melting enthalpy of 100% crystalline PLA given as 93 J/g in the literature [98]. DSC first heating thermograms of the specimens were given in Figure 3.10, while all the related data determined were tabulated in Table 3.2.

It is seen that incorporation of micron and nano sized titania had almost no influence on the T_g and T_m of the PLA matrix; however, there was certain reduction in its cold crystallization temperature (T_c). Depending on the TiO_2 contents, this reduction was from

125ºC (neat PLA) down to the range of 110-120ºC for the PLA matrices of the composites. This can be interpreted that cold crystallization in the PLA matrix of the composites started at lower temperatures possibly due to the TiO_2 particles acting as heterogeneous nucleation sites. Of course, these TiO_2 particles in the polymer melt can also reduce both the energy required to create a new surface and the nucleus size for crystal growth [58] promoting the crystallinity of PLA matrix. Therefore, Table 3.2 shows that the use of 10 wt. % m-TiO_2 increased crystallinity amount of PLA from 3.76% to 6.93%; that is an increase of almost 2 times. Moreover, due to their higher surface area/volume ratio, use of only 2 wt. % n-TiO_2 increased crystallinity amount to 10.86%; which was an increase of almost 3 times. Beyond these loading amounts, TiO_2 particles resulted in slight reduction in the crystallinity amount of the PLA matrix. One reason leading to the development of this trend might be the deterioration of homogenous distribution preventing the formation of new nucleation sites with increasing TiO_2 content. Another possible reason of decreasing crystallinity at higher TiO_2 compositions can be the hindrance of growing spherulitic crystals by other TiO_2 particles constraining the conformational mobility of PLA chains required for spherulitic growth. Similar results have been also reported in the literature for PLA/TiO_2 nanocomposites [35, 45].

Table 3.2 Transition Temperatures (T_g, T_c, T_m), Enthalpies (ΔH_m, ΔH_c) and Crystallinity Percent (X_C) values of neat PLA, PLA/m-TiO_2 and PLA/n- TiO_2 composites obtained from the first heating profile of DSC thermograms

Specimens	T_g (°C)	T_c (°C)	T_m (°C)	ΔH_m (J/g)	ΔH_c (J/g)	X_C (%)
PLA	60.1	124.6	150.2	17.2	13.7	3.76
PLA/m-TiO_2 1%	60.2	121.2	150.6	27.5	22.8	5.10
PLA/m-TiO_2 2%	60.1	118.5	149.8	27.3	22.3	5.49
PLA/m-TiO_2 5%	59.8	115.2	149.4	27.9	22.2	6.00
PLA/m-TiO_2 10%	59.7	109.8	148.9	21.8	16.0	6.93
PLA/m-TiO_2 15%	59.6	111.4	148.6	19.9	15.3	5.82
PLA/n-TiO_2 0.5%	59.5	121.5	150.2	18.3	12.1	6.70
PLA/n-TiO_2 1%	60.2	118.2	149.1	24.5	16.5	8.69
PLA/n-TiO_2 2%	59.7	117.9	149.2	28.1	13.2	10.86
PLA/n-TiO_2 3%	60.1	115.8	149.7	28.3	20.0	9.20
PLA/g-MA/n-TiO_2 2%	59.2	117.8	149.2	24.6	15.6	9.87

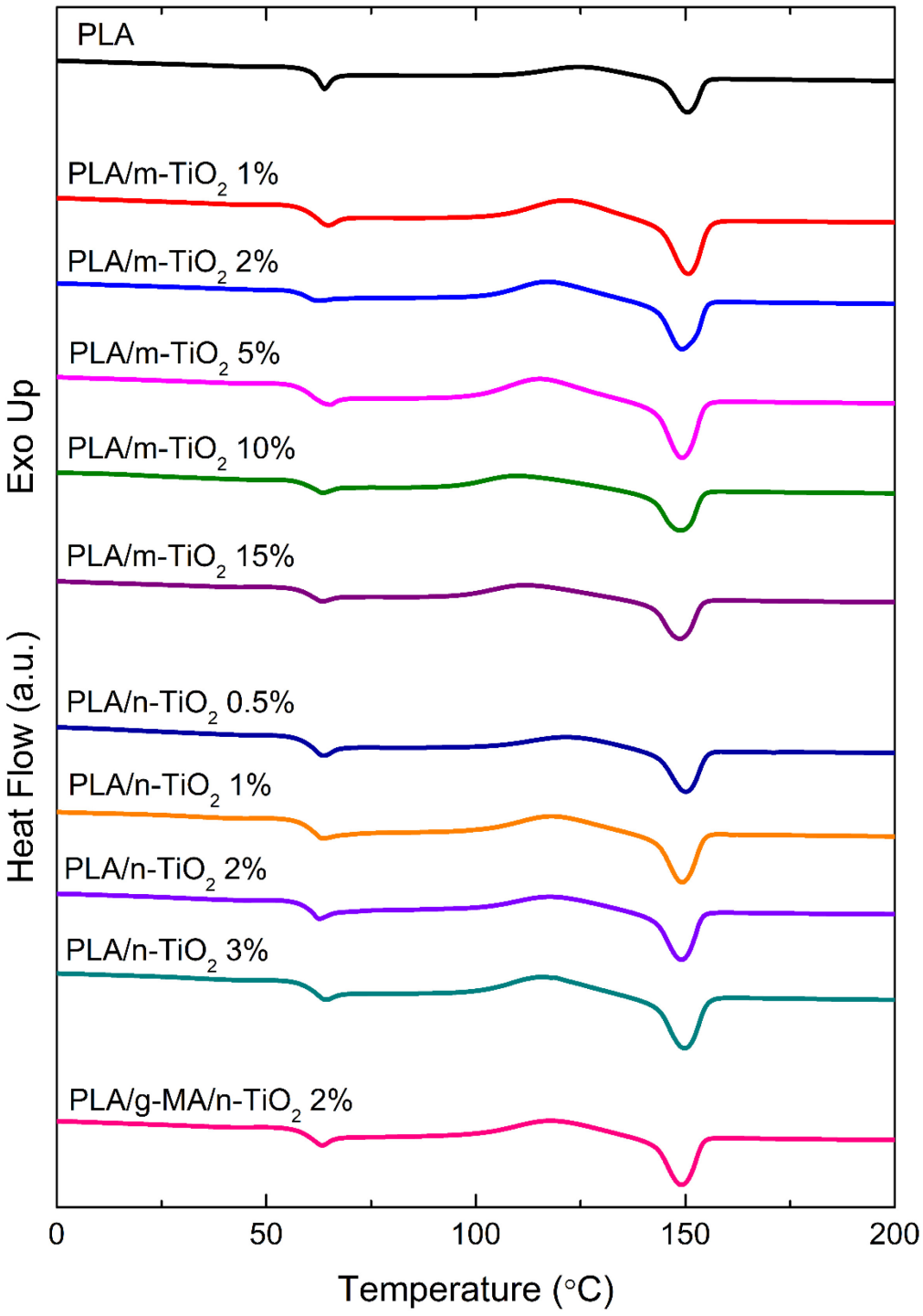

Figure 3.10 First heating DSC thermograms of neat PLA, PLA/m-TiO_2 and PLA/n-TiO_2 composites

PLA is a biodegradable aliphatic polyester, which is prone to degradation by various factors such as heat, moisture and UV radiation. Therefore, the second analysis conducted was thermogravimetric analyses (TGA) to determine the thermal degradation temperatures of each specimen. TG curves were given in Figure 3.11, while the data determined were tabulated in Table 3.3 as $T_{5\%}$, $T_{10\%}$ and $T_{25\%}$ representing the degradation temperatures at 5%, 10% and 25% mass losses; and T_{max} representing the temperature at maximum mass loss. In the table %residue of each specimen determined at 550ºC was also included.

Results provided in Table 3.3 simply indicated that the use of nano sized (50 nm) TiO_2 particles improved thermal degradation temperatures of the PLA matrix only by a few degrees. It is seen that the highest improvement for the nanocomposites was in the 5 wt. % mass loss temperature ($T_{5\%}$) i.e. an increase from 332 to 340ºC. This increase can be due to the heat barrier effect of TiO_2 particles at the early stages of thermal decomposition. Similar results for the slight improvements in the thermal decomposition temperatures of PLA/TiO_2 nanocomposites have been reported in the literature [59,63,64,100]; and these improvements have been attributed to the thermal stability of titania and its shielding effect against transportation of heat and volatile products formed during thermal decomposition.

On the other hand, for the micron sized (200 nm) TiO_2 particles, no improvement was observed; instead, there were certain degrees of reductions in the all thermal degradation temperatures. It is stated in the literature that the decomposition temperatures can be decreased due to the agglomeration and decreased homogeneity of the distribution of TiO_2 particles [96,100]. It is also mentioned by Li *et al.* [47] that availability of surface hydroxyl groups on the surfaces TiO_2 fillers can catalyze the thermal decomposition of PLA at elevated temperatures.

Table 3.3 Thermal degradation temperatures ($T_{5\%}$, $T_{10\%}$, $T_{25\%}$) at 5, 10 and 25 wt. % mass losses, the maximum mass loss temperature (T_{max}) and %Residue at 550ºC of neat PLA, PLA/m-TiO_2 and PLA/n-TiO_2 composites

Specimens	$T_{5\%}$ (ºC)	$T_{10\%}$ (ºC)	$T_{25\%}$ (ºC)	T_{max} (ºC)	%Residue at 550 ºC
PLA	332	342	353	362	0.16
PLA/m-TiO_2 1%	333	342	352	359	0.31
PLA/m-TiO_2 2%	333	340	344	355	2.29
PLA/m-TiO_2 5%	330	337	345	352	4.84
PLA/m-TiO_2 10%	326	334	343	350	12.49
PLA/m-TiO_2 15%	323	331	341	349	14.00
PLA/n-TiO_2 0.5%	337	345	355	363	1.01
PLA/n-TiO_2 1%	336	345	355	363	1.99
PLA/n-TiO_2 2%	339	346	355	364	2.35
PLA/n-TiO_2 3%	340	347	356	364	3.66
PLA/g-MA/n- TiO_2 2%	331	340	352	364	2.52

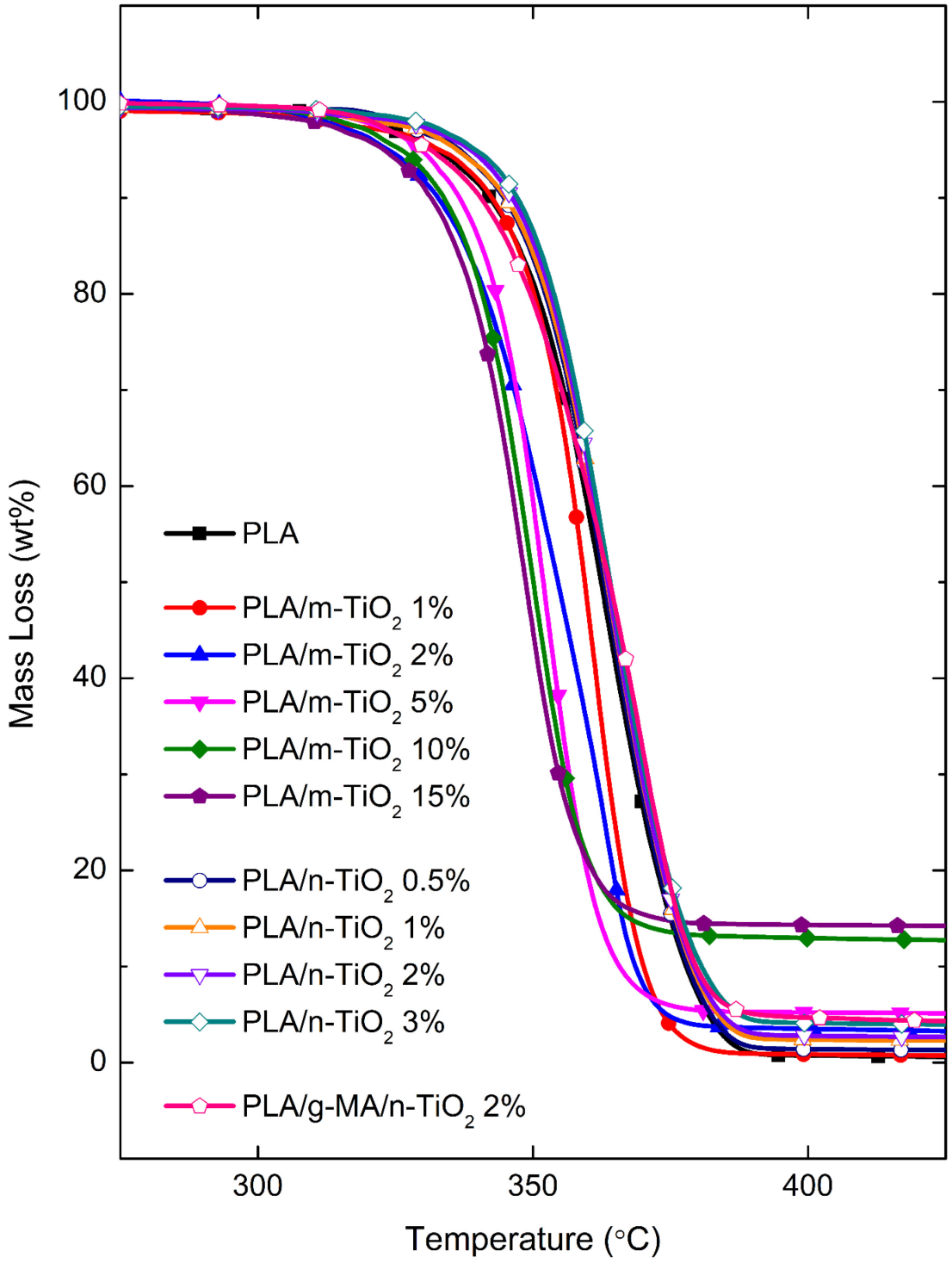

Figure 3.11 Thermogravimetric curves of neat PLA, PLA/m-TiO_2 and PLA/n-TiO_2 composites

3.2 Effects of Micro and Nano Titania on the UV Irradiation Resistance of PLA with and without an Organic UV Absorber

In the following sections, changes in the performance of UV irradiated neat PLA and its compounds containing micron or nano sized TiO_2 particles with and without organic UV absorber were evaluated in terms of % weight loss, changes in color and chemical structure, including the decreases in the mechanical and thermal properties.

3.2.1 Weight Loss after UV Irradiation

Degree of the weight loss in the mass of polymeric materials exposed to UV irradiation could be an indication of their stability or resistance against UV photodegradation. In the literature [63,77,80,81], it was reported that if the PLA based materials were especially in the form of thin sheets (e.g.100-200 μm), and if they are exposed to high energy irradiations (e.g. 50-100 W/m^2) for prolonged periods (e.g. 10-40 days), then percent weight loss can be as much as 15-40%.

In the second part of this thesis, before and after 24 days of UV irradiation, at least four fracture toughness test specimens of all compositions were weighted using a high precision balance. The average % weight loss values with standard deviations are tabulated in Table 3.4, while the weight loss trends are indicated in Figure 3.12.

Table 3.4 and Figure 3.12 show that, since the specimens used in this thesis were 2 mm thick bulk specimens, not thin sheets of micron thicknesses, %wt loss values are all rather very low, being less than 1 wt. %. However, the values indicate the trends observed in each specimen composition. It was seen that the highest %wt loss occurs in the neat PLA specimen. When it is filled with UVA, micron and nano sized TiO_2, then %wt loss values decreases substantially, of course due to their UV absorbing capabilities. Moreover, Table 3.4 and Figure 3.12 revealed that the least %wt loss takes place when UVA was added together with micro and nano TiO_2 particles. This can be

interpreted that UVA has synergistic UV absorbing action when used together with titania particles.

Table 3.4 Percent Weight Loss values of the Specimens after (24d) UV irradiation

Specimens	Weight Loss (%)
PLA	0.23 ± 0.045
PLA/UVA	0.19 ± 0.012
PLA/m-TiO_2	0.21 ± 0.004
PLA/n-TiO_2	0.20 ± 0.008
PLA/UVA/m-TiO_2	0.11 ± 0.023
PLA/UVA/n-TiO_2	0.09 ± 0.020

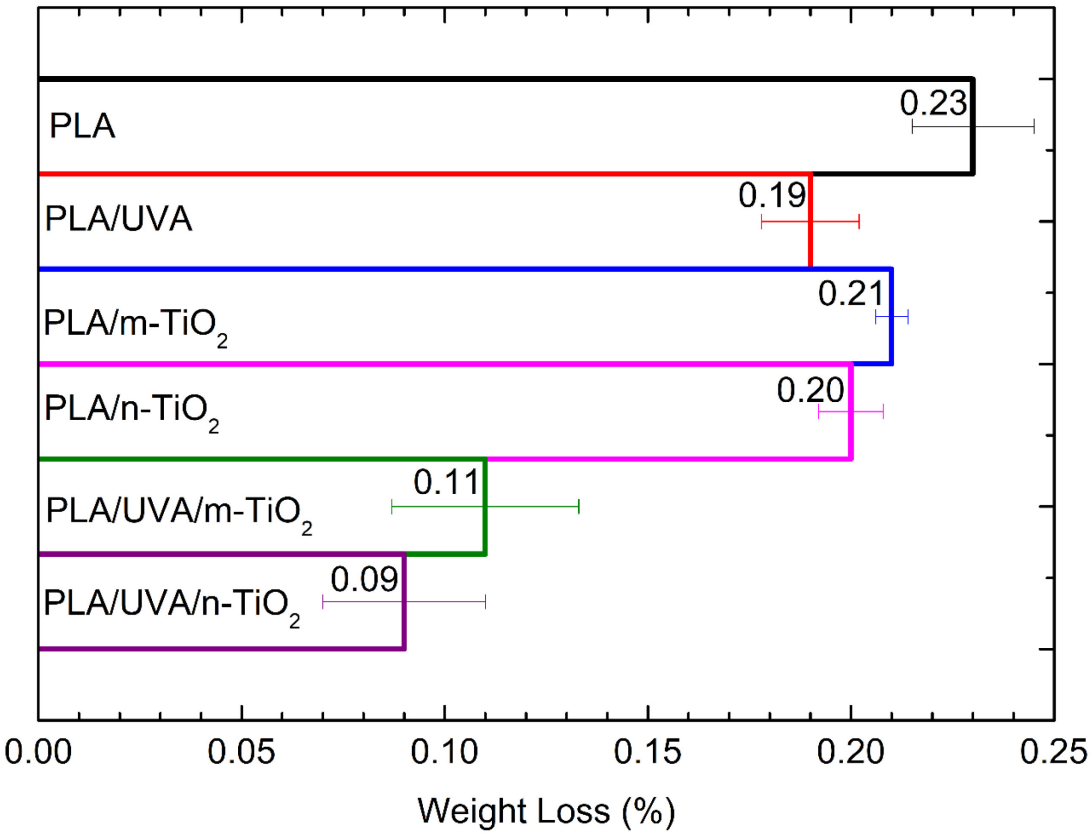

Figure 3.12 Percent weight loss trends of the specimens after (24d) UV irradiation

3.2.2 Color Change after UV Irradiation

In the polymer industry, from consumers' point of view, change in the color of the polymeric components can be very problematic, which can take place when these component are exposed to UV irradiation during their outdoor use under sunlight or sterilization under UV lamps. Therefore, in the second part of this thesis, possible color changes in each specimen composition after (24d) UV irradiation period were evaluated first visually by the photographic images (Figure 3.13) and then also quantitatively by the CEILAB color space parameters (L*, a*, b*, ΔE*) via diffused reflectance analyses (DRA), results of which are provided in Table 3.5.

It is seen in Figure 3.13 that the neat PLA specimen before (0d) irradiation appears very transparent, due to the very slow melt crystallization rate. PLA had no ability to crystallize during the high cooling rate of the compression molding process used for shaping of the specimens. Therefore, all neat PLA specimens had very high level of amorphous structure. During UV irradiation tests, the temperature in the unit was 50ºC, which was insufficient for the start of cold crystallization of PLA. Therefore, even after 24 days, the amorphous transparent structure of neat PLA specimen remained almost the same. Similarly, Table 3.5 shows that during UV irradiation of the neat PLA there was slight changes in the CIELAB color space parameters (L*, a*, b*), in which the total color change (ΔE*) value was only around 3. By the addition of 2 wt. % UVA into the PLA matrix, it was observed that PLA/UVA specimen appeared with a very slightly yellowish tone, again with very high level of amorphous transparent structure. After 24 days of UV irradiation, color space parameters (L*, a*, b*) again changing slightly, this time the total color change (ΔE*) value was around 4.5.

Due to the very well-known perfect whiteness of titania particles, Figure 3.13 indicated that, with the addition of only 2 wt. % micro or nano TiO_2 particles, the specimens appeared opaque and very white, both before (0d) and after (24d) UV irradiation. Similarly, the quantitative color parameters in Table 3.5 revealed that, the values of L* parameter which represents "whiteness" for these components were all above 96, while L* values for the neat PLA and PLA/UVA were around 30. After irradiation,

ΔE*total color change value for the m-TiO_2 and n-TiO_2 filled composites were extremely low, being less than 1.

When TiO_2 particles were added together with UVA, no significant color changes were observed; L* value being again more than 96, and ΔE* value becoming slightly above 1.

Therefore, it can be stated that use of micro and nano titania particles either alone or together with a benzotriazole type organic UV absorber could be very effective to keep white color of the PLA products under prolonged UV irradiation conditions.

Table 3.5 Changes in the CIELAB color space parameters (L*, a*, b*) and total color change (ΔE*) values of the specimens after (24d) UV irradiation

Specimens	***L****	***a****	***b****	***ΔE****
PLA-0d	30.00±1.02	-0.24±0.05	-0.72±0.03	
PLA-24d	32.72±1.15	-0.27±0.04	-1.59±0.14	2.91±1.03
PLA/UVA-0d	28.71±0.89	-0.61±0.09	-0.10±0.08	
PLA/UVA-24d	33.13±0.72	-0.53±0.06	-0.60±0.22	4.46±0.31
PLA/m-TiO_2-0d	95.97±0.09	-0.85±0.04	2.63±0.14	
PLA/m-TiO_2-24d	96.56±0.11	-0.78±0.01	2.07±0.09	0.82±0.14
PLA/n-TiO_2-0d	96.21±0.09	-0.97±0.04	2.67±0.20	
PLA/n-TiO_2-24d	96.74±0.13	-0.80±0.03	1.85±0.03	0.99±0.09
PLA/UVA/m-TiO_2-0d	96.08±0.30	-1.08±0.02	3.11±0.11	
PLA/UVA/m-TiO_2-24d	96.57±0.05	-1.49±0.06	4.60±0.17	1.62±0.05
PLA/UVA/n-TiO_2-0d	96.17±0.15	-1.09±0.03	3.05±0.05	
PLA/UVA/n-TiO_2-24d	96.08±0.05	-1.43±0.03	4.23±0.05	1.24±0.05

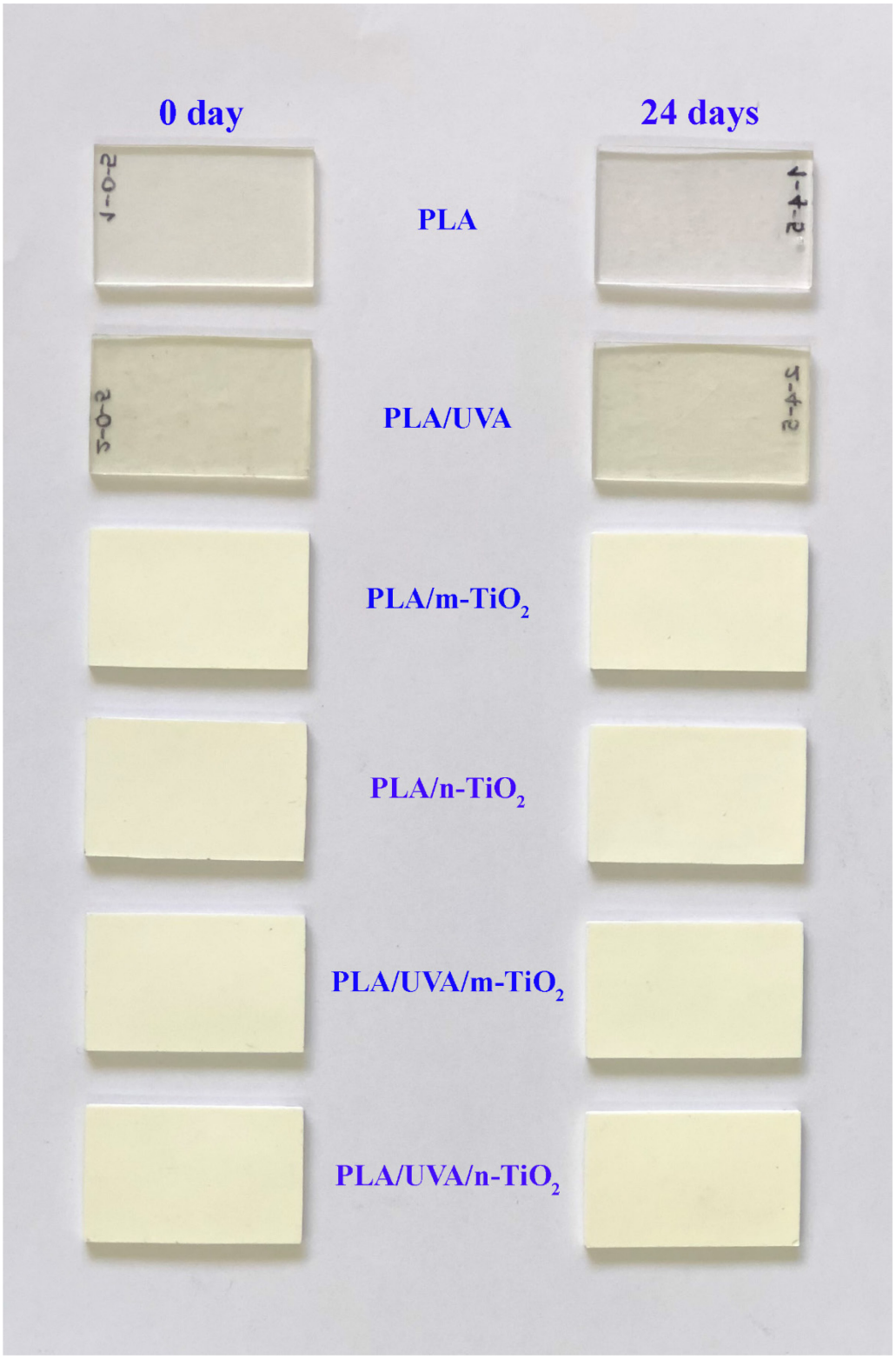

(a)

Figure 3.13 Photographic images of the **(a)** Flexural test and, **(b)** Fracture toughness specimens; showing their color before (0d) and after (24d) UV irradiation

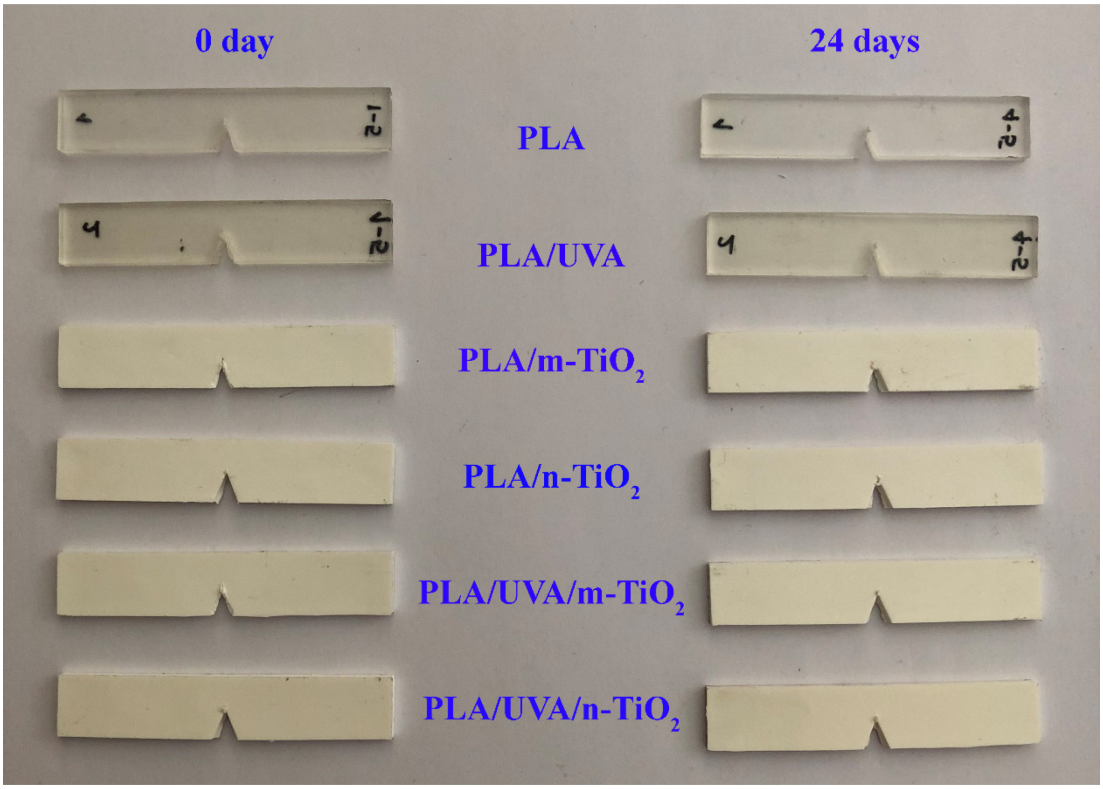

(b)

Figure 3.13 (continued)

3.2.3 Chemical Structure Change after UV Irradiation

It is known that the most significant deteriorative effects of UV irradiation influencing all mechanical properties of PLA would be in the form of molecular weight (M_w) decrease via chain scission reactions. Therefore, in order to determine the level of molecular weight reduction of PLA matrix after (24d) UV irradiation, gel permeation chromatography (GPC) analysis was used. GPC analysis revealed that the weight average molecular weight (M_w) of unirradiated (0d) neat PLA matrix being 105.80×10^3 g/mol reduced down to 86.98×10^3 g/mol after 24 days of UV irradiation. As will be evaluated in the next section, this level of reduction in the M_w of PLA matrix led to substantial decreases in the mechanical properties of all specimen compositions.

Apart from the reduction in the M_w of PLA matrix, in order to observe other changes in the chemical structure of each specimen, ATR-FTIR analyses were conducted. Their spectra before (0d) and after (24d) UV irradiation are compared in Figure 3.14 (a) and (b). The first spectrum in Figure 3.14 (a) belongs to unirradiated (0d) neat PLA specimen indicating the well-known typical five main absorption bands of the PLA as described in section 3.1.3

In the literature [22,25,80] it has been indicated that, upon absorption of a photon during UV irradiation, photo degradation mechanisms known as "photolysis" and "photo-oxidation" leading to "chain scission" i.e. breakage of the PLA backbone structure especially takes place in the C-O and C-C bonds of the ester linkage, resulting in the decreased IR intensity of these bands.

Figure 3.14 (a) and (b) show that, for all specimen compositions, compared to their unirradiated (0d) IR spectrum, IR intensities of not only C-O and C-C bonds, but also other typical bands of the UV irradiated (24d) specimens were decreased. Of course, it was very clear that the most significant decrease in the IR intensity of the bonds occurred in the neat PLA specimen. In the irradiated (24d) specimens having either UVA, micron or nano sized TiO_2 particles, the decrease in the intensity of IR bands were much lower. Moreover, it was observed that, due to the synergism, when UVA was added together with micron or nano sized TiO_2, the decrease in the IR intensities were almost negligible.

Apart from decreased intensity of IR bands, it has been also discussed [77,79,81] that, upon UV irradiation, there might be formation of new C=C bands (around 1600 cm^{-1}) and O-H bands (around 3500 cm^{-1}). The formation of the first new band is believed to be due to the excitation of the C=O ester carbonyl during the main photodegradation reaction known as Norrish II type photocleavage. The second new band that might appear would be due to the formation of hydroperoxides at the terminals of the new broken PLA chains. In this thesis, closer examination of the 24d irradiated IR spectrum of the neat PLA and UVA, micron and nano sized TiO_2 filled specimens, revealed that there were tiny broad peaks for the new C=C band at 1636, 1646 and 1654 cm^{-1}; while

for the new –O-H band at 3629, 3649 and 3676 cm^{-1} (Figure 3.14 (a) and (b)). However, for the specimens having UVA and micron or nano sized TiO_2 together, these tiny new peaks were not observed.

Copinet *et al.*[25] and Santonja-Blasco *et al.* [26] indicated that, apart from new peak formations, UV irradiation might also lead to shifting of the certain IR peaks of the typical PLA bands to lower wavenumbers. In this thesis upon (24d) UV irradiation of the neat PLA specimen, the (O=)C–O and C–C–O stretching bands shifted from 1180 cm^{-1} to 1179 cm^{-1}, 1264 cm^{-1} to 1263 cm^{-1}; and from 1042 cm^{-1} to 1040 cm^{-1},respectively; while the C=O carbonyl stretching peaks shifted from 1747 cm^{-1} to 1744 cm^{-1}. However, for the specimens containing UVA, micro or nano TiO_2 particles, alone or together, these shifts were not observed.

Therefore, it can be pointed out that, compared to neat PLA, due to the efficient photon absorbing abilities of UVA and TiO_2 particles, the change in the chemical structure of PLA matrix i.e. the degree of "chain scission" in these filled compositions were rather lower.

3.2.4 Mechanical Property Changes after UV Irradiation

In the second part of this thesis, in order to determine the degree of the reductions in the mechanical properties of the UV irradiated specimens, two types of tests were conducted. The first one, 3-point bending, was used to compare "Flexure Strength, σ_{Flex}" and "Flexure Modulus, E_{Flex}" values; while the second one was used to compare "K_{IC} and G_{IC} Fracture Toughness" values. It should be pointed out that, since during UV irradiation test of the specimens, the temperature exposure unit was 50ºC, all unirradiated specimens were first dried in a vacuum oven at 50ºC in order to make proper comparison.

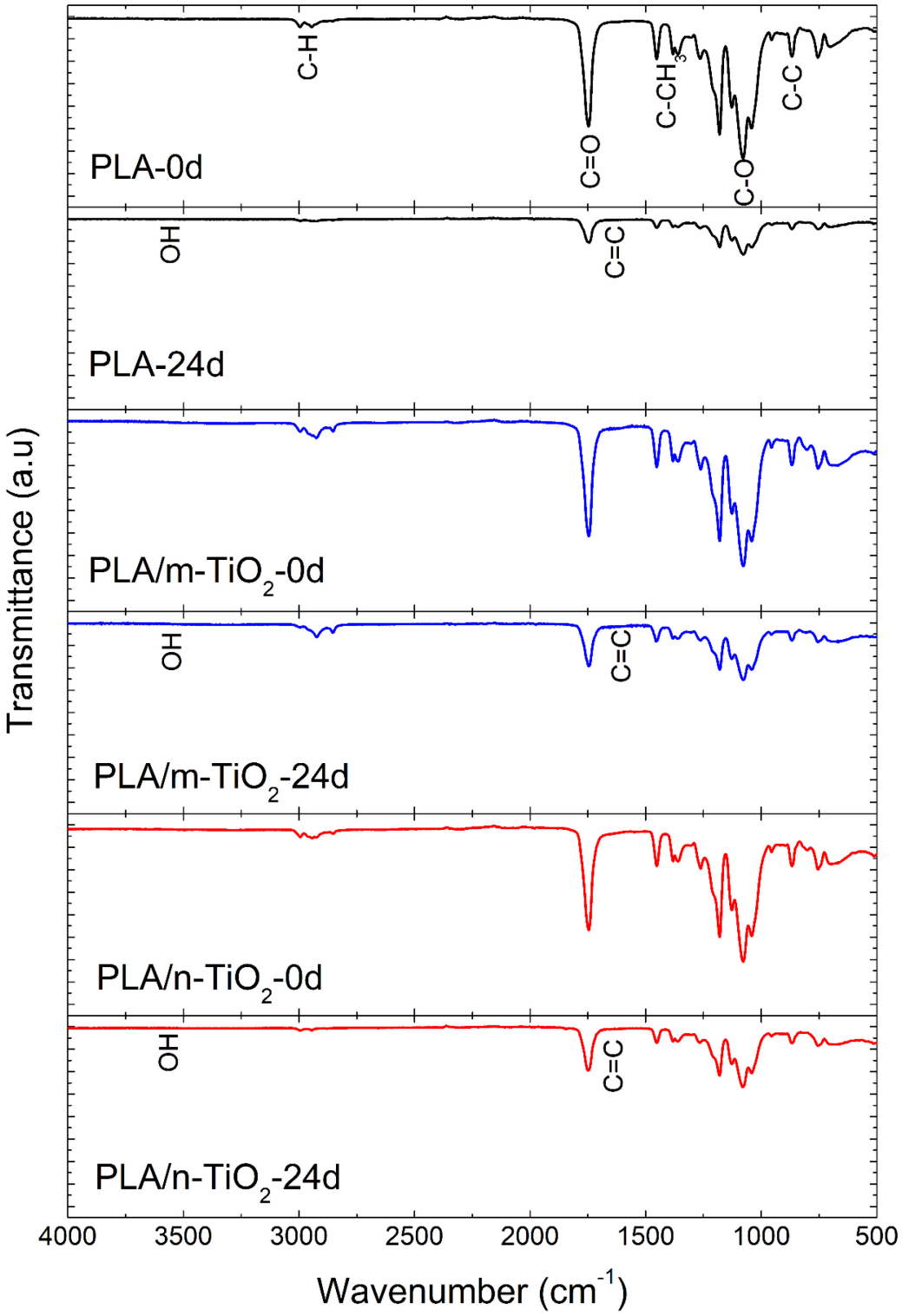

(a)

Figure 3.14 Comparison of ATR-FTIR spectra of the **(a)** PLA, PLA/m-TiO_2, PLA/n-TiO_2, **(b)** PLA/UVA, PLA/UVA/m-TiO_2, PLA/UVA/n-TiO_2 specimens before (0d) and after (24d) UV irradiation:

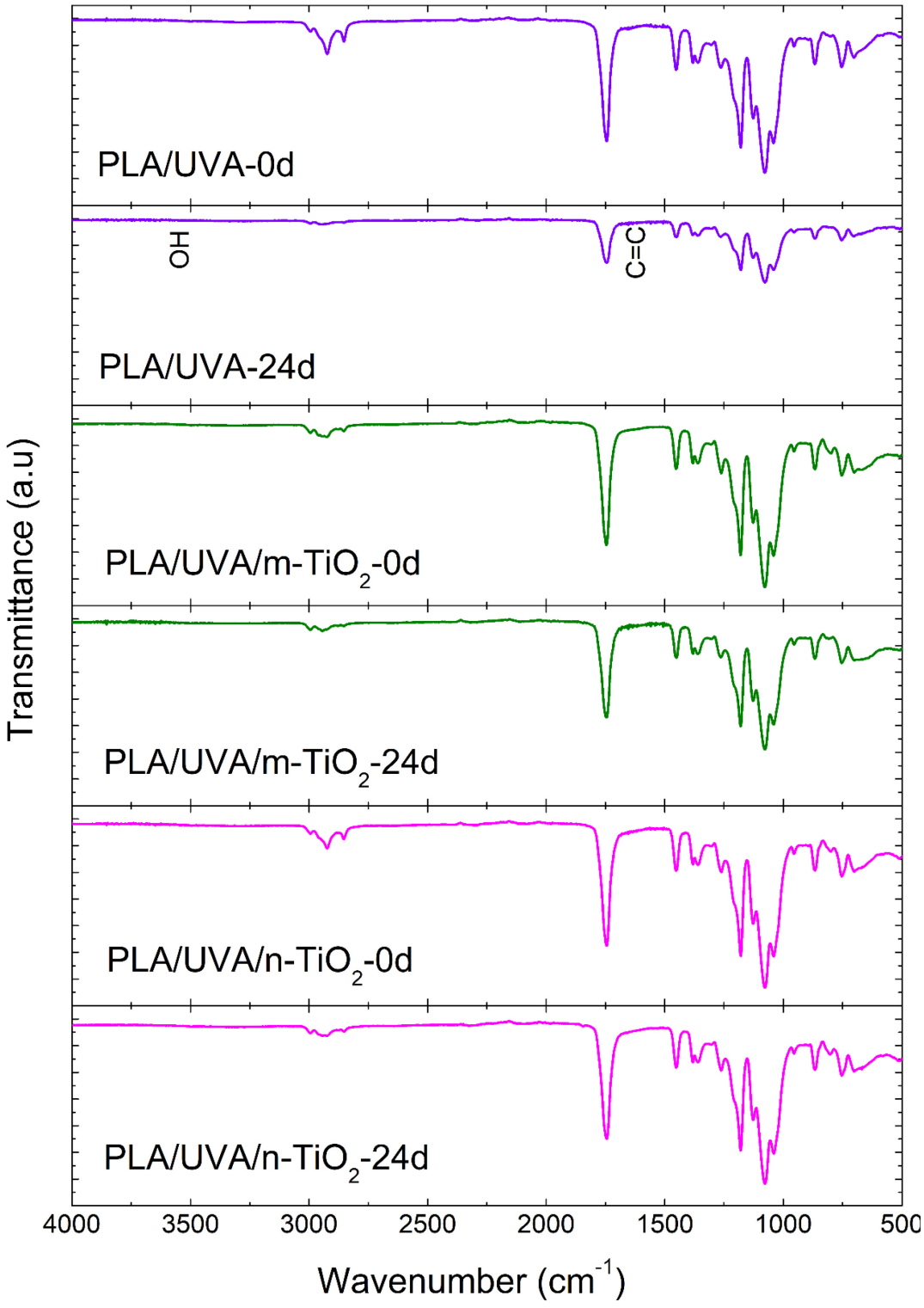

(b)

Figure 3.14 (continued)

Results of the first test are given in Figure 3.15 (a) and (b) in the form of "flexural stress-strain curves", while the σ_{Flex} and E_{Flex} data determined from these curves are tabulated in Table 3.6. Moreover effects of 12d and 24d UV irradiation on these strength and modulus values are shown in Figure 3.16.

Figures 3.15, 3.16 and Table 3.6 revealed that the flexural stress-strain curves of all specimens were affected from 24 days of UV irradiation leading to certain decreases in the values of both flexural strength and modulus (σ_{Flex} and E_{Flex}). It is clear that the most significant deterioration in the strength and modulus values were for the neat PLA specimen. The reduction in the σ_{Flex} and E_{Flex} values of this specimen after 24d irradiation was 15% and 10%, respectively. This was because of the photodegradation reactions leading to "chain scissions" and the consequent decrease in the molecular weight of PLA structure.

However, due to the UV absorbing actions of both TiO_2 particles and UVA molecules, decreasing the level of chain scissions in their PLA matrix, these reductions were lower in the specimens of PLA/UVA, PLA/m-TiO_2 and PLA/n-TiO_2. When these fillers were added together, the lowest level of reductions were obtained. For example, for the PLA/UVA/n-TiO_2 specimen, the reductions in the σ_{Flex} and E_{Flex} values after 24d irradiation were both only 3%.

Benefits in the strength and elastic modulus values of the specimen filled with micro and nano TiO_2 particles were especially due to their inorganic rutile phase having very high chemical stability during UV irradiation. Consequently, these TiO_2 filled specimen exhibited higher σ_{Flex} and E_{Flex} values not only before (0d) but also after (24d) UV irradiation. Because, these compositions kept their function on the well-known composite strengthening and stiffening mechanisms of "load transfer from the matrix" and "decreased mobility of the matrix chains" also during UV irradiation..

The possible reason of the synergistic behavior when UVA was used together with TiO_2 particles can be due to the higher efficiency during absorption of the UV photons

and then transformation of the energy of these photons into less harmful heat by higher degree of electron hole recombination.

Changes in the fracture toughness, i.e. ability of the structure to hinder crack initiation and propagation leading to fracture, of the specimens were determined in terms of "Critical Stress Intensity Factor (K_{IC})" and "Critical Strain Energy Release Rate (G_{IC})" values as given in Table 3.6. Effects of 12d and 24d UV irradiation periods on these fracture toughness values were evaluated in Figure 3.17.

Just like in the case of σ_{Flex} and E_{Flex}, Table 3.6 and Figure 3.17 showed that, the reductions in the fracture toughness values K_{IC} and G_{IC} in the 24d irradiated neat PLA specimen was significant being as much as 18% and 36%, respectively. Similarly, these reductions were again much lower in the specimens having UVA and TiO_2 particles either alone or together. For instance, in the specimen of PLA/UVA/n-TiO_2 the reductions in the K_{IC} and G_{IC} values after 24d irradiation were only 7% and 19%, respectively.

The contribution of the organic UVA molecules and the inorganic TiO_2 particles to the fracture toughness values of the PLA matrix before and after UV irradiation could be discussed in two manner. First of all, since they have high chemical stability under UV irradiation; they could keep their function in the composite toughening mechanisms. For instance UVA might act as plasticizing agent for the "shear banding or plastic deformation" mechanism, while micro and nano TiO_2 particles keep their action in the mechanisms of "crack deflection", "crack bowing", "particle debonding" and "particle pull-out". Secondly, their very efficient UV absorbing actions decreasing the level of photodegradation (i.e. chain scission) in their PLA matrix would result in lower amount of crack initiation and propagation.

Table 3.6 Changes in the flexural Modulus (E_{Flex}), Flexural Strength (σ_{Flex}) and Fracture Toughness (K_{IC} and G_{IC}) values of the specimens before (0d) and after UV irradiation periods of 12d and 24d.

Specimens	E_{Flex} (GPa)	σ_{Flex} (MPa)	K_{IC} (MPa$\sqrt{m}$)	G_{IC} (kJ/m^2)
PLA-0d	117.23 ± 1.75	3.77 ± 0.01	3.57 ± 0.06	5.88 ± 0.54
PLA-12d	112.67 ± 0.29	3.58 ± 0.27	3.38 ± 0.06	4.84 ± 0.19
PLA-24d	99.44 ± 0.84	3.38 ± 0.04	2.92 ± 0.18	3.79 ± 0.39
PLA/UVA-0d	114.71 ± 0.83	3.74 ± 0.13	3.64 ± 0.13	6.31 ± 1.27
PLA/UVA-12d	113.27 ± 0.24	3.71 ± 0.01	3.58 ± 0.02	6.10 ± 0.18
PLA/UVA-24d	105.85 ± 0.82	3.49 ± 0.01	3.31 ± 0.06	4.78 ± 0.09
PLA/m-TiO$_2$-0d	118.83 ± 2.31	3.97 ± 0.06	3.76 ± 0.10	7.05 ± 0.13
PLA/m-TiO$_2$-12d	113.91 ± 4.33	3.84 ± 0.18	3.71 ± 0.14	6.66 ± 0.52
PLA/m-TiO$_2$-24d	107.66 ± 0.06	3.68 ± 0.02	3.43 ± 0.04	5.43 ± 0.11
PLA/n-TiO$_2$-0d	123.25 ± 3.70	4.09 ± 0.18	3.85 ± 0.12	7.42 ± 0.76
PLA/n-TiO$_2$-12d	115.14 ± 1.16	3.86 ± 0.04	3.73 ± 0.04	6.79 ± 0.58
PLA/n-TiO$_2$-24d	108.73 ± 0.19	3.72 ± 0.05	3.59 ± 0.02	5.81 ± 0.71
PLA/UVA/m-TiO$_2$-0d	118.01 ± 0.71	3.93 ± 0.15	3.92 ± 0.33	7.33 ± 1.18
PLA/UVA/m-TiO$_2$-12d	116.74 ± 2.08	3.90 ± 0.04	3.73 ± 0.08	6.69 ± 0.25
PLA/UVA/m-TiO$_2$-24d	110.73 ± 2.28	3.72 ± 0.10	3.56 ± 0.04	5.46 ± 0.09
PLA/UVA/n-TiO$_2$-0d	120.06 ± 6.24	4.05 ± 0.27	3.94 ± 0.30	7.59 ± 1.66
PLA/UVA/n-TiO$_2$-12d	118.36 ± 1.50	3.97 ± 0.05	3.83 ± 0.18	7.18 ± 0.78
PLA/UVA/n-TiO$_2$-24d	115.52 ± 4.13	3.90 ± 0.23	3.68 ± 0.09	6.12 ± 0.34

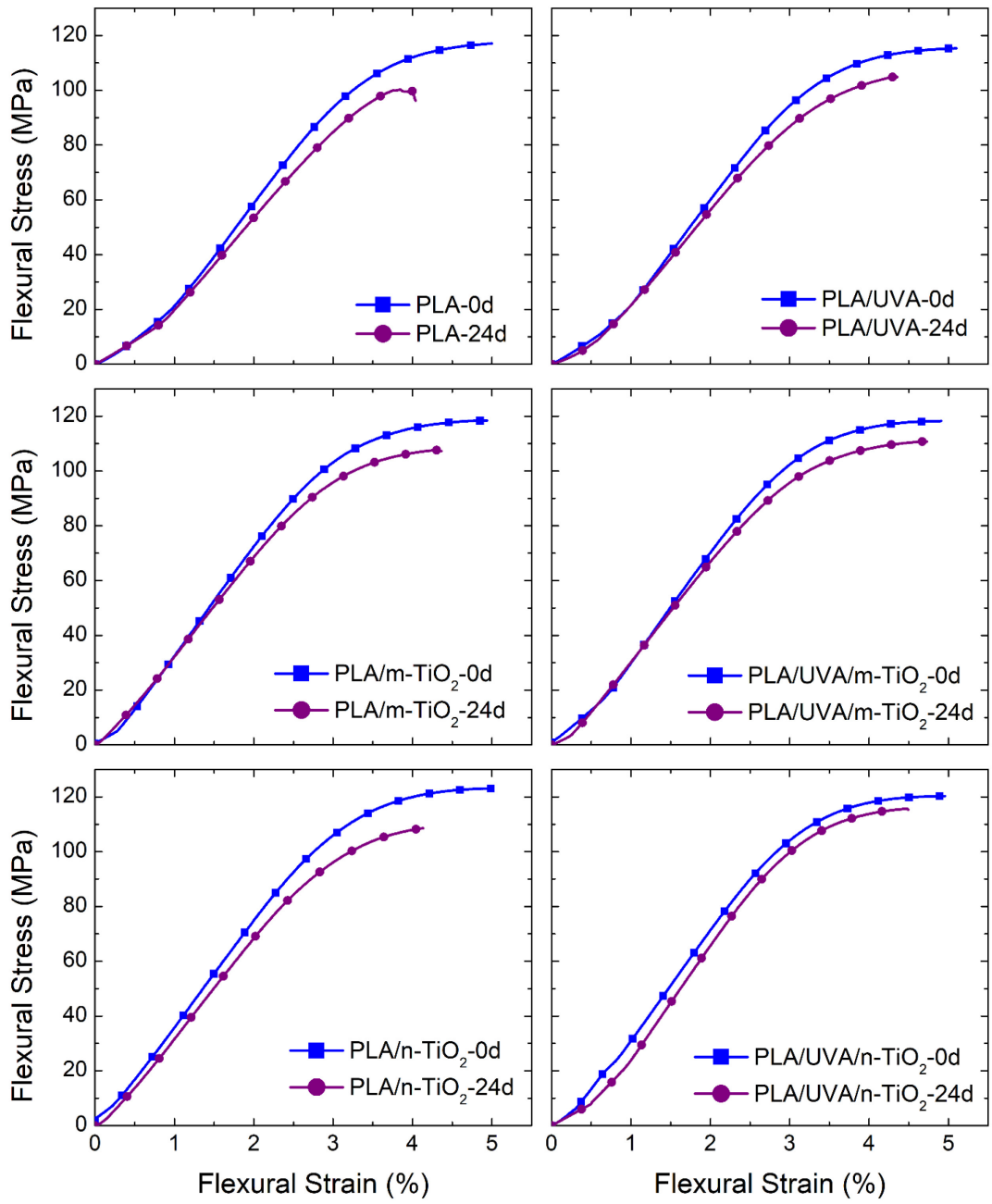

Figure 3.15 Changes in the flexural stress strain curves of **(a)** each specimen and **(b)** all specimens together; before (0d) and after (24d) UV irradiation

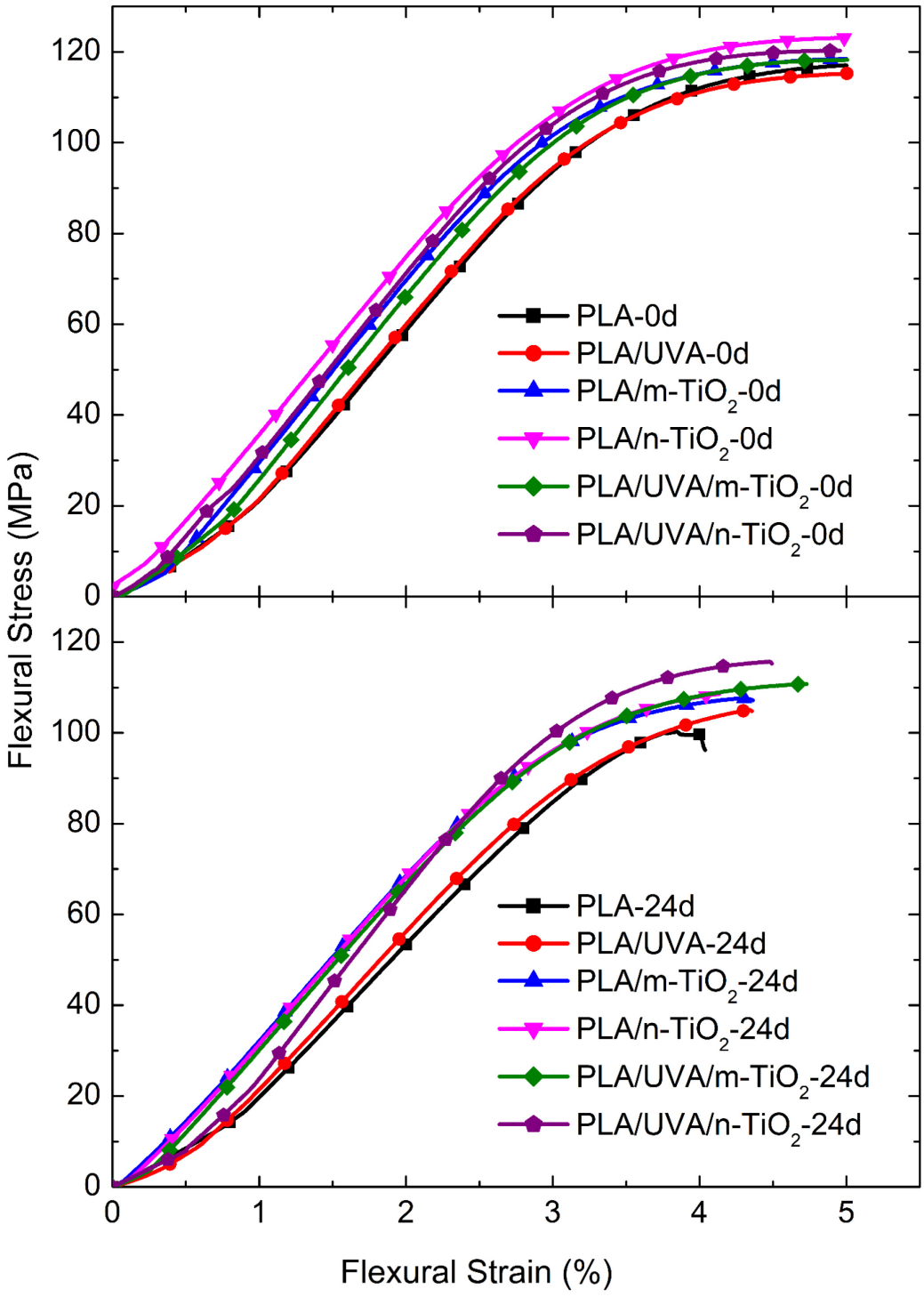

(b)

Figure 3.15 (continued)

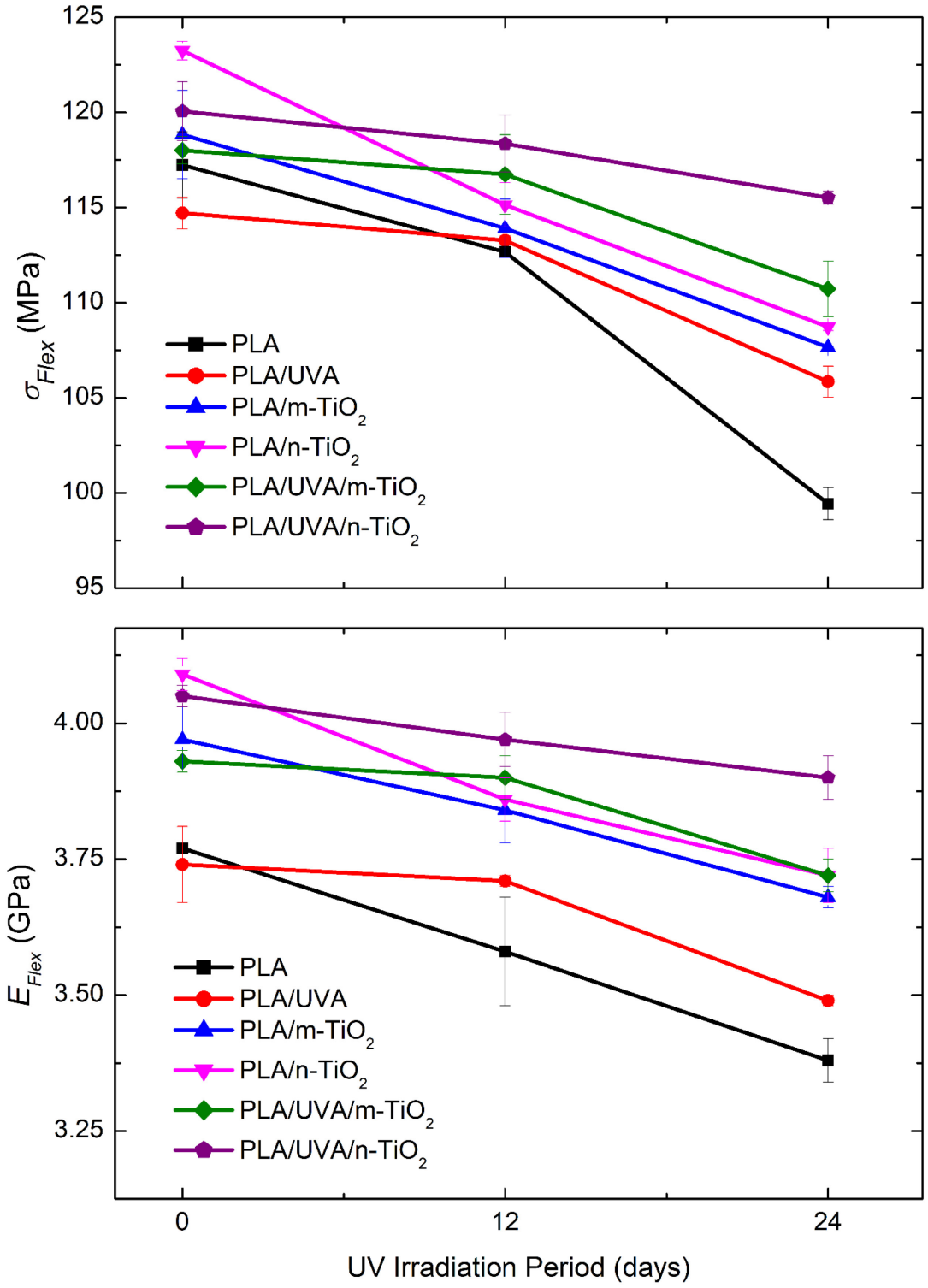

Figure 3.16 Effects of 12d and 24d UV irradiation periods on the flexural strength (σ_{Flex}) and flexural modulus (E_{Flex}) of the specimens (The lines are for visual aid only)

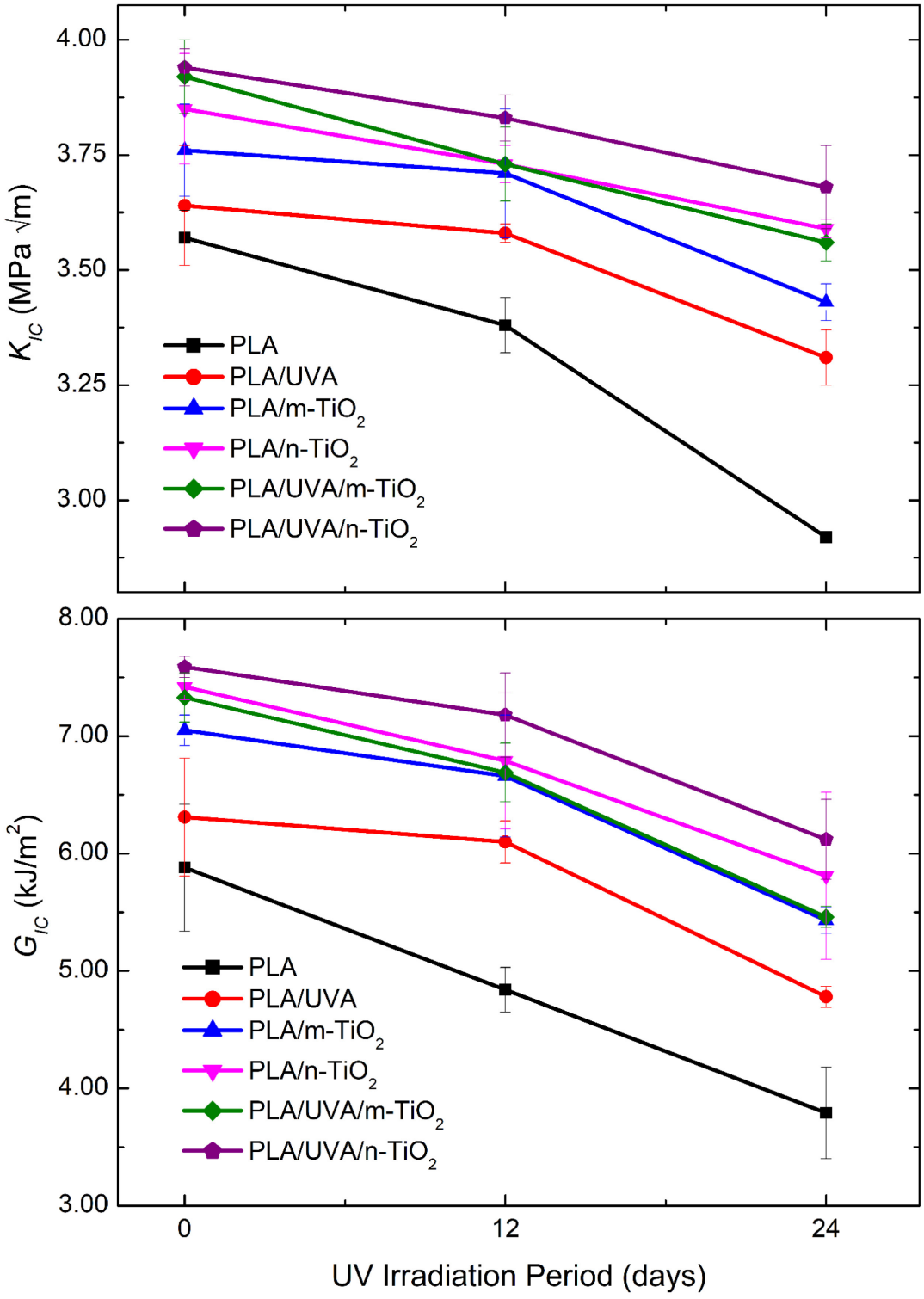

Figure 3.17 Effects of 12d and 24d UV irradiation periods on the fracture toughness (K_{IC} and G_{IC}) of the specimens (The lines are for visual aid only)

In this section finally, in order to reveal benefits of using UVA and TiO_2 filled compositions rather than using neat PLA, all the mechanical properties of these filled specimens before (0d) and after (24d) UV irradiation were compared and provided in Figure 3.18. Note that benefits of using these filled compositions compared to PLA-0d and PLA-24d specimens are shown in terms of "% Increase" in each mechanical property at 0d and 24d.

Figure 3.18 revealed that in terms of all mechanical properties, the use of micro or nano TiO_2 particles alone or together with a benzotriazole type UVA in PLA matrix would be quite beneficial not only under normal conditions but also under UV irradiation conditions. % Increase data given in Figure 3.18 indicated that if TiO_2 particles were used together with UVA, then the benefits would be much higher. For instance, for the specimen of PLA/UVA/n-TiO_2-24d, the %Increase in σ_{Flex} and E_{Flex} values were 16% and 15%, respectively; while in K_{IC} and G_{IC} values, %Increase were as much as 26% and 61%, respectively.

It can be once more stated that synergistic benefits of using micro and nano TiO_2 particles together with benzotriazole type UVA were not only due to the effective stiffening, strengthening and toughening actions of titania particles but also due to their very significant "UV screening" actions absorbing the photons of the UV irradiation, thus decreasing the degree of the detrimental photodegradation reactions in their PLA matrix. This was also reported for other polymeric matrices in the literature [90,91].

Therefore, it can be concluded that, since PLA/UVA/n-TiO_2 specimen had very close or higher mechanical properties even after 24 days of UV irradiation compared to unirradiated neat PLA specimen; use of this composition can be as an alternative PLA based material for automobile and biomedical applications having durability requirement especially in terms of UV resistance.

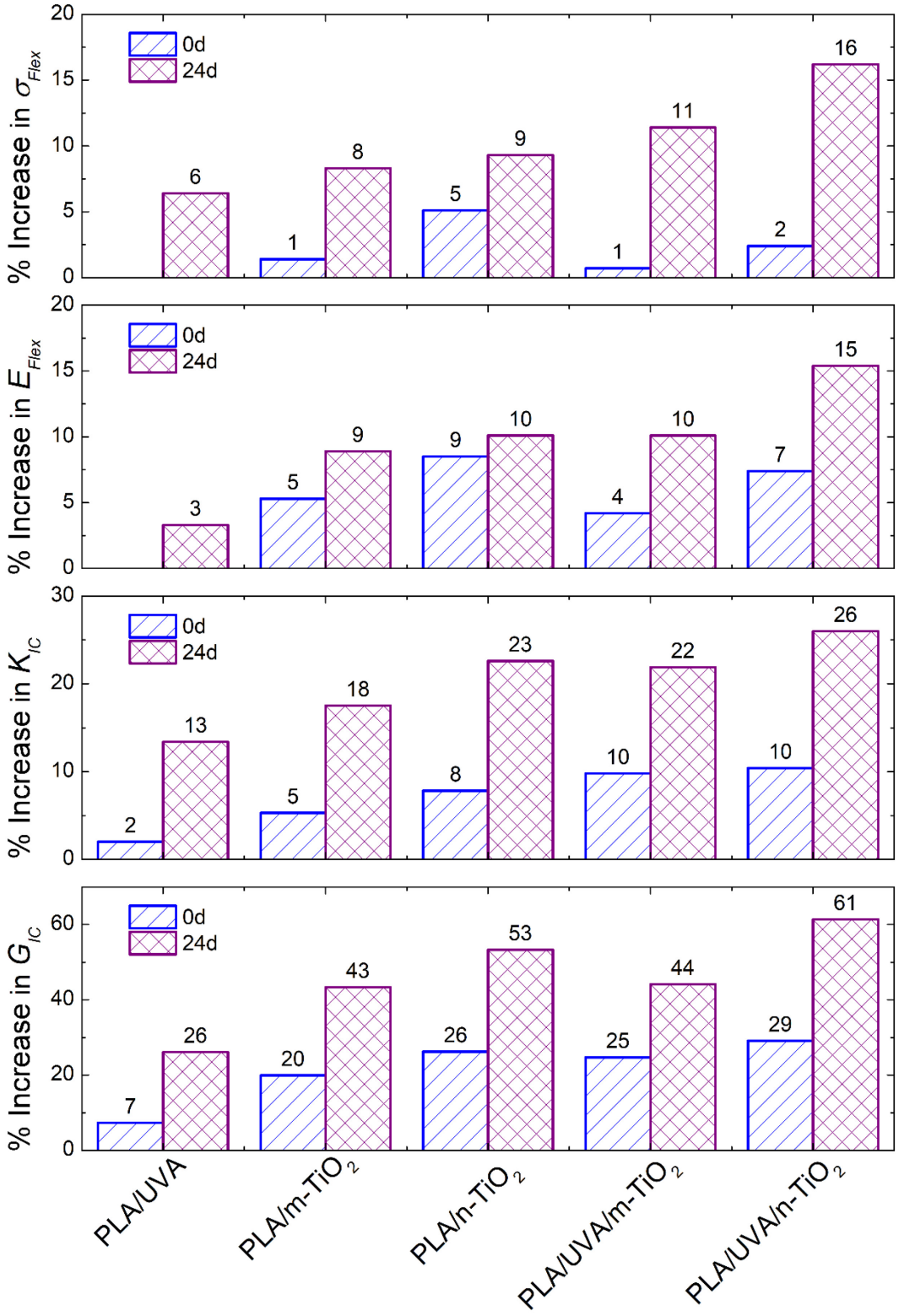

Figure 3.18 Compared to neat PLA-0d and PLA-24d specimens, "% Increase" in the mechanical properties of each filled specimen before (0d) and after (24d) UV irradiation

3.2.5 Fracture Surface Morphology Changes after UV Irradiation

In order to observe the changes in the fracture surface morphology, SEM analysis were conducted on the fracture surfaces of the fracture toughness test specimens of all compositions before (0d) and after 24 days of UV irradiation and SEM images as given in Figure 3.19 (a) and (b), respectively. All the images of the left hand side of Figure 3.19 belong to the unirradiated (0d) specimens. In this group, it is seen that fracture surfaces of neat PLA and only organic UVA filled PLA are rather very smooth and flat, representing the well-known inherently brittle character of PLA structure. When 2 wt. % micro or nano TiO_2 particles were added, it was observed that these titania particles were all rather homogeneously distributed in the PLA matrix, and the smooth fracture surface morphology did not change much.

On the other hand, in the images of the right hand side of Figure 3.19 belonging to the 24d UV irradiated specimens, it was seen that all the images were obscured; with very tortuous and rough fracture surface morphology. It was even not possible to recognize the TiO_2 particles in the matrix. Due to the photodegradation reactions leading to significant deteriorative chemical changes in the PLA matrix of the specimens, certain number of main and secondary cracks and cleavages were also observed in the fracture surfaces of all irradiated specimens.

3.2.6 Thermal Property Changes after UV Irradiation

In order to evaluate changes in the thermal properties of the UV irradiated specimens two different thermal analysis were conducted namely differential scanning calorimetry (DSC) analyses and thermogravimetric analyses (TGA).

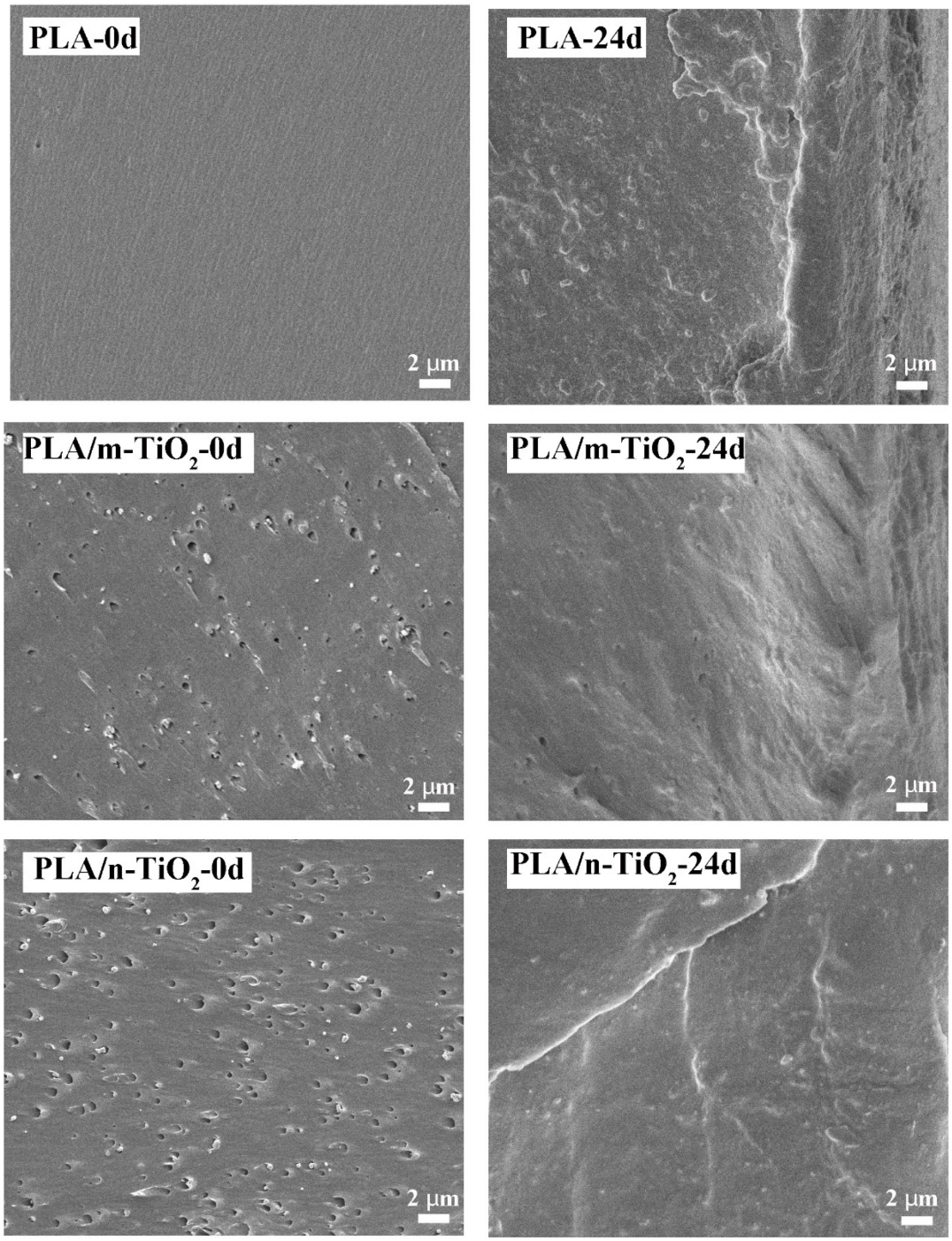

(a)

Figure 3.19 SEM fracture surface morphology of **(a)** PLA, PLA/m-TiO_2, PLA/n-TiO_2; and **(b)** PLA/UVA, PLA/UVA/m-TiO_2, PLA/UVA/n-TiO_2 specimens before (0d) and after (24d) UV irradiation:

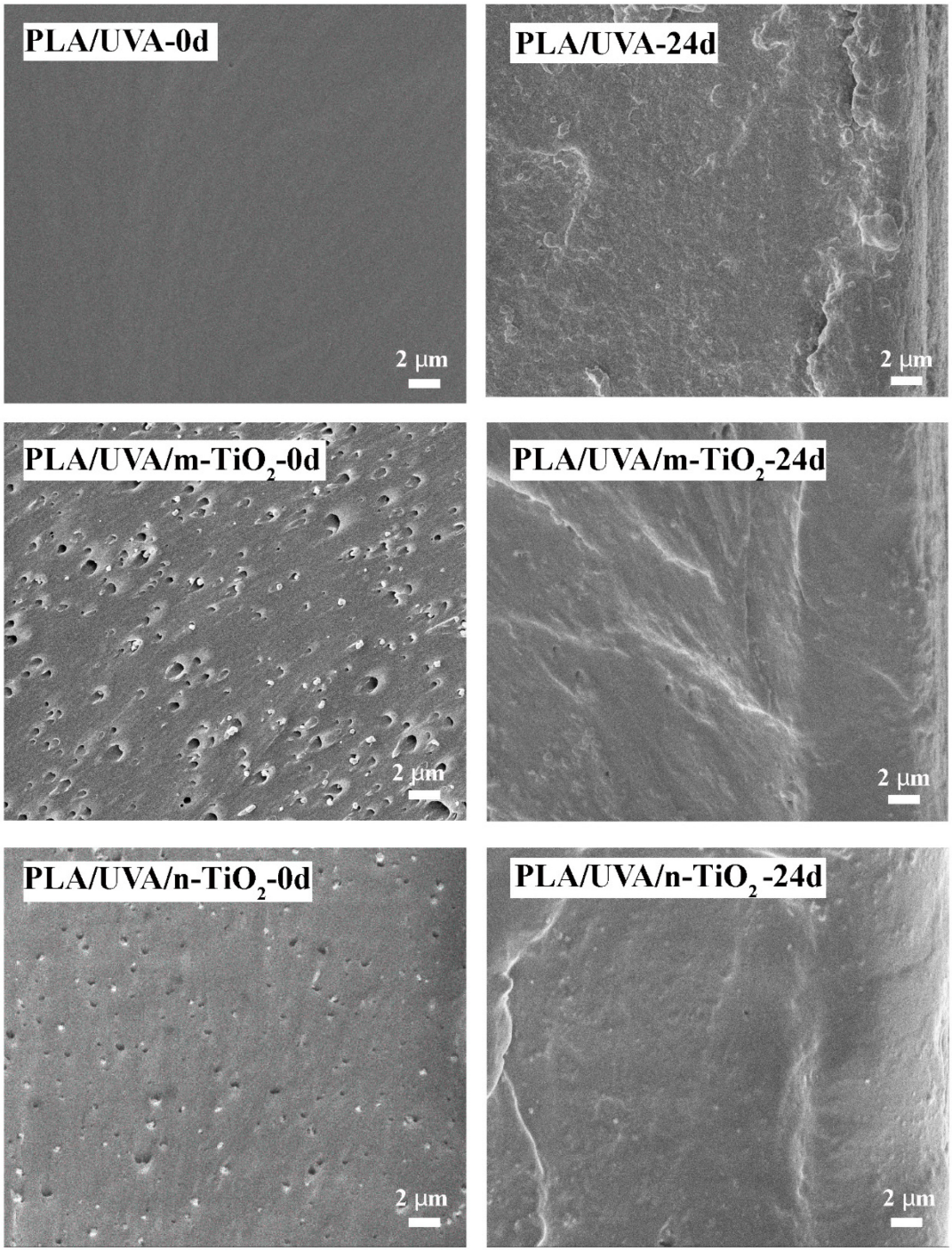

(b)

Figure 3.19 (continued)

First heating DSC thermograms of all specimens before (0d) and after (24d) UV irradiation were given in Figure 3.20, while in Table 3.7 glass transition (T_g), cold crystallization (T_c) and melting (T_m) temperatures together with the enthalpies of melting (ΔH_m) and crystallization (ΔH_c) including the percent crystallinity (Xc) values were tabulated. The relation used in the calculation of the percent crystallinity is given in Section 3.1.4.

Table 3.7 and Figure 3.20 indicated that there were important changes in only two parameters; T_g and X_c. Due to the deteriorative actions of the photodegradation reactions on the chemical structure of PLA matrices, glass transition temperature T_g of the PLA specimen decreased by 5ºC after 24d UV irradiation. The decrease in the T_g values of the specimens, filled with UVA, micro and nano TiO_2 particles, were all less than 5ºC.

Another reduction observed for all UV irradiated specimens was the amount of the percent crystallinity X_c in their PLA matrices. This can be interpreted that all those deteriorative photodegradation reactions were occurred not only in the amorphous regions of the PLA matrices, but also in the crystalline regions of the matrix. That behavior was also discussed in detail by Tsuji *et al.* [22] for the PLA matrix.

As the second thermal analysis, thermogravimetric (TG) curves of all specimen compositions before (0d) and after (24d) UV irradiation were obtained as given in Figure 3.21. Then, the thermal degradation temperatures of $T_{5\%}$, $T_{10\%}$, $T_{25\%}$ representing the mass loss temperatures at 5, 10, 25 wt. %; T_{max} representing the temperature at maximum mass loss; and %residue of each specimen determined at 550ºC were tabulated in Table 3.8.

Table 3.7 Changes in the transition temperatures (T_g, T_c, T_m), enthalpies (ΔH_m, ΔH_c) and crystallinity percent (X_c) of the specimens after (24d) UV irradiation

Specimens	T_g(ºC)	T_c(ºC)	T_m(ºC)	ΔH_m(J/g)	ΔH_c(J/g)	X_C(%)
PLA-0d	60.1	124.6	150.2	17.2	13.7	3.76
PLA-24d	55.7	122.7	149.3	5.69	6.58	0.96
PLA/UVA-0d	58.4	124.1	149.8	10.2	14.1	4.30
PLA/UVA-24d	57.0	122.9	149.3	3.11	4.15	1.14
PLA/m-TiO_2-0d	60.1	118.5	149.8	27.3	22.3	5.49
PLA/m-TiO_2-24d	56.0	118.1	149.4	6.98	7.95	1.06
PLA/n-TiO_2-0d	60.2	118.2	149.1	24.5	16.5	8.69
PLA/n-TiO_2-24d	57.2	117.8	148.7	7.80	9.63	2.01
PLA/UVA/m-TiO_2-0d	59.2	122.6	148.9	4.85	3.19	1.86
PLA/UVA/m-TiO_2-24d	58.1	120.6	148.7	5.24	3.91	1.49
PLA/UVA/n-TiO_2-0d	59.0	121.5	149.5	7.74	6.00	1.95
PLA/UVA/n-TiO_2-24d	58.2	119.5	149.0	8.07	6.53	1.72

Figure 3.21 and Table 3.8 revealed that, because of the deteriorations in the chemical structure of the PLA matrices upon 24d UV irradiation, there were certain reductions in all thermal degradation temperatures of all specimen compositions. It can be deduced from Table 3.8 that the most significant reduction occurred in the onset degradation temperature of $T_{5\%}$; which is being as much as 10ºC for the neat PLA specimen. That reduction was gradually decreased in the specimens filled with UVA, micro and nano TiO_2 particles. It was seen that when benzotriazole type UVA and TiO_2 particles were added together, i.e. the synergistic compositions, the reduction in the values of $T_{5\%}$ were only 2-3ºC.

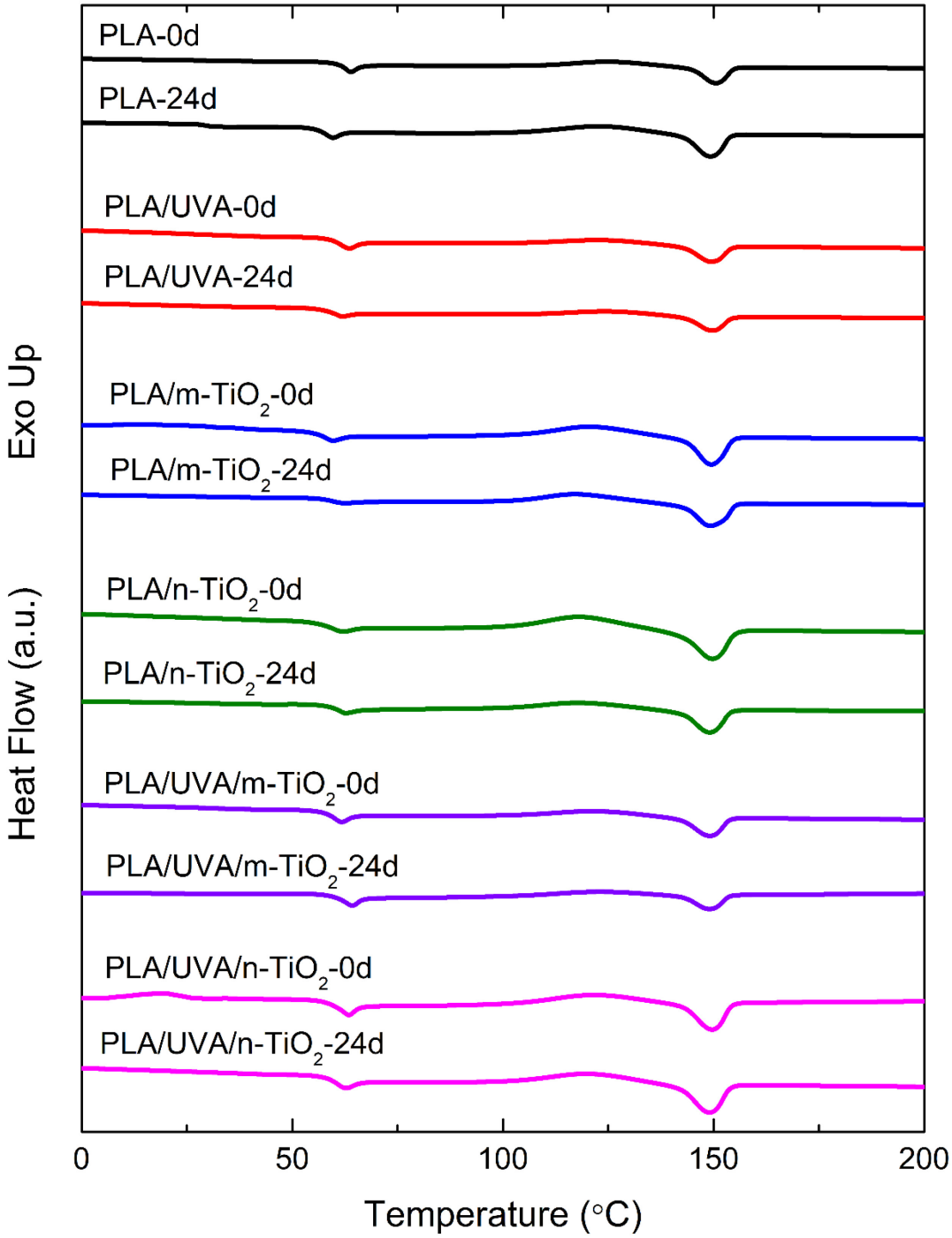

Figure 3.20 Changes in the first heating DSC thermograms of all specimens before (0d) and after (24d) UV irradiation

Table 3.8 also indicated that, for the specimens containing micro and nano TiO_2 particles, the values of the %Residue at 550ºC were all around 2 wt. % before (0d) and after (24d) UV irradiation. This could be interpreted that photodegradation reactions resulted in no significant changes in the structure of these inorganic TiO_2 particles.

Table 3.8 Changes in the thermal degradation temperatures ($T_{5\%}$, $T_{10\%}$, $T_{25\%}$) of the specimens at 5, 10 and 25 wt. % mass losses and the maximum mass loss temperature (T_{max}); and the %Residue at 550ºC after (24d) UV irradiation

Specimens	$T_{5\%}$**(ºC)**	$T_{10\%}$**(ºC)**	$T_{25\%}$**(ºC)**	T_{max}**(ºC)**	**%Residue at 550 ºC**
PLA-0d	332.2	342.2	353.4	362.4	0.16
PLA-24d	323.5	335.4	349.8	361.2	0.06
PLA/UVA-0d	330.3	340.2	352.4	363.3	0.10
PLA/UVA-24d	325.5	337.0	350.3	361.4	0.01
PLA/m-TiO_2-0d	332.7	340.2	344.3	355.0	2.29
PLA/m-TiO_2-24d	321.8	332.3	343.8	351.4	2.18
PLA/n-TiO_2-0d	338.6	346.2	355.5	363.6	2.35
PLA/n-TiO_2-24d	321.4	335.7	350.1	361.8	2.20
PLA/UVA/m-TiO_2-0d	326.8	336.5	348.9	359.8	2.11
PLA/UVA/m-TiO_2-24d	324.1	335.0	347.7	358.8	2.06
PLA/UVA/n-TiO_2-0d	334.0	342.7	354.1	364.3	2.22
PLA/UVA/n-TiO_2-24d	331.4	340.9	353.1	363.7	2.09

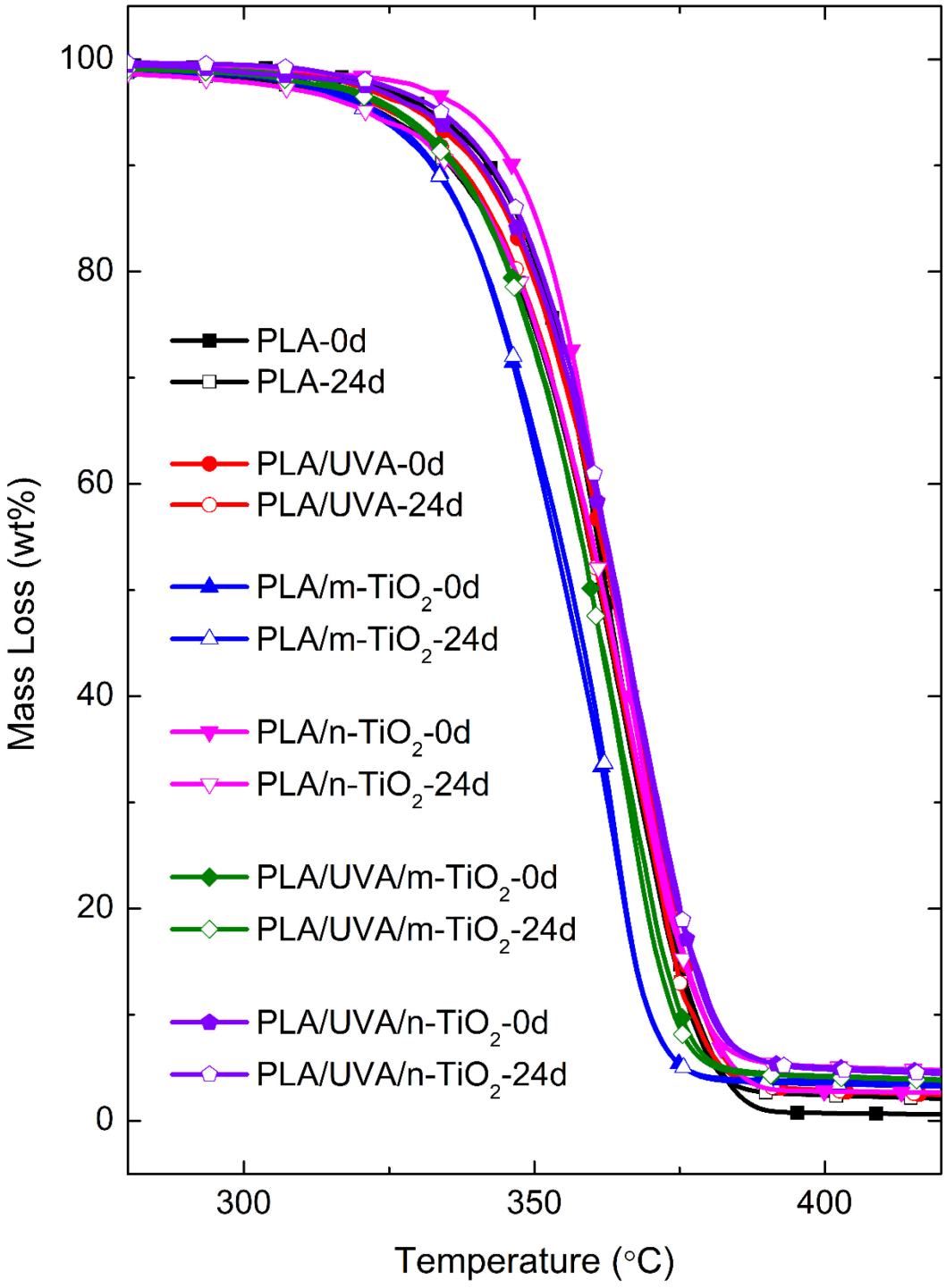

Figure 3.21 Changes in the thermogravimetric curves of all specimens before (0d) and after (24d) UV irradiation

CHAPTER 4

CONCLUSIONS

The main conclusions drawn from the two different parts of this thesis can be summarized as follows:

(i) Effects of Micro-Nano Titania Contents and Maleic Anhydride Compatibilization on the Mechanical Performance of PLA

- SEM analyses revealed that at low filler contents both micron sized (200 nm) and nano sized (50 nm) TiO_2 particles were distributed rather homogeneously in the PLA matrix. On the other hand, at higher filler contents, i.e. beyond 5 wt. % for m-TiO_2 and 2 wt. % for n-TiO_2 particles, there were certain level of particle agglomeration.

- Mechanical tests indicated that due to their efficient strengthening, stiffening and toughening actions, use of both micron and nano sized TiO_2 improved all strength, elastic modulus and fracture toughness values of the neat PLA to a certain extent. The main difference observed between them was the filler content necessary for the best improvement. That is, use of only 2 wt. % n-TiO_2 resulted in either similar or higher improvements compared to the use of 5 wt. % m-TiO_2.

- According to the FTIR analysis, the proposed interaction between the PLA matrix and TiO_2 particles was formation of the certain level of hydrogen bonding; while after maleic anhydride grafted copolymer (PLA-g-MA) compatibilization, certain level of covalent chemical bonding was also expected.

- Due to the improved interfacial adhesion, use of PLA-g-MA compatibilization for the specimen of PLA/2 wt. % n-TiO_2 composition resulted in the highest improvements in the mechanical performance of neat PLA. The improvements were 14% in tensile strength, 20% in flexural modulus and as much as 67% in G_{IC} fracture toughness.

- Thermal analyses by DSC and TGA indicated that use of titania particles had no significant contribution to the transition temperatures and thermal degradation temperatures of PLA. However, first heating DSC thermograms revealed that crystallinity amount of PLA matrix could be increased almost two times by 10 wt. % m-TiO_2 or almost three times by 2 wt. % n-TiO_2 due to especially their heterogeneous nucleation site actions.

(ii) Effects of Micro and Nano Titania on the UV Irradiation Resistance of PLA with and without an Organic UV Absorber

- Visual photographic images and quantitative CEILAB color space parameters indicated that use of micron and nano sized titania particles either alone or together with a benzotriazole type organic UV absorber (UVA) could be very effective to keep white color of the PLA products under prolonged UV irradiation conditions.

- GPC analysis revealed that the weight average molecular weight (M_w) of unirradiated (0d) neat PLA matrix reduced from 105.80×10^3 down to 86.98×10^3 g/mol after 24 days of UV irradiation via chain scission actions of the photodegradation reactions, leading to consequent reductions in the mechanical properties of the specimens.

- Three-point bending tests showed that after 24d UV irradiation the most significant deterioration in the σ_{Flex} strength and E_{Flex} modulus values were for the neat PLA specimen being 15% and 10%, respectively. When UVA, m-TiO_2 or n-TiO_2 were added alone or together, then much lower reductions were obtained, e.g. being only 3% reduction for the PLA/UVA/n-TiO_2 specimen.

- Similarly, fracture toughness tests indicated that K_{IC} and G_{IC} values of the neat PLA specimen was reduced as much as 18% and 36%; while for the synergistic specimen composition PLA/UVA/n-TiO_2 these reductions after 24d UV irradiation were 7% and 19%, respectively.

- Synergistic benefits of using micron and nano sized TiO_2 particles together with benzotriazole type UVA were not only due to the effective stiffening, strengthening and toughening actions of titania particles but also due to their very significant "UV screening" actions absorbing the photons of the UV irradiation, thus decreasing the degree of the detrimental photodegradation reactions in their PLA matrix.

- Therefore, it could be concluded that, since PLA/UVA/n-TiO_2 specimen had very close or higher mechanical properties even after 24 days of UV irradiation compared to unirradiated neat PLA specimen; use of this composition could be considered as an alternative PLA based material for automobile and biomedical applications having durability requirement especially in terms of UV resistance.

- DSC and TGA analyses indicated that PLA specimens filled with UVA, micron and nano sized TiO_2 particles would be also beneficial in terms of keeping the glass transition temperature T_g and the onset degradation temperature $T_{5\%}$ of the PLA matrices after UV irradiation.

REFERENCES

[1] Auras R, Harte B, Selke S. An Overview of Polylactides as Packaging Materials. Macromol Biosci 2004;4:835–64. doi:10.1002/mabi.200400043.

[2] Rasal RM, Janorkar A V, Hirt DE. Poly(lactic acid) modifications. Prog Polym Sci 2010;35:338–56. doi:10.1016/j.progpolymsci.2009.12.003.

[3] Zeng JB, Li KA, Du AK. Compatibilization strategies in poly(lactic acid)-based blends. RSC Adv 2015;5:32546–65. doi:10.1039/c5ra01655j.

[4] Nampoothiri KM, Nair NR, John RP. An overview of the recent developments in polylactide (PLA) research. Bioresour. Technol., vol. 101, Elsevier Ltd; 2010, p. 8493–501. doi:10.1016/j.biortech.2010.05.092.

[5] Peng B, Hou H, Song F, Wu L. Synthesis of high molecular weight poly(l -lactic acid) via melt/solid state polycondensation. II. Effect of precrystallization on solid state polycondensation. Ind Eng Chem Res 2012;51:5190–6. doi:10.1021/ie202192q.

[6] Anderson KS, Schreck KM, Hillmyer MA. Toughening polylactide. Polym Rev 2008;48:85–108. doi:10.1080/15583720701834216.

[7] Chen X, Mao SS. Titanium Dioxide Nanomaterials : Synthesis , Properties , Modifications , and Applications. Chem Rev 2007;107:2891–959. doi:10.1021/cr0500535.

[8] Wunderlich W, Oekermann T, Miao L, Hue NT, Tanemura S, Tanemura M. Electronic properties of Nano-porous TiO 2 - and ZnO-Thin Films-comparison of simulations and experiments. J Ceram Process Res 2004;5:343–54.

[9] Mo S-D, Ching WY. Electronic and optical properties of three phases of titanium dioxide: Rutile, anatase, and brookite. Phys Rev B 1995;51:13023–32. doi:10.1103/PhysRevB.51.13023.

[10] Macwan DP, Dave PN, Chaturvedi S. A review on nano-TiO 2 sol–gel type syntheses and its applications. J Mater Sci 2011;46:3669–86. doi:10.1007/s10853-011-5378-y.

[11] Li G, Chen L, Graham ME, Gray KA. A comparison of mixed phase titania photocatalysts prepared by physical and chemical methods: The importance of

the solid-solid interface. J Mol Catal A Chem 2007;275:30–5. doi:10.1016/j.molcata.2007.05.017.

[12] Shen Q. Photoexcited hole dynamics in TiO 2 nanocrystalline films characterized using a lens-free heterodyne detection transient grating technique 2006;419:464–8. doi:10.1016/j.cplett.2005.11.109.

[13] Pinto D, Bernardo L, Amaro A, Lopes S. Mechanical properties of epoxy nanocomposites using titanium dioxide as reinforcement – A review. Constr Build Mater 2015;95:506–24. doi:10.1016/j.conbuildmat.2015.07.124.

[14] Rhim JW, Park HM, Ha CS. Bio-nanocomposites for food packaging applications. Prog Polym Sci 2013;38:1629–52. doi:10.1016/j.progpolymsci.2013.05.008.

[15] Kemp TJ, McIntyre RA. Transition metal-doped titanium(IV) dioxide: Characterisation and influence on photodegradation of poly(vinyl chloride). Polym Degrad Stab 2006;91:165–94. doi:10.1016/j.polymdegradstab.2005.04.033.

[16] Yuwono AH, Liu B, Xue J, Wang J, Elim HI, Ji W, et al. Controlling the crystallinity and nonlinear optical properties of transparent TiO 2 –PMMA nanohybrids. J Mater Chem 2004;14:2978–87. doi:10.1039/B403530E.

[17] Yuwono AH, Xue J, Wang J, Elim HI, Ji W, Li Y, et al. Transparent nanohybrids of nanocrystalline TiO2 in PMMA with unique nonlinear optical behavior. J Mater Chem 2003;13:1475–9. doi:10.1039/b211976e.

[18] Fajzulin I, Zhu X, Mo M. Nanoparticulate inorganic UV absorbers : a review 2015;12:617–32. doi:10.1007/s11998-015-9683-2.

[19] Sakai W, Tsutsumi N. Photodegradation and Radiation Degradation. Poly(Lactic Acid), Hoboken, NJ, USA: John Wiley & Sons, Inc.; 2010, p. 413–21. doi:10.1002/9780470649848.ch24.

[20] McNeill IC, Leiper HA. Degradation studies of some polyesters and polycarbonates—2. Polylactide: Degradation under isothermal conditions, thermal degradation mechanism and photolysis of the polymer. Polym Degrad Stab 1985;11:309–26. doi:10.1016/0141-3910(85)90035-7.

[21] Ikada E. Photo- and Bio-degradable Polyesters . Photodegradation Behaviors of Aliphatic Polyesters. J Photopolym Sci Technol 1997;10:265–9.

doi:10.2494/photopolymer.10.265.

[22] Tsuji H, Echizen Y, Nishimura Y. Photodegradation of biodegradable polyesters: A comprehensive study on poly(l-lactide) and poly(ε-caprolactone). Polym Degrad Stab 2006;91:1128–37. doi:10.1016/j.polymdegradstab.2005.07.007.

[23] Janorkar A V, Metters AT, Hirt DE. Degradation of poly(L-lactide) films under ultraviolet-induced photografting and sterilization conditions. J Appl Polym Sci 2007;106:1042–7. doi:10.1002/app.24692.

[24] Bocchini S, Fukushima K, Blasio A Di, Fina A, Frache A, Geobaldo F. Polylactic Acid and Polylactic Acid-Based Nanocomposite Photooxidation. Biomacromolecules 2010;11:2919–26. doi:10.1021/bm1006773.

[25] Copinet A, Bertrand C, Govindin S, Coma V, Couturier Y. Effects of ultraviolet light (315 nm), temperature and relative humidity on the degradation of polylactic acid plastic films. Chemosphere 2004;55:763–73. doi:10.1016/j.chemosphere.2003.11.038.

[26] Santonja-Blasco L, Ribes-Greus A, Alamo RG. Comparative thermal, biological and photodegradation kinetics of polylactide and effect on crystallization rates. Polym Degrad Stab 2013;98:771–84. doi:10.1016/j.polymdegradstab.2012.12.012.

[27] Farah S, Anderson DG, Langer R. Physical and mechanical properties of PLA, and their functions in widespread applications — A comprehensive review. Adv Drug Deliv Rev 2016;107:367–92. doi:10.1016/j.addr.2016.06.012.

[28] Masirek R, Kulinski Z, Chionna D, Piorkowska E, Pracella M. Composites of Poly(L-lactide) with Hemp Fibers: Morphology and Thermal and Mechanical Properties. J Appl Polym Sci 2007;105:255–68. doi:10.1002/app.

[29] Xia X, Liu W, Zhou L, Liu H, He S, Zhu C. Study on flax fiber toughened poly (lactic acid) composites. J Appl Polym Sci 2015;132:1–10. doi:10.1002/app.42573.

[30] Rajesh G, Prasad AR, Gupta A. Preparation and Properties of Successive Alkali Treated Completely Biodegradable Short Jute Fiber-Reinforced PLA Composites. Polym Compos 2016;37:2160–70. doi:10.1002/pc.

[31] Yu T, Ren J, Li S, Yuan H, Li Y. Effect of fiber surface-treatments on the

properties of poly(lactic acid)/ramie composites. Compos Part A Appl Sci Manuf 2010;41:499–505. doi:10.1016/j.compositesa.2009.12.006.

[32] Rajesh G, Prasad AR, Gupta A. Mechanical and degradation properties of successive alkali treated completely biodegradable sisal fiber reinforced poly lactic acid composites. J Reinf Plast Compos 2015;34:951–61. doi:10.1177/0731684415584784.

[33] Oksman K, Skrifvars M, Selin JF. Natural fibres as reinforcement in polylactic acid (PLA) composites. Compos Sci Technol 2003;63:1317–24. doi:10.1016/S0266-3538(03)00103-9.

[34] Wan YZ, Wang YL, Li QY, Dong XH. Influence of surface treatment of carbon fibers on interfacial adhesion strength and mechanical properties of PLA-based composites. J Appl Polym Sci 2001;80:367–76. doi:10.1002/1097-4628(20010418)80:3<367::AID-APP1108>3.0.CO;2-U.

[35] Xiu H, Qi X, Liu Z, Zhou Y, Bai H, Zhang Q, et al. Simultaneously reinforcing and toughening of polylactide/carbon fiber composites via adding small amount of soft poly(ether)urethane. Compos Sci Technol 2016;127:54–61. doi:10.1016/j.compscitech.2016.02.025.

[36] Haque P, Barker IA, Parsons A, Thurecht KJ, Ahmed I, Walker GS, et al. Influence of compatibilizing agent molecular structure on the mechanical properties of phosphate glass fiber-reinforced PLA composites. J Polym Sci Part A Polym Chem 2010;48:3082–94. doi:10.1002/pola.24086.

[37] Varsavas SD, Kaynak C. Effects of glass fiber reinforcement and thermoplastic elastomer blending on the mechanical performance of polylactide. Compos Commun 2018;8:24–30. doi:10.1016/j.coco.2018.03.003.

[38] Kaynak C, Erdogan AR. Mechanical and thermal properties of polylactide/talc microcomposites: Before and after accelerated weathering. Polym Adv Technol 2016;27:812–22. doi:10.1002/pat.3721.

[39] Liuyun J, Chengdong X, Lixin J, Lijuan X. Effect of hydroxyapatite with different morphology on the crystallization behavior, mechanical property and in vitro degradation of hydroxyapatite/poly(lactic-co-glycolic) composite. Compos Sci Technol 2014;93:61–7. doi:10.1016/j.compscitech.2013.12.026.

[40] Kasuga T, Maeda H, Kato K, Nogami M, Hata KI, Ueda M. Preparation of

poly(lactic acid) composites containing calcium carbonate (vaterite). Biomaterials 2003;24:3247–53. doi:10.1016/S0142-9612(03)00190-X.

[41] Murariu M, Da Silva Ferreira A, Degée P, Alexandre M, Dubois P. Polylactide compositions. Part 1: Effect of filler content and size on mechanical properties of PLA/calcium sulfate composites. Polymer (Guildf) 2007;48:2613–8. doi:10.1016/j.polymer.2007.02.067.

[42] Kim MW, Song YS, Youn JR. Effects of interfacial adhesion and crystallization on the thermoresistance of poly(lactic acid)/mica composites. Compos Part A Appl Sci Manuf 2010;41:1817–22. doi:10.1016/j.compositesa.2010.08.016.

[43] Dogu B, Kaynak C. Behavior of polylactide/microcrystalline cellulose biocomposites: effects of filler content and interfacial compatibilization. Cellulose 2016;23:611–22. doi:10.1007/s10570-015-0839-0.

[44] Wang N, Zhang X, Ma X, Fang J. Influence of carbon black on the properties of plasticized poly(lactic acid) composites. Polym Degrad Stab 2008;93:1044–52. doi:10.1016/j.polymdegradstab.2008.03.023.

[45] Park SH, Lee SG, Kim SH. Isothermal crystallization behavior and mechanical properties of polylactide/carbon nanotube nanocomposites. Compos Part A Appl Sci Manuf 2013;46:11–8. doi:10.1016/j.compositesa.2012.10.011.

[46] Wu F, Lan X, Ji D, Liu Z, Yang W, Yang M. Grafting polymerization of polylactic acid on the surface of nano-SiO2 and properties of PLA/PLA-grafted-SiO2 nanocomposites. J Appl Polym Sci 2013;129:3019–27. doi:10.1002/app.38585.

[47] Valapa RB, Pugazhenthi G, Katiyar V. Effect of graphene content on the properties of poly(lactic acid) nanocomposites. RSC Adv 2015;5:28410–23. doi:10.1039/C4RA15669B.

[48] Wu T-M, Chiang M-F. Fabrication and characterization of biodegradable poly(lactic acid)/layered silicate nanocomposites. Polym Eng Sci 2005;45:1615–21. doi:10.1002/pen.20370.

[49] Sari B, Kaynak C. Effects of Montmorillonite Content and Maleic Anhydride Compatibilization on the Mechanical Behavior of Polylactide Nanocomposites 2016. doi:10.3139/217.3226.

[50] Fukushima K, Tabuani D, Camino G. Nanocomposites of PLA and PCL based

on montmorillonite and sepiolite. Mater Sci Eng C 2009;29:1433–41. doi:10.1016/j.msec.2008.11.005.

[51] Turan D, Sirin H, Ozkoc G. Effects of POSS Particles on the Mechanical, Thermal, and Morphological Properties of PLA and Plasticised PLA. J Appl Polym Sci 2011;121:1067–75. doi:10.1002/app.33802.

[52] Yuanyuan Chen, Luke M Geever, John A. Killion, John G. Lyons, Clement L. Higginbotham DMD, Chen Y, Geever LM, Killion JA, Lyons JG, Higginbotham CL, et al. Halloysite nanotube reinforced polylactic acid composite. Polym Compos 2015;16:1–8. doi:10.1002/pc.

[53] Kaygusuz I, Kaynak C. Influences of halloysite nanotubes on crystallisation behaviour of polylactide. Plast Rubber Compos 2015;44:41–9. doi:10.1179/1743289814Y.0000000116.

[54] Qian S, Zhang H, Yao W, Sheng K. Effects of bamboo cellulose nanowhisker content on the morphology, crystallization, mechanical, and thermal properties of PLA matrix biocomposites. Compos Part B Eng 2018;133:203–9. doi:10.1016/j.compositesb.2017.09.040.

[55] Chen D, Caruso RA. Recent progress in the synthesis of spherical titania nanostructures and their applications. Adv Funct Mater 2013;23:1356–74. doi:10.1002/adfm.201201880.

[56] Dural-Erem A, Erem HH, Ozcan G, Skrifvars M. Anatase titanium dioxide loaded polylactide membranous films: preparation, characterization, and antibacterial activity assessment. J Text Inst 2015;106:571–6. doi:10.1080/00405000.2014.929274.

[57] Farhoodi M, Dadashi S, Mousavi SMA, Sotudeh-Gharebagh R, Emam-Djomeh Z, Oromiehie A, et al. Influence of TiO2 nanoparticle filler on the properties of PET and PLA nanocomposites. Polym 2012;36:745–55. doi:10.7317/pk.2012.36.6.745.

[58] Fonseca C, Ochoa A, Ulloa MT, Alvarez E, Canales D, Zapata PA. Poly(lactic acid)/TiO2 nanocomposites as alternative biocidal and antifungal materials. Mater Sci Eng C 2015;57:314–20. doi:10.1016/j.msec.2015.07.069.

[59] Zhang H, Huang J, Yang L, Chen R, Zou W, Lin X, et al. Preparation, characterization and properties of PLA/TiO $_2$ nanocomposites based on a novel

vane extruder. RSC Adv 2015;5:4639–47. doi:10.1039/C4RA14538K.

[60] Lu X, Lv X, Sun Z, Zheng Y. Nanocomposites of poly(l-lactide) and surface-grafted TiO2 nanoparticles: Synthesis and characterization. Eur Polym J 2008;44:2476–81. doi:10.1016/j.eurpolymj.2008.06.002.

[61] Luo Y-B, Li W-D, Wang X-L, Xu D-Y, Wang Y-Z. Preparation and properties of nanocomposites based on poly(lactic acid) and functionalized TiO2. Acta Mater 2009;57:3182–91. doi:10.1016/j.actamat.2009.03.022.

[62] Meng B, Tao J, Deng J, Wu Z, Yang M. Toughening of polylactide with higher loading of nano-titania particles coated by poly(ε-caprolactone). Mater Lett 2011;65:729–32. doi:10.1016/j.matlet.2010.11.029.

[63] Zhuang W, Liu J, Zhang JH, Hu BX, Shen J. Preparation, characterization, and properties of TiO 2 /PLA nanocomposites by in situ polymerization. Polym Compos 2009;30:1074–80. doi:10.1002/pc.20658.

[64] Marra A, Silvestre C, Kujundziski AP, Chamovska D, Duraccio D. Preparation and characterization of nanocomposites based on PLA and TiO2 nanoparticles functionalized with fluorocarbons. Polym Bull 2017;74:3027–41. doi:10.1007/s00289-016-1881-2.

[65] Niaounakis M. Automotive Applications. Biopolym. Appl. Trends, Elsevier; 2015, p. 257–89. doi:10.1016/B978-0-323-35399-1.00006-5.

[66] Savaris M, Santos V dos, Brandalise RN. Influence of different sterilization processes on the properties of commercial poly(lactic acid). Mater Sci Eng C 2016;69:661–7. doi:10.1016/j.msec.2016.07.031.

[67] Kaynak C, Kaygusuz I. Consequences of accelerated weathering in polylactide nanocomposites reinforced with halloysite nanotubes. J Compos Mater 2016;50:365–75. doi:10.1177/0021998315575038.

[68] Kaynak C, Sarı B. Accelerated weathering performance of polylactide and its montmorillonite nanocomposite. Appl Clay Sci 2016;121:86–94. doi:10.1016/j.clay.2015.12.025.

[69] Varsavas SD, Kaynak C. Weathering degradation performance of PLA and its glass fiber reinforced composite. Mater Today Commun 2018;15:344–53. doi:10.1016/j.mtcomm.2017.11.008.

[70] Kaynak C, Dogu B. Effects of Accelerated Weathering in Polylactide

Biocomposites Reinforced with Microcrystalline Cellulose. Int Polym Process 2016;31:410–22. doi:10.3139/217.3197.

[71] Gugumus F. Possibilities and limits of synergism with light stabilizers in polyolefins 2 . UV absorbers in polyolefins. Polym Degrad Stab 2002;75:309–20.

[72] Silvia Díaz-Cruz M, Llorca M, Barceló D, Barceló D. Organic UV filters and their photodegradates, metabolites and disinfection by-products in the aquatic environment. TrAC Trends Anal Chem 2008;27:873–87. doi:10.1016/j.trac.2008.08.012.

[73] Muasher M, Sain M. The efficacy of photostabilizers on the color change of wood filled plastic composites. Polym Degrad Stab 2006;91:1156–65. doi:10.1016/j.polymdegradstab.2005.06.024.

[74] Stark NM, Matuana LM. Ultraviolet weathering of photostabilized wood-flour-filled high-density polyethylene composites. J Appl Polym Sci 2003;90:2609–17. doi:10.1002/app.12886.

[75] Xiang X, Chai R, Chen S, Zhang J. Effect of the combination of a benzotriazole-type ultraviolet absorber with thermal stabilizers on the photodegradation of poly(vinyl chloride). J Vinyl Addit Technol 2010;21:175–82. doi:10.1002/vnl.20232.

[76] Zhang M, Xie W, Tang B, Sun L, Wang X. Synthesis of TiO 2 &SiO 2 nanoparticles as efficient UV absorbers and their application on wool. Text Res J 2017;87:1784–92. doi:10.1177/0040517516659375.

[77] Li Y, Chen C, Li J, Sun XS. Photoactivity of poly(lactic acid) nanocomposites modulated by TiO2 nanofillers. J Appl Polym Sci 2014;131:1–7. doi:10.1002/app.40241.

[78] Man C, Zhang C, Liu Y, Wang W, Ren W, Jiang L, et al. Poly (lactic acid)/titanium dioxide composites: Preparation and performance under ultraviolet irradiation. Polym Degrad Stab 2012;97:856–62. doi:10.1016/j.polymdegradstab.2012.03.039.

[79] Xiu H, Qi X, Bai H, Zhang Q, Fu Q. Simultaneously improving toughness and UV-resistance of polylactide/titanium dioxide nanocomposites by adding poly(ether)urethane. Polym Degrad Stab 2017;143:136–44.

doi:10.1016/j.polymdegradstab.2017.07.002.

[80] Buzarovska A, Grozdanov A. Biodegradable poly(L-lactic acid)/TiO2 nanocomposites: Thermal properties and degradation. J Appl Polym Sci 2012;123:2187–93. doi:10.1002/app.34729.

[81] Nakayama N, Hayashi T. Preparation and characterization of poly(l-lactic acid)/TiO2 nanoparticle nanocomposite films with high transparency and efficient photodegradability. Polym Degrad Stab 2007;92:1255–64. doi:10.1016/j.polymdegradstab.2007.03.026.

[82] Rabie ST, Nada AA. Glucoside/(UV absorber) mixtures as photostabilizers for rigid PVC. J Vinyl Addit Technol 2008;14:79–83. doi:10.1002/vnl.20143.

[83] Rajan V V., Wäber R, Wieser J. Influence of different types of UV absorber/UV stabilizer combination on the photodegradation of PC/ABS blend. J Appl Polym Sci 2012;124:4007–15. doi:10.1002/app.34560.

[84] Chang ST, Chou PL. Photodiscoloration inhibition of wood coated with UV-curable acrylic clear coatings and its elucidation. Polym Degrad Stab 2000;69:355–60. doi:10.1016/S0141-3910(00)00082-3.

[85] Kuo CJ, Lan WL, Chen C, Tsai H. Property modification and process parameter optimization design of polylactic acid composite materials. Part I: polylactic acid toughening and photo-degradation modification and optimized parameter design. Text Res J 2015;85:13–25. doi:10.1177/0040517514540766.

[86] Shi QF, Gao JY, Zhao DD, Xu SA. Synergism effect between modified carbon black and organic ultraviolet absorber in polymer matrix for ultraviolet protection. J Appl Polym Sci 2010;116:2566–72. doi:10.1002/app.31775.

[87] Blanchard V, Blanchet P. Color Stability for Wood Products During Use: Effects of Inorganic Nanoparticles. Bioresources 2011;6:1219–29.

[88] Auclair N, Riedl B, Blanchard V, Blanchet P. Improvement of Photoprotection of Wood Coatings by Using Inorganic Nanoparticles as Ultraviolet Absorbers. For Prod J 2011;61:20–7. doi:10.13073/0015-7473-61.1.20.

[89] Forsthuber B, Müller U, Teischinger A, Grüll G. Chemical and mechanical changes during photooxidation of an acrylic clear wood coat and its prevention using UV absorber and micronized TiO2. Polym Degrad Stab 2013;98:1329–38. doi:10.1016/j.polymdegradstab.2013.03.029.

[90] Mahltig B, Böttcher H, Rauch K, Dieckmann U, Nitsche R, Fritz T. Optimized UV protecting coatings by combination of organic and inorganic UV absorbers. Thin Solid Films 2005;485:108–14. doi:10.1016/j.tsf.2005.03.056.

[91] Yao Q, Du M, Sun M. Improving anti-aging coatings by coupling of organic and inorganic ultraviolet absorbers. Adv Mater Res 2013;652–654:1723–7. doi:10.4028/www.scientific.net/AMR.652-654.1723.

[92] Santos RM, Botelho GL, Machado A V. Development of acrylonitrile-butadiene-styrene composites with enhanced UV stability. J Mater Sci 2014;49:510–8. doi:10.1007/s10853-013-7728-4.

[93] Kaynak C, Meyva Y. Use of maleic anhydride compatibilization to improve toughness and other properties of polylactide blended with thermoplastic elastomers. Polym Adv Technol 2014;25:1622–32. doi:10.1002/pat.3415.

[94] Lin-Vien D, Colthup NB, Fateley WG, Grasselli JG. The Handbook of Infrared and Raman Characteristic Frequencies of Organic Molecules. San Diego, CA: Academic Press; 1991.

[95] Nakayama N, Hayashi T. Preparation and Characterization of TiO2 and Polymer Nanocomposite Films with High Refractive Index. J Appl Polym Sci 2007;105:3662–72. doi:10.1002/app.

[96] Liao H-T, Wu C-S. New biodegradable blends prepared from polylactide, titanium tetraisopropylate, and starch. J Appl Polym Sci 2008;108:2280–9. doi:10.1002/app.27901.

[97] Wilson JN, Titheridge DJ, Kieu L, Idriss H. Reactions of maleic anhydride over TiO2 (001) single crystal surfaces. J Vac Sci Technol a-Vacuum Surfaces Film 2000;18:1887–92. doi:10.1116/1.582441.

[98] Fischer EW, Sterzel HJ, Wegner G. Investigation of the structure of solution grown crystals of lactide copolymers by means of chemical reactions. Kolloid-Zeitschrift Zeitschrift Für Polym 1973;251:980–90. doi:10.1007/BF01498927.

[99] Phetwarotai W, Tanrattanakul V, Phusunti N. Synergistic effect of nucleation and compatibilization on the polylactide and poly(butylene adipate-co-terephthalate) blend films. Chinese J Polym Sci (English Ed 2016;34:1129–40. doi:10.1007/s10118-016-1834-0.

[100] Zhang Q, Li D, Zhang H, Su G, Li G. Preparation and properties of poly(lactic

acid)/sesbania gum/nano-TiO2 composites. Polym Bull 2017;75:623–35. doi:10.1007/s00289-017-2059-2.